TU/e EINDHOVEN UNIVERSITY OF TECHNOLOGY

# Surfaces of fluorinated polymer systems

*Citation for published version (APA):*
van de Grampel, R. D. (2002). *Surfaces of fluorinated polymer systems*. [Phd Thesis 1 (Research TU/e / Graduation TU/e), Chemical Engineering and Chemistry]. Technische Universiteit Eindhoven. https://doi.org/10.6100/IR554350

*DOI:*
10.6100/IR554350

*Document status and date:*
Published: 01/01/2002

*Document Version:*
Publisher's PDF, also known as Version of Record (includes final page, issue and volume numbers)

*Please check the document version of this publication:*

• A submitted manuscript is the version of the article upon submission and before peer-review. There can be important differences between the submitted version and the official published version of record. People interested in the research are advised to contact the author for the final version of the publication, or visit the DOI to the publisher's website.
• The final author version and the galley proof are versions of the publication after peer review.
• The final published version features the final layout of the paper including the volume, issue and page numbers.

Link to publication

*General rights*
Copyright and moral rights for the publications made accessible in the public portal are retained by the authors and/or other copyright owners and it is a condition of accessing publications that users recognise and abide by the legal requirements associated with these rights.

• Users may download and print one copy of any publication from the public portal for the purpose of private study or research.
• You may not further distribute the material or use it for any profit-making activity or commercial gain
• You may freely distribute the URL identifying the publication in the public portal.

If the publication is distributed under the terms of Article 25fa of the Dutch Copyright Act, indicated by the "Taverne" license above, please follow below link for the End User Agreement:

www.tue.nl/taverne

*Take down policy*
If you believe that this document breaches copyright please contact us at:

openaccess@tue.nl

providing details and we will investigate your claim.

Download date: 16. Nov. 2023

# Surfaces of Fluorinated Polymer Systems

R. D. van de Grampel

CIP-DATA LIBRARY TECHNISCHE UNIVERSITEIT EINDHOVEN

Grampel, Robert D. van de

Surfaces of fluorinated polymer systems / by Robert D. van de Grampel. -
Eindhoven : Technische Universiteit Eindhoven, 2002.
Proefschrift. – ISBN 90-386-2863-3
NUGI 813

Trefwoorden: gefluorideerde polymeren / polymeeroppervlakken / dunne lagen / bevochtiging ; oppervlaktespanning / lage-energie-ionenverstrooiing ; LEIS / foto-elektronspectroscopie ; XPS / fysisch-chemische simulatie en modelering ; SCF-theorie
Subject headings: fluorinated polymers / polymer surfaces / thin films / wettability ; surface tension / low-energy ion scattering ; LEIS / X-ray photoelectron spectroscopy ; XPS / physicochemical simulation and modeling ; SCF theory

© 2002, Robert van de Grampel

Druk: Universiteitsdrukkerij Technische Universiteit Eindhoven

Kaftontwerp / Cover design: Mariana Amador Asensio and Emilio Jiménez Piqué

# Surfaces of Fluorinated Polymer Systems

PROEFSCHRIFT

ter verkrijging van de graad van doctor aan de
Technische Universiteit Eindhoven, op gezag van de
Rector Magnificus, prof.dr. R.A. van Santen, voor
een commissie aangewezen door het College voor
Promoties in het openbaar te verdedigen op
donderdag 18 april 2002 om 16.00 uur

door

Robert Dirk van de Grampel

geboren te Paterswolde

Dit proefschrift is goedgekeurd door de promotoren:

prof.dr. R. van der Linde

en

prof.dr. G. de With

Copromotor:

dr. J. Laven

This research has been financially supported by the Council for Chemical Sciences of the Netherlands Organization for Scientific Research (CW-NWO) in the Priority Program for Materials Research (PPM)

*Aan mijn ouders*

*Voor Annemieke*

# Contents

**Chapter 1 Introduction** 11

1.1 Historical Perspective 11
1.2 Fluorinated Polymer Films 12
1.2.1 Fluorinated Surfaces 12
1.2.2 Fluorinated Polymer Systems 12
1.3 Fluorine-Containing Coatings 13
1.4 Aim and Survey of this Thesis 14
1.5 References 15

**Chapter 2 Surface Analysis: Background and Experimental Considerations** 19

2.1 Introduction 20
2.2 Surface Composition 21
2.2.1 X-Ray Photoelectron Spectroscopy (XPS) 21
2.2.2 Low-Energy Ion Scattering (LEIS) 24
2.3 Determination of Surface Tension 27
2.3.1 Surface Tension Component Approach 29
2.3.2 Equation of State Approach 31
2.4 Self-Consistent Field Model 32
2.5 Experimental Considerations 34
2.5.1 XPS 34
2.5.2 LEIS 34
2.5.3 Contact Angles 35
2.6 References 35

**Chapter 3 Quantification of Fluorine in Fluorinated Surfaces** 37

3.1 Introduction 38
3.2 Experimental 39
3.2.1 Materials 39
3.2.2 Sample Preparation 39
3.2.3 Surface Techniques 40
3.3 Results and Discussion 40
3.3.1 LiF (100) Single Crystal 40
3.3.2 Fluorinated Self-Assembled Monolayers 42
3.4 Conclusions 46
3.5 References 46

**Chapter 4 Fluorinated Polymethacrylates** 49

4.1 Introduction 50
4.2 Experimental 52
4.2.1 Materials 52

4.2.2 Characterization Techniques 52
4.2.3 Monomer and Polymer Synthesis. 53
*Synthesis of 1H,1H-perfluorodecyl methacrylate* 53
4.2.4 Film Preparation 53
4.2.5 Surface Techniques 54
4.2.6 Surface Tension Calculations 54
4.3 Synthesis of Fluorinated Polymethacrylates 54
4.3.1 1H,1H-perfluorodecyl methacrylate 54
4.3.2 Partially Fluorinated Polymethacrylates 55
4.4 Surface Tension of Fluorinated Polymethacrylates 58
4.5 Surface Composition 60
4.5.1 X-Ray Photoelectron Spectroscopy (XPS) 60
4.5.2 Low Energy Ion Scattering (LEIS) 62
4.6 Discussion 65
4.7 Conclusions 68
4.8 References 68

**Chapter 5 The Influence of Polymer Architecture on Surface Structure** 71

5.1 Introduction 72
5.2 Molecular Modeling 73
5.3 Theory 75
5.3.1 Discretization Scheme for Branched Systems within the Scheutjens-Fleer Theory 75
5.3.2 Evaluation of the Surface Tension 79
*5.3.2.1 The surface tension of a molecularly homogeneous bulk in equilibrium with a vapor.* 79
*5.3.2.2 The surface tension for a system wherein the bulk is micro-phase segregated* 80
5.3.3 The Molecules 81
5.3.4 The Parameters 82
5.4 Results 83
5.4.1 Surface Tensions 84
5.4.2 The Structure of the Surface 85
5.4.3 Chain Length Dependence 90
5.4.4 Chemical Composition Variation 91
5.4.5 Chain Architecture 92
5.5 Discussion 94
5.6 Conclusions 96
5.7 References 97

**Chapter 6 Fluorinated Epoxy Films** 101

6.1 Introduction 102
6.2 Experimental 103
6.2.1 Materials 103
6.2.2 Sample Preparation 103
6.2.3 Surface Techniques 104

6.2.4 Surface Tension Calculations 104
6.2.5 Atomic Force Microscopy 105
6.2.6 Raman Spectroscopy 105
6.3 Results and Discussion 105
6.3.1 Surface Tension of Starting Materials 105
6.3.2 Surface Tension of the Epoxy Films 106
6.3.3 Surface Structures 110
6.3.4 Surface Composition 110
6.3.5 Network Formation 112
6.4 Conclusions 114
6.5 References 115

**Chapter 7 Fluorinated Oligoesters** 117

7.1 Introduction 118
7.2 Experimental 118
7.2.1 Materials 118
7.2.2 Synthesis of Oligoesters 119
7.2.3 Synthesis of Partially Fluorinated Oligoester 119
7.2.4 Characterization Techniques 120
7.2.5 Film Preparation 120
7.3 Results and Discussion 121
7.3.1 Synthesis and Characterization of Oligoesters 121
7.3.2 Characterization of Fluorinated Oligoesters 124
7.3.3 Wetting Characteristics from Contact Angles 128
7.3.4 Chemical Composition of Fluorinated Oligoester Films 131
7.4 Conclusions 134
7.5 References 135

**Chapter 8 Epilogue** 137

8.1 General Considerations 137
8.2 Domain Formation in the Surface 138
8.3 Self-Stratifying Coatings 138
8.4 Which Surface is more Hydrophobic ? 140
8.5 References 140

**Summary** 141

**Samenvatting** 145

**Dankwoord** 149

**Curriculum Vitae** 151

# Chapter 1

# Introduction

## 1.1 HISTORICAL PERSPECTIVE

The serendipitous discovery of polytetrafluoroethylene (PTFE) by Plunkett and coworkers[1] at DuPont opened a new field of special polymeric materials. The outstanding properties of PTFE, such as low surface tension, low coefficient of friction, excellent chemical and thermal stability combined with excellent dielectric properties, have favored the application of PTFE in many areas. Pipes, valves, optical fibers, surgical implants, and the well-known nonstick coatings for cookware are some typical examples for the application of PTFE. The features of PTFE are the result of weak intermolecular forces and a strong C-F bond in its molecular structure. The possibilities for processing of PTFE, however, are limited to the aqueous dispersion or to its granular form with high melt-viscosity, as the homopolymer is insoluble in any solvent. These unattractive features have challenged further research, striving for materials with comparable properties but more flexible processing. For this purpose, a variety of comonomers have been introduced in the PTFE chains to obtain copolymers of lower molar mass and reduced melt-viscosity, while maintaining adequate mechanical and physical properties. Examples of such copolymers are those comprising hexafluoropropylene (FEP) and perfluoroalkyl-vinyl-ethers (PFAs), or perfluoro-(2,2-dimethyl-1,3-dioxole) (Teflon AF).[2] Recently, Smith and coworkers[3] at ETH Zürich developed a processing window for PTFE using medium melt-viscosities/medium molecular weights grades of PTFE. They demonstrated that PTFE could be shaped by ordinary melt processing into objects with proper mechanical properties that resemble those of high-density

polyethylene. These findings allow the fabrication of a broad spectrum of entirely new products, as well as compounding and recycling of this unique material.[4]

## 1.2 FLUORINATED POLYMER FILMS

### 1.2.1 Fluorinated Surfaces

Fluorinated surfaces derive their characteristics from the unique molecular properties associated with the C-F bond that imparts a specific, unique chemistry and physics at interfaces. Their low surface tensions, low electrostatic loading, and low friction coefficient can play an essential role in microelectronics, antifogging and antifouling applications and are promising in medical applications.

It is well known that there are materials that have a lower surface tension than PTFE. These surfaces are often dominated by mainly $CF_3$ groups in the surface compared to the $CF_2$ groups of PTFE. The higher effectiveness of $CF_3$ compared to $CF_2$ groups in lowering the surface tension is attributed to the bulky F atom leading to a lower density of attractive centers per unit area at the surface.[5] Zisman established that the surface tension depends on the constituent groups and decreases in the order of $CH_2$ (36 mN/m) > $CH_3$ (30 mN/m) > $CF_2$ (23 mN/m) > $CF_3$ (15 mN/m).[6]

The properties of fluorinated surfaces depend not only on the coverage of the surface by the fluorocarbons but also on the degree of order in the surface.[7] A uniformly organized array of $CF_3$ groups can create a surface with a surface tension as low as 6 mN/m.[6]

### 1.2.2 Fluorinated Polymer Systems

It has been shown that self-assembled monolayers of perfluoroalkyl chains, where the surface is formed by a close-packed array of $CF_3$ groups, possess the lowest surface energy attainable.[6] Similar low surface tensions have been reported for macromolecules with pendant perfluoroalkyl groups that have been introduced by the incorporation of fluorinated monomers. Examples of such polymers are partly-fluorinated polysiloxanes[8-10], poly(acrylates),[11-14] polymethacrylates,[13,15-25] and polystyrenes.[26-28] The pendant perfluoroalkyl-chains introduced by the fluorinated monomer orientate in the surface perpendicular to the substrate leading to ultra-low surface tensions.

Several research groups have reported polymer systems exhibiting a low surface tension by grafting perfluoroalkyl groups to polymer chains.[29-31] Other polymer architectures

like end-functionalized polymers[32-36] and block copolymers[37-44] have also been employed to obtain fluorinated polymer surfaces with low surface tensions.

Investigations of surface structures and surface properties of polymeric systems have been carried out extensively, both experimentally[45] and theoretically[46]. In accordance with the specific surface properties of fluorinated polymer materials, continuing efforts have been made towards the understanding of the relation between the microscopic surface structure and the macroscopic surface properties. It is well known that some of the important factors for low surface tension surfaces include both the precise nature of the atomic population at the surface and their physical arrangement. However, the search for a correlation has often been impeded by a missing link, namely, the knowledge of the composition in the outermost atomic layer.

## 1.3 FLUORINE-CONTAINING COATINGS

Fluorine-containing materials are not only used as engineering plastics and high-tech elastomers, but also find considerable application in the coatings industry because of their interesting properties like water and oil repellency, low coefficient of friction, and chemical resistance. Fluorine-containing coatings can be divided into two classes *viz.*, coatings based on thermoplastic binders and coatings based on thermosetting binders.[2] Examples of thermoplastic binders are poly(vinyl fluoride) (*e.g.* Tedlar from DuPont), poly(vinylidene fluoride) (*e.g.* Kynar from Atochem), and poly(tetrafluoroethylene) (*e.g.* Teflon from DuPont). The fluorine content and its distribution along the chain of these polymers determine the properties of these materials. In general, the higher the fluorine content, the larger the chemical and thermal stability, the solvent resistance, and the better the weatherability. As already mentioned for PTFE (Section 1.1), perfluorinated homopolymers are insoluble in common organic solvents, which renders them intractable materials. This problem can partially be solved by copolymerization of perfluorinated monomers with conventional, non-fluorinated monomers.

Two main groups of thermosetting materials can be distinguished. The first group is Lumiflon from Asahi Glass Co, which can be considered as alternating copolymers of chlorotrifluoroethylene and various modified vinyl ethers. These modified vinyl ethers introduce functional groups into the polymers, which improve the properties of the coatings. For instance, the introduction of an acid-functionalized ether makes the resin more compatible with pigments and at the same time provides the resin reactivity for adhesion at the substrate,

whereas hydroxy-functionalized vinyl ethers introduce crosslinkable groups for network formation. The second major type of fluorine-containing thermosetting binders is Fluorobase from Ausimont. Fluorobase resins are functional derivatives of perfluoropolyethers available in a range of molecular weights ($1000 < M_n < 4000$ g/mol).

However, the synthesis and high costs of these fluorinated bulk materials and the additional intrinsic processing problems have limited their application to niche segments of the market.

## 1.4 AIM AND SURVEY OF THIS THESIS

The first objective of this thesis is to better understand the correlation between surface properties and surface composition. The work in this thesis will be concentrated on the

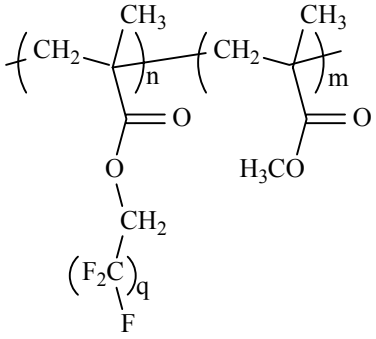

**Figure 1.1** Chemical structure of a random copolymer of MMA and perfluoroalkyl methacrylate.

investigation of the molecular origin of the surface tension of partially fluorinated polymers. Therefore, polymers were investigated with the same polymethacrylate backbone but with different perfluoroalkyl side groups according to the structure depicted in Figure 1.1.

In addition to the study of the molecular nature of the surface tension of partially fluorinated polymethacrylates, the second objective of the present study will be the exploration of novel coating systems following the strategy of surface enrichment with fluorinated species. In such systems, the fluorinated species will migrate to the coating-air interface to give a fluorine-rich topcoat, introducing the exceptional surface properties of expensive fluoropolymers to less expensive bulk materials.

In **Chapter 1** an general introduction to fluorinated surfaces of polymeric materials, focusing on their peculiar and intriguing aspects, has been given.

In **Chapter 2** a number of surface characterization techniques is introduced which are used in this thesis. Advantages and disadvantages for each of the methods are contrasted. The techniques chosen are usually selected on the basis of their applicability.

**Chapter 3** describes the quantification of the fluorine concentration in the outermost atomic surface layer by Low Energy Ion Scattering (LEIS), using LiF (100) single crystals as reference material. This successfully led to the determination of the fluorine density in the outermost atomic layer of perfluorinated self-assembled monolayers.

The molecular aspects of surfaces of partially fluorinated polymethacrylates are considered in **Chapter 4**. These polymers have a perfluoroalkyl side chain, which preferentially orientates towards the surface (*intra*-molecular segregation). The nature of the atomic origin of the surface tension of these polymers will be deduced and discussed in detail using the quantification as described in Chapter 3.

Complementary to the experimental surface analyses, a theoretical framework is applied for the description of both the bulk and interfacial properties of the polymethacrylate chains. A detailed Self-Consistent Field (SCF) lattice theory is used for this purpose. The results of these analyses are described in **Chapter 5**. In these theoretical calculations the influence of polymer architectures (random copolymers, end-capped polymers, and block copolymers) is illustrated, providing essential knowledge to design tailor-made surface.

**Chapters 6 and 7** are concerned with novel low surface tension coating systems for practical applications *viz*. an epoxy-amine coating and a solventless liquid oligoester system. Low surface tensions could be obtained by the introduction of small quantities of fluorinated species, which are enriched at the surface during the formation of crosslinked networks.

The last Chapter (**Chapter 8**) summarizes the main findings of the present thesis. Final remarks considering future work conclude this chapter.

## 1.5 REFERENCES


1 Plunkett, R. J. *U. S. Pat.* US 2230654.

2 Scheirs, J. Ed. *Modern Fluoropolymers* Wiley: New York, 1997.

3 Tervoort, T.; Visjager, J.; Graf, B.; Smith, P. *Macromolecules* **2000**, 33, 6460.

4 Smith, P.; Visjager, J.; Bastiaansen, C.; Tervoort, T. *Int. Pat. Appl*. WO 00/08071.

5 Johnson, R. E., Jr.; Dettre, R. H. in *Wettability*; Berg, J. C., Ed.; Marcel Dekker: New York, 1993; Chapter 1.

[6] Zisman, W. A. *Contact Angle, Wettability, and Adhesion,* Advances in Chemistry Series 43, Am. Chem. Soc.: Washington DC, 1964.

[7] Genzer, J.; Sivaniah, E.; Kramer, E. J.; Wang, J.; Körner, H.; Xiang, M.; Char, K.; Ober, C. K.; DeKoven, B. M.; Bubeck, R. A.; Chaudhury, M. K.; Sambasivan. S.; Fischer, D. A. *Macromolecules* **2000**, 33, 1882.

[8] Kobayashi, H.; Owen, M. J. *Trends Polym. Sci*. **1995**, 3, 10.

[9] Thorpe, A. A.; Young, S. A.; Nevell, T. G.; Tsibouklis, J. *J. Appl. Surf. Sci*. **1998**, 136, 99.

[10] Perutz, S.; Wang, J.; Kramer, E. J.; Ober, C. K.; Ellis, K. *Macromolecules* **1998**, 31, 4272.

[11] DeSimone, J. M.; Guan, Z.; Elsbernd, C. S. *Science* **1992**, 257, 945.

[12] Guyot, B.; Ameduri, B.; Boutevin, B. *J. Fluorine Chem*. **1995**, 74, 233.

[13] Ameduri, B.; Boutevin, B.; Guida-Pietrasanta, F.; Rousseau *J. Fluorine Chem*. **2001**, 107, 397.

[14] Morita, M.; Ogisu, H.; Kubo, M. *J. Appl. Polym. Sci*. **1999**, 73, 1741.

[15] Schmidt, D. L.; Coburn, C. E.; DeKoven, B. M.; Potter, G. E.; Meyers, G. F.; Fisher, D. A. *Nature* **1994**, 368, 39.

[16] Takahashi, S.; Kasemura, T.; Asano, K. *Polymer* **1997**, 38, 2107.

[17] Katano, Y.; Tomono, H.; Nakajima, T. *Macromolecules* **1994**, 27, 2342.

[18] Park, I. J.; Lee, S.-B.; Choi, C. K.; Kim, K.-J. *J. Colloid. Inter. Sci*. **1996**, 181, 284.

[19] Krupers, M.; Slangen, P.-J.; Möller, M. *Macromolecules* **1998**, 31, 2552.

[20] Kassis, C. M.; Steehler, J. K.; Betts, D. E.; Guan, Z. B.; Romack, T. J.; DeSimone, J. M.; Linton, R. W. *Macromolecules* **1996**, 29, 3247.

[21] Seiko, S.; Lermann, E.; Möller, M. *Langmuir* **1996**, 12, 4015.

[22] Bongiovanni, R.; Malucelli, G.; Lombardi, V.; Priola, A.; Siracusa, V.; Tonelli, C.; Di Meo, A. *Polymer* **2001**, 42, 2299.

[23] Thomas, R. R.; Anton, D. R.; Graham, W. F.; Darmon, M. J.; Sauer, B. B.; Stika, K. M.; Swartzfager, D. G. *Macromolecules* **1997**, 30, 2883.

[24] Tsibouklis, J.; Graham, P.; Eaton, P. J.; Smith, J. R.; Nevell, T. G.; Smart, J. D.; Ewen, R. J. *Macromolecules* **2000**, 33, 8460.

[25] Ciardelli, F.; Aglietto, M.; Montagnini di Mirabello, L.; Passaglia, E.; Giancristoforo, S.; Castelvetro, V.; Ruggeri, G. *Prog. Org. Coat*. **1997**, 32, 43.

[26] Höpken, J.; Möller, M. *Macromolecules* **1992**, 25, 2482.

[27] Bouteiller, V.; Garnault, A. M.; Teyssié, D.; Boileau, S.; Möller, M. *Polym. Int.* **1999**, 48, 765.

[28] Kato, S.; Ueno, Y.; Kishida, A.; Miyazaki, T.; Matsumoto, T.; Murata, Y.; Akashi, M. *J. Appl. Polym. Sci*. **1999**, 71, 1049.

[29] Hwang, S. S.; Ober, C. K.; Perutz, S. M.; Iyengar, D. R.; Schneggenburger, L. A.; Kramer, E. J. *Polymer* **1995**, 36, 1321.

[30] Perutz, S. M.; Dai, C.-A.; Ober, C. K.; Kramer, E. J. *Macromolecules* **1996**, 29, 1229.

[31] Park, I. J.; Lee, S.-B.; Choi, C. K. *Polymer* **1997**, 38, 2523.

[32] Albert, B.; Jerome, R.; Teyssié, P. *Macromol. Chem*. **1984**, 185, 579.

[33] Hunt, Jr., M. O.; Belu, A. M.; Linton, R. W.; DeSimone, J. M. *Macromolecules* **1993**, 26, 4854.

[34] McLain, S. J.; Sauer, B. B.; Firment, L. E. *Macromolecules* **1996**, 29, 8211.

[35] Su, Z.; Wu, D.; Hsu, S. L.; McCarthy, T. J. *Macromolecules* **1997**, 30, 840.

[36] Lee, W.-K.; Losito, I.; Gardella, Jr., J. A.; Hicks, Jr., W. L. *Macromolecules* **2001**, 34, 3000.

[37] Wang, J.; Mao, G.; Ober, C. K.; Kramer, E. J. *Macromolecules* **1997**, 30, 1906.

[38] Krupers, M. J.; Bartelink, C. F.; Grünhauer, H. J. M.; Möller, M. *Polymer* **1998**, 39, 2049.

[39] Grundke, K.; Pospiech, D.; Kollig, W.; Simon, F.; Janke, A. *Colloid Polym. Sci*. **2001**, 279, 727.

[40] Zhang, Z.; Ying, S.; Zhang, Q.; Xu, X. *J. Polym. Sci. Part A: Polym. Chem*. **2001**, 39, 2670.

[41] Xiang, M.; Li, X.; Ober, C. K.; Char, K.; Genzer, J.; Sivaniah, E.; Kramer, E. J.; Fischer, D. A. *Macromolecules* **2000**, 33, 6106.

[42] Genzer, J.; Sivaniah, E.; Kramer, E. J.; Wang, J.; Körner, H.; Xiang, M.; Char, K.; Ober, C. K.; DeKoven, B. M.; Bubeck, R. A.; Fischer, D. A.; Sambasivan. S. *Langmuir* **2000**, 16, 1993.

[43] Matsumoto, K.; Kubota, M.; Matsuoka, H.; Yamaoka, H. *Macromolecules* **1999**, 32, 7122.

[44] Hayakawa, T.; Wang, J.; Xiang, M.; Li, X.; Ueda, M.; Ober, C. K.; Genzer, J.; Sivaniah, E.; Kramer, E. J.; Fischer, D. A. *Macromolecules* **2000**, 33, 8012.

[45] a) Chaudhury, M. K.; Whitesides, G. M. *Science* **1992**, 255, 1230. b) Olbris, D. J.; Ulman, A.; Shnidman, Y. *J. Chem. Phys*. **1995**, 102, 6865. c) Ulman, A. *Thin Solid Films*, **1996**, 273, 48. d) Mach, P.; Huang, C. C.; Nguyen, H. T. *Phys. Rev. Lett*. **1998**, 80, 732. e) Fadeev, A. Y.; McCarthy, T. J. *Langmuir* **1999**, 15, 3759. f) Castner, D. G.; Lweis, Jr., K. B.; Fischer, D. A.; Ratner, B. D.; Gland, J. L. *Langmuir* **1993**, 9, 537. g) Lüning, J.; Stöhr,

J.; Song, K. Y.; Hawker, C. J.; Ionidice, P.; Nguygen, C. V.; Yoon, D. Y. *Macromolecules*, **2001**, 34, 1128.

[46] Jones, R. A. L.; Richards, R. W. *Polymers at Surfaces and Interfaces*, Cambridge University Press: Cambridge, 1999, and references therein.

# Chapter 2

# Surface Analysis: Background and Experimental Considerations

## 2.0 ABSTRACT

*In this Chapter some basic physical principles and experimental considerations of surface characterization techniques are described which have been used frequently in this thesis. Besides, a short introduction to a theoretical approach to study surfaces (self-consistent field analysis) will be given. More comprehensive and detailed descriptions of the reviewed techniques can be found in the references quoted.*

## 2.1 INTRODUCTION

During recent years, many surface sensitive techniques have been developed to analyze polymer surfaces. However, the surface investigated by one technique may be the bulk if studied by another. An appropriate definition of a surface, *e.g.*, the sampling depth observed, is therefore very important. Figure 2.1 gives an overview of several *analytical* surface techniques. X-ray photoelectron spectroscopy (XPS) analyses the composition within a few tens of Ångströms from the surface. Secondary ion mass spectroscopy (SIMS) gives information about the composition of roughly the first five Ångström from the surface. Information about the atomic composition of the *outermost* atomic layer (~ 1 Å) can be obtained from low energy ion scattering (LEIS).

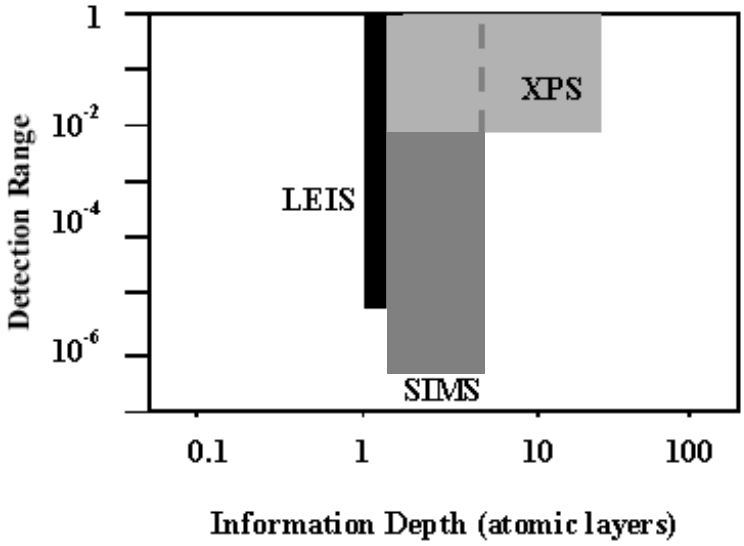


**Figure 2.1** A comparison of average sampling depth for some surface analysis techniques.

The techniques mentioned above provide compositional information for different depths below the surface. When *structural* information (surface topology, lateral heterogeneity) is required various types of microscopy techniques are appropriate, such as scanning electron microscopy (SEM), transmission electron microscopy (TEM) and more recently atomic force microscopy (AFM). The descriptions of these techniques, however, are beyond the scope of this thesis.

The choice of a suitable analytical surface technique involves the consideration of what kind of surface information is needed. Contact angle data (*macroscopic*), which are extremely surface sensitive, are important for the determination of surface tensions of the solid surface. However, these data do not provide direct information about the chemical

nature of the surface. In this respect XPS, SIMS or LEIS have to be used. The combination of several techniques can provide complementary types of surface information and thus, in turn, can result in a more detailed view of chemical composition and component distribution, particularly in relation to a better understanding of the phenomena of wetting and adhesion. In the following sections short reviews will be given for XPS, LEIS, contact angle measurements, being the main techniques used in this thesis. Besides an introduction of theoretical modeling to study surface properties is given.

## 2.2 SURFACE COMPOSITION

### 2.2.1 X-Ray Photoelectron Spectroscopy (XPS)

X-ray photoelectron spectroscopy, also known as electron spectroscopy for chemical analysis (ESCA), is probably the most widely used technique to study the chemical composition of polymer surfaces.[1] The technique is based on the photoelectrical effect, which provides information on elemental and functional group composition, and oxidation state.

In an XPS experiment the surface is irradiated with X-rays. The energy of the incident X-ray photons is that high that electrons can be ejected from electron shells. These ejected electrons are referred to as photoelectrons. A schematic representation of the XPS process is given in Figure 2.2.

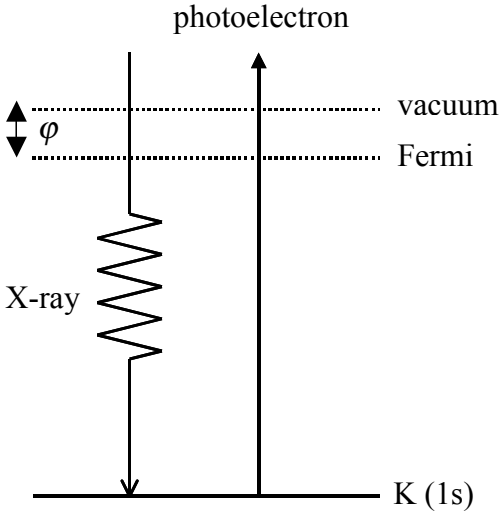


**Figure 2.2** Schematic depiction of the XPS process**.**

From the difference between the known energy of the X-ray photons and the measured kinetic energy of the photoelectrons, the binding energy can be calculated according to:[2]

$$E_b = h\nu - E_k - \varphi \qquad (2.1)$$

where $E_b$ denotes the binding energy of the photoelectron in the excited electron shell, $E_k$ the kinetic energy of the photoelectron, *h* Planck's constant, *v* the frequency of the X-ray, and $\varphi$ the work function of the spectrometer. Elements can be recognized by their binding energy, which depends slightly on oxidation state and chemical environment.

Some experimental problems can occur in XPS. First, insulating samples (polymers) may become charged during the measurement, because photoelectrons leave the sample. Due to the positive charge on the samples, all XPS peaks in the spectrum shift by the same amount to apparently higher binding energies. Calibration is therefore necessary and in case of organic polymers the $-CH_2-$ peak at 284.5 eV is often used. Secondly, organic polymers are damaged during XPS by the impact of photoelectrons and secondary electrons generated from them.[3,4] This gives rise to the generation of free radicals which react to give various products like crosslinked structures. In order to minimize this polymer degradation, the acquisition times must be limited.[6]

The surface sensitivity of XPS is not related to the penetration depth of the incident X-rays, which is many micrometers, but to the probability of the generated photoelectrons being able to leave the surface. Generally it is accepted that 95% of the signal of the photoelectron originates from 3 times the inelastic mean free path ($\lambda$).[5] If an electron is emitted from a deeper layer, it will almost certainly lose its information due to energy loss during collision within the solid material and will only contribute to the XPS background. Therefore, the sampling depth *d* (from which 95% of the emitted electrons originates) in XPS is usually defined as:[6]

$$d = 3\lambda \cos\theta \qquad (2.2)$$

where $\theta$ represents the angle between the surface normal and the electron detector. This means that measurements can be made more sensitive to the outer surface region by increasing $\theta$, and thus decreasing the actual probing depth (angle dependent XPS, see Figure 2.3). In this way depth profiles of chemical composition are obtained in a non-destructive way.

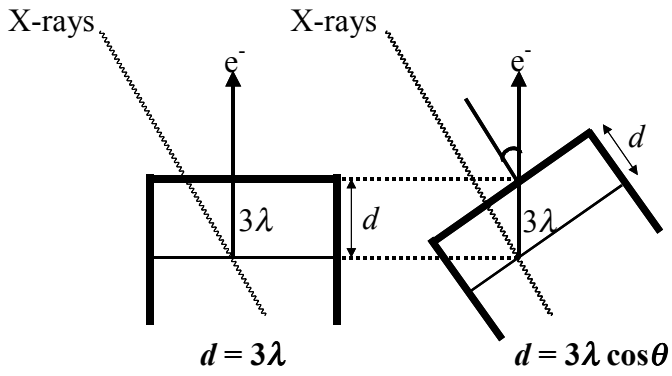


**Figure 2.3** Schematic representation of an angle-dependent XPS.

Quantitative surface analyses by XPS have been reviewed extensively by many authors.[6] Usually, a uniform distribution of atoms is assumed with depth. The quantification of the surface composition for XPS can be obtained from the peak areas after correction for the background. Several methods are available for background correction. The most widely used are a linear background subtraction, the Shirley method, and the Tougaard method.[7] The simple linear approach has been recommended for the analysis of polymers over the Shirley method. The Tougaard method is not a proven method for polymers and hence has not been applied. After correction for the background the atomic concentration $C_i$ of an element $i$ can be calculated from:

$$C_i = \frac{A_i / S_i}{\sum_j^m A_j / S_j} \tag{2.3}$$

where $m$ is the number of elements in the sample, and $A_i$ and $S_i$ are the peak area and the relative sensitivity factor for element $i$, respectively. These relative sensitivity factors parameters are defined as the ratio of the XPS intensity divided by the number of atoms of the element per unit volume, taking one elemental peak as standard. It is important to note that relative sensitivity factors have to be determined by calibration as they depend on the spectrometer used.

Another important point is that the sampling depth, defined as the layer thickness that contributes to the XPS signal, varies from element to element (Table 2.1). A direct comparison of atomic concentrations as 'determined by XPS' is therefore not possible when dealing with non-homogeneous samples. Therefore, when dealing with organic polymers the

best procedure to evaluate the surface composition from XPS data is by curve fitting the $C_{1s}$ region. In this case the emitted photoelectrons originate from the same sampling depth.[8]

**Table 2.1** XPS sampling depth as a function of the core level binding energy and the angle from the surface normal.[6]

| Core level | BE (eV) | Sampling depth (95% of the signal) (nm) | | | | | |
|---|---|---|---|---|---|---|---|
| | | Mg Kα | | | Al Kα | | |
| | | 80° | 45° | 0° | 80° | 45° | 0° |
| | | | | | | | |
| $F_{1s}$ | 686 | 0.8 | 3.4 | 4.8 | 1.1 | 4.5 | 6.3 |
| $O_{1s}$ | 531 | 1.0 | 4.1 | 5.8 | 1.3 | 5.2 | 7.3 |
| $N_{1s}$ | 402 | 1.1 | 4.7 | 6.6 | 1.4 | 5.7 | 8.0 |
| $C_{1s}$ | 287 | 1.3 | 5.2 | 7.3 | 1.5 | 6.2 | 8.7 |

### 2.2.2 Low-Energy Ion Scattering (LEIS)

In a LEIS experiment, also referred to as ion scattering spectroscopy (ISS), the sample is bombarded with low-energy (noble gas) ions (Figure 2.4). The energy of the ions that are elastically backscattered provides direct information on the masses of the atoms from which the ions are scattered. LEIS is a technique sensitive only to the outermost atomic layer only.[9] This is due to the fact that primary ions that collide with sample atoms below the first atomic layer have a high probability to capture an electron leading to neutralization (neutral species are not detected because the analyzer/detector uses electrostatic deflection).

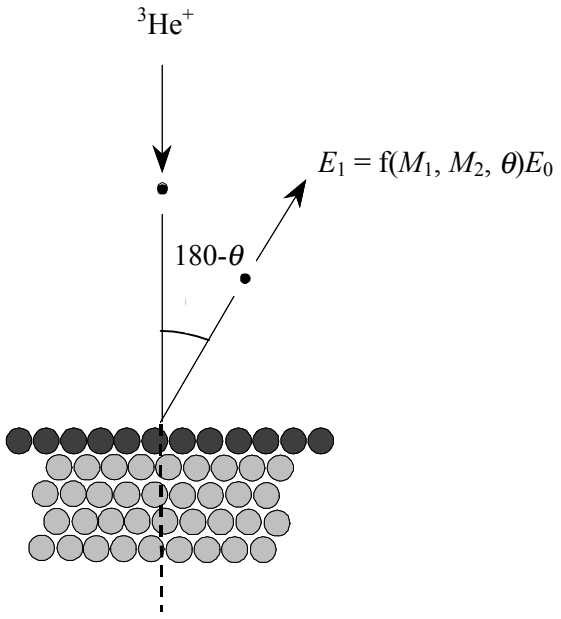


**Figure 2.4** Schematic representation of scattering in a LEIS experiment. $E_1$ is the energy of the ion after collision.

It follows from the laws of conservation of energy and momentum, that for a given scattering angle $\theta$, the energy of the backscattered ion is characteristic for the mass of the target atoms from which they are scattered. The energy of the backscattered ion $E_1$ is given by:[10]

$$\frac{E_1}{E_0} = \frac{M_1^2}{(M_1 + M_2)^2}\left[\cos\theta + \left(\frac{M_2^2}{M_1^2} - \sin^2\theta\right)^{1/2}\right]^2 \tag{2.4}$$

where $E_0$ represents the energy of the ion before the collision, $M_1$ denotes the mass of the impinging ion, and $M_2$ is the mass of the atom at the surface. Since the mass of the ion, its incident energy, and the scattering angle are fixed in the LEIS experiment, there is a direct relation between the mass of the target atom and the energy of the back-scattered ion. The energy spectrum can thus directly be interpreted as a mass spectrum of the surface atoms.

Both the detectable mass range and the mass resolution of LEIS depend on the mass and the energy of the primary noble gas ion. For detection of mass numbers lower than 50, $He^+$ ions are used. For the detection of heavier elements $Ne^+$ or $Ar^+$ ions are applied as primary ions.

In a LEIS experiment the ion scattering yield, $S_i$, of an ion scattered from element *i* is given by:

$$S_i \propto Ic_i(d\sigma_i / d\Omega)P_i^+ \tag{2.5}$$

where $I$ is the incident ion current, $c_i$ the effective atomic surface density of element $i$, $(d\sigma_i / d\Omega)$ the differential scattering cross-section for scattering from element $i$, and $P_i^+$ the ion fraction after scattering from element $i$. The neutralization of the ions depends on the interaction time. The ion fraction is generally given by:

$$P_i^+ = \exp(-v_c / v) \tag{2.6}$$

where $v$ denotes the velocity of the ion and $v_c$ a characteristic neutralization constant. Since the ion neutralization involves the electron transfer from the surface to the ion, one would

expect that the precise electronic structure determines the value of $P_i^+$. However, this is generally not the case. From energy (velocity) dependent experiments it is found, for instance, that $P_{Al}^+$ is the same for scattering from Al in Al or $Al_2O_3$.[11] Likewise, no difference for the value of $P_{Si}^+$ was found for scattering from Si in Si or $SiO_2$.[12] Thus, in these cases there is no matrix effect. More recently, similar observations of the absence of a matrix effect have been made also for organic materials.[13]

The LEIS measurements were performed with the Calipso set-up, which is an improved version of the ERISS configuration.[14] A cross-section of the analyzer is given in Figure 2.5. The primary ions are incident along the axis of the double toroidal electrostatic energy analyzer. Ions that are backscattered over 145° by the atoms in the target are accepted by the analyzer. The ions with the higher energy are less affected by the electrostatic field and imaged near the centre of the detector, while the lower energy ions are imaged at a larger radius. Using a two-dimensional ring-shaped detector, the analyzer and detector enable parallel detection of the backscattered ions. In comparison to conventional electrostatic energy analyzers, this unique design gives a very high efficiency for the detection of the scattered particles. The sensitivity of the Calipso set-up is therefore about a factor of 1000 higher than that of conventional LEIS set-ups. This allows the use of low doses (non-destructive "static" analysis) with still good statistics in the spectra. This is very important for polymers, for which the signals are generally very low. Charging of the sample is avoided by using a ring shaped filament that floods the surface with low-energy electrons. This compensation is relatively simple, since there are no electrostatic fields in the target region.

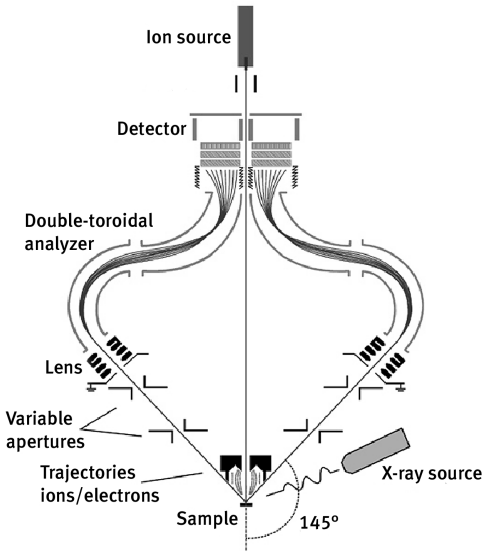


**Figure 2.5** A schematic cross-section of the double toroidal analyzer for LEIS.

A good sensitivity in LEIS is generally obtained when the mass of the target atom is at least 2.5 times higher than that of the bombarding ion. When this condition is met, the highest sensitivity is obtained for the noble gas ion having the highest atomic number. If an ion has more than one isotope, the sensitivity for the lighter isotope is higher but the mass resolution is lower. Since for polymers the mass resolution of the surface atoms is good enough when using $^3$He ions, these ions are preferred for the analysis.

One has to keep in mind that polymer surfaces can be easily damaged under ion bombardment. Hence, to avoid damage of the polymer surfaces during LEIS measurement, the ion dose must be kept low (s*tatic* LEIS).[15]

As mentioned previously the sensitivity of the LEIS technique differs from element to element. It depends on the mass and nuclear charge of the projectile ion, the mass of the target atom, and the energy levels of, in particular, the inner-shell electrons of the target atom in relation to the levels of the ion. With a given probing ion, the sensitivity for most elements in the periodic table of elements does not differ by more than a factor of 10. Results as published in the literature[16] usually are hampered by the lack of an absolute calibration method. The reason is that it is very difficult to determine $P^+$ accurately. Therefore, when absolute calibration is necessary, reference samples with a well-defined composition in the outermost atomic layer are needed. In Chapter 3 we will present the absolute quantification of fluorine in the first atomic layer in more detail using a single crystal of LiF.

## 2.3 DETERMINATION OF SURFACE TENSION

The combined use of the first and the second law of thermodynamics, gives the variation of the internal energy $U$ of a macroscopically homogeneous bulk phase:

$$dU = TdS - pdV + \sum_i \mu_i dn_i \qquad (2.7)$$

where $S$ is the entropy, $V$ the volume, and $\mu$ the chemical potential. The index $i$ refer to the type of molecules. For a thermodynamic description of bulk properties this equation is adequate but considering surfaces it has to be extended since the boundary of the system is the locus of some excess energy. This excess term is proportional to the change in surface area $A$ and the associated intensive variable is the surface tension $\gamma$ so that Eq. (2.7) becomes:

$$dU = TdS - pdV + \sum_i \mu_i dn_i + \gamma dA \tag{2.8}$$

Probably the surface tension γ, is the most important quantity that characterizes a surface. Thermodynamically, the surface tension of a solid material in contact with vapor ($\gamma_{sv}$) is thus defined as the change in energy ($U$) of the whole system with change in surface area ($A$) at constant entropy ($S$), volume ($V$) and number moles of the component involved ($n$). It can be shown that $\gamma$ is also equal to the change in Gibbs energy ($G$) at constant temperature ($T$), pressure ($p$) and number of moles ($n$), *i.e.*[17]

$$\gamma_{sv} = \left(\frac{dU}{dA}\right)_{S,V,n} = \left(\frac{dG}{dA}\right)_{T,p,n} \tag{2.9}$$

For liquids there are several direct methods, *e.g.* Wilhelmy plate, capillary rise and pendant drop, for direct determination of the surface tension. However, it is impossible to measure directly the surface tension of a solid, such as a polymer. Therefore indirect methods have to be used, as the liquid homologue method, the polymer melt method and contact angle measurements. The last method is perhaps the simplest and most widely used method for the evaluation of surface tension. Various approaches have been developed to calculate surface tensions of solids from contact angle measurements. They all rest on the Young's equation in which the relation is given between the surface tension ($\gamma$) and contact angle ($\theta$) for a (pure) solid in contact with a (pure) liquid.

When a droplet of a wetting liquid makes contact with the solid surface (Figure 2.6) the balance between the forces along the three phase boundaries is defined by the Young's equation:

$$\gamma_{\mathrm{lv}} \cos\theta = \gamma_{\mathrm{sv}} - \gamma_{\mathrm{sl}} \tag{2.10}$$

where $\gamma_{\mathrm{lv}}$, $\gamma_{\mathrm{sv}}$, and $\gamma_{\mathrm{sl}}$ denote the interfacial tension of the liquid-vapor, the solid-vapor and the solid-liquid interfaces, respectively. The terms on the left hand side are readily obtained experimentally leaving $\gamma_{\mathrm{sv}}$ and $\gamma_{\mathrm{sl}}$ as unknowns. As only the value of $\gamma_{\mathrm{sv}}$ - $\gamma_{\mathrm{lv}}$ can

be obtained from contact angle measurements, the value of $\gamma_{sl}$ is needed for the evaluation of $\gamma_{sv}$. Numerous approximate models have been developed to determine the surface tension of solids from contact angle measurements. For instance, the critical surface tension concept of Zisman,[18] the surface tension components approach of Fowkes,[19] and the equation of state approach of Neumann[20]. The last two methods will be discussed in brief. In spite of the extensive studies, a definite theoretical framework has yet not been established and all models are more or less subject to arguments.

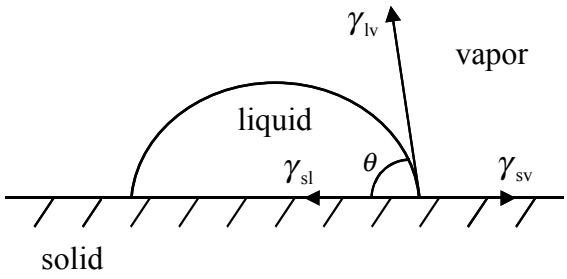


**Figure 2.6** Balance of interfacial tensions between a solid, a liquid and a vapor.

### 2.3.1 Surface Tension Component Approach

Fowkes[21] pioneered the approach of surface tension components. He assumed that the total surface tension ($\gamma$) is composed of different surface tension components, each of which arises from specific intermolecular or inter-atomic forces at the interface. Then the surface tension can be written as:

$$\gamma = \gamma^d + \gamma^p + \gamma^h + \gamma^i + \gamma^m + .. \tag{2.11}$$

where $\gamma^d$, $\gamma^p$, $\gamma^h$, $\gamma^i$, $\gamma^m$ are the contribution due to London dispersive forces, Keesom permanent dipole-dipole forces, hydrogen bonds, the Debye induction forces, and metallic interactions, respectively. For a two phase system in which only dispersive forces are operative ($\gamma = \gamma^d$) across the interface $\gamma_{12}$ can be written (using a geometric mean approach) as:

$$\gamma_{12} = \gamma_1 + \gamma_2 - 2(\gamma_1\gamma_2)^{1/2} = \gamma_1^d + \gamma_2^d - 2(\gamma_1^d\gamma_2^d)^{1/2} \tag{2.12}$$

where subscript 1 and 2 represent phase 1 and 2, respectively. For a solid-liquid interface Eq. (2.12) results in:

$$\gamma_{sl}^{d} = \gamma_{sv}^{d} + \gamma_{lv}^{d} - 2(\gamma_{sv}^{d}\gamma_{lv}^{d})^{1/2} \tag{2.13}$$

Owens, Wendt and Kaelble[22] extended this concept by considering both dispersive and polar forces. By using the geometrical mean approach in combination with the Young's equation they proposed:

$$\gamma_{lv}(1+\cos\theta) = 2(\gamma_{sv}^{d}\gamma_{lv}^{d})^{1/2} + 2(\gamma_{sv}^{p}\gamma_{lv}^{p})^{1/2} \tag{2.14}$$

The surface tension $\gamma_{sv}$ of the solid surface and its components ($\gamma_{sv}^{d}$ and $\gamma_{sv}^{p}$) can be determined according to Eq. (2.14) by using two different liquids with known dispersive ($\gamma_{lv}^{d}$) and polar components ($\gamma_{lv}^{p}$) of their surface tensions.

Wu[19] suggested another empirical approximation in which the 'harmonic-mean' instead of a geometric mean approach was used for the interfacial tension. Substitution in the Young's equation leads to:

$$\gamma_{lv}(1+\cos\theta) = 4\left(\frac{\gamma_{lv}^{d}\gamma_{sv}^{d}}{\gamma_{lv}^{d}+\gamma_{sv}^{d}} + \frac{\gamma_{lv}^{p}\gamma_{sv}^{p}}{\gamma_{lv}^{p}+\gamma_{sv}^{p}}\right) \tag{2.15}$$

Similar to the geometric-mean approach, two relationships are obtained after substituting the contact angles of two wetting liquids into Eq. (2.15), with $\gamma_{sv}^{d}$ and $\gamma_{sv}^{p}$ as unknown parameters. Solution of these equations results in the dispersive and polar contribution of the surface tension of the solid substrate. Although there is no theoretical background for the use of the harmonic-mean approach, Wu claimed that surface tensions of a number of polymers, obtained by the harmonic-mean method, are comparable to those obtained by the polymer melt method. Both Eq. (2.14) and (2.15) have been used extensively to determine the wettability of polymer surfaces.

An analogous approach was used by Van Oss and coworkers.[23] In this method the surface tension of a solid can be divided into two parts:

$$\gamma = \gamma^{LW} + \gamma^{AB} \tag{2.16}$$

where $\gamma^{LW}$ denotes the non-covalent long range Lifshitz-Van der Waals interactions and $\gamma^{AB}$ the short-range Lewis acid-base interactions. The long-range interactions are a summation of:

$$\gamma^{LW} = \gamma^{d} + \gamma^{i} + \gamma^{p} \tag{2.17}$$

Moreover the short-range interactions can be expressed as a function of the geometric mean of the electron-acceptor ($\gamma^{+}$) and the electron-donor ($\gamma^{-}$) parts:

$$\gamma_{sv}^{AB} = 2\sqrt{(\gamma_{sv}^{+}\gamma_{sv}^{-})} \tag{2.18}$$

Taking the geometric mean of the Lifshitz-Van der Waals component and the electron-acceptor and the electron donor part and combining this with Young's equations the following equation can be obtained:

$$\gamma_{lv}(1+\cos\theta) = 2\sqrt{(\gamma_{lv}^{LW}\gamma_{sv}^{LW})} + 2\sqrt{(\gamma_{lv}^{+}\gamma_{sv}^{-})} + 2\sqrt{(\gamma_{lv}^{-}\gamma_{sv}^{+})} \tag{2.19}$$

To determine the three parameters for the solid surface (($\gamma_{sv}^{LW}$, $\gamma_{sv}^{+}$, and $\gamma_{sv}^{-}$), three independent equations are obtained by measuring the contact angles of three liquids (two of which must be polar) with known values of $\gamma_{lv}^{LW}$, $\gamma_{lv}^{+}$, and $\gamma_{lv}^{-}$ on the solid surface.

### 2.3.2 Equation of State Approach

On phenomenological grounds, Neumann *et al.*[20] have proposed an equation of state approach for solid-liquid interfacial tensions interaction:

$$\gamma_{sl} = \gamma_{lv} + \gamma_{sv} - 2\sqrt{\gamma_{lv}\gamma_{sv}}\; e^{-\beta(\gamma_{lv}-\gamma_{sv})^2} \tag{2.20}$$

where $\beta$ is a constant which was found to be 0.0001247 $(m^2/mJ)^2$. The combination of this equation with Young's relation results in an equation of state approach, where the relation between $\cos\theta$ and $\gamma_{lv}$ is given by:

$$1 + \cos\theta = 2\sqrt{\frac{\gamma_{sv}}{\gamma_{lv}}}\, e^{-\beta(\gamma_{lv} - \gamma_{sv})^2} \tag{2.21}$$

When the liquid surface tension $\gamma_{lv}$ is known and the contact angle $\theta$ is measured, $\gamma_{sv}$ can easily be calculated.

Although there are still some controversies between both methods, the surface tension components approach and the equation of state of approach are both used in literature. In our case the Lifshitz-Van der Waals/Acid-Base method is used to determine the surface tensions of solids.

## 2.4 SELF-CONSISTENT FIELD MODEL

Besides the experimental approaches to study the surface as described in Section 2.2. and Section 2.3 we also adapted a complementary theoretical approach, to study the behavior of polymers at surfaces.

A possible route to analyze surfaces and interfaces is by the use of square gradient theories. Gradient theories offer the possibility to predict density profiles at the surface of the polymer melt.[24] A general strategy is to calculate the composition gradients of polymers at the surface, count all interactions, derive the Gibbs free energy of the system and minimize it. But this method is generally unfeasible as the number of conformations is too large. Therefore, approximations and model assumptions have to be made. One method to facilitate the counting of conformations is to make use of a lattice. Here, every polymer segment occupies a lattice site. The use of a lattice means basically only the discretisation of space. One-way of counting the statistically weight of all possible conformations is described in self-consistent field (SCF) calculations. The statistical weight of a conformation is proportional to the potential fields, felt by its segments. The potential field is often called self-consistent because it is computed from the concentration profiles on the one hand and it influences the concentration profiles on the other hand. The solution characterized by the fixed point that the potential fields are *consistent* with the concentration profiles and the other way around, is

called the self-consistent field solution. It is typically found iteratively in a numerical procedure.

The SCF calculations used in this thesis are based on the approach developed by Scheutjens and Fleer.[25,26] This approach is in essence an extension of the conventional Flory-Huggins (zero-mean field) theory including gradients. In this theory, the interfacial behavior of polymer systems is modeled by combining Markov chain statistics with a mean field approximation. This method is described in detail by Fleer *et al*.[27] Here only some basic starting points are discussed. Details can be found in references 25-27. As explained, in the SCF model it is necessary to define a self-consistent potential, which represents the average effect of surrounding molecules. The averaging is expected to be accurate if the fluctuations in the local averaged properties are small. In the potential energy field intermolecular interactions are accounted for by Flory-Huggins parameters. It is expected for a surface, that the densities are more or less constant parallel to the surface and that the important density variations develop perpendicular to the surface. For this reason the properties of the system only depend on the z-direction and therefore the properties of the system are averaged in the x-y plane parallel to the surface. The z-direction is kept as the relevant one, leading to a one-dimensional model.

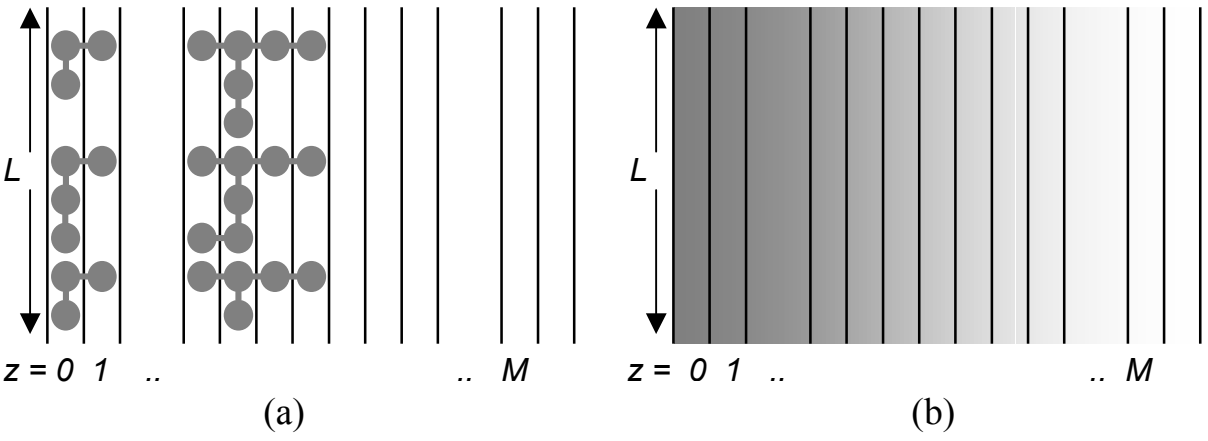


**Figure 2.7** a) A two dimensional representation of the layer model used in the numerical SCF theory. The spheres represent the segments of the polymers. b) The corresponding gray scaling gives the density of polymer in the system, which in this case goes from a high value at low z to a low value at high z.

In Figure 2.7 the lattice layers are depicted with the distribution of molecules in the system depicted by (a) spheres or by (b) gray scaling. These densities vary actually stepwise because a discretisation of space is made. The layers are numbered arbitrarily from unity to a

large value $M$: $z$ = 1,……, $M$. The parameter $M$ should be large enough to ensure that the bulk values are reached.

From a given SCF solution, not only thermodynamic information, *i.e.*, surface tension is readily obtained, it is also possible to evaluate structural information, *i.e.*, density profiles. In Chapter 5 a molecular-level SCF theory is used to analyze physical and thermodynamic properties of partially fluorinated polymer systems.

## 2.5 EXPERIMENTAL CONSIDERATIONS

In this Section some experimental considerations are given with respect to the techniques employed in this thesis for the characterization of the polymer surfaces.

### 2.5.1 XPS

XPS measurements were performed using a non-monochromized VG Mg Ka X-ray beam operated at 20 mA emission at 12.5 kV and a VG Clam II hemispherical analyzer. As fluoropolymers can undergo degradation when irradiated by X-rays,[28] XPS measurement time was limited to 10 min or less. Under these conditions surface damage due to radiation was minimized. All $C_{1s}$ peaks corresponding to hydrocarbons were calibrated at a binding energy of 285.0 eV to correct for the energy shift caused by charging. For peak fitting the program XPSPEAK Version 4.0 of Kwok[29] was used. All peaks were fitted with a 30 % Lorenzian and a 70 % Gaussian peak shape.

### 2.5.2 LEIS

The LEIS measurements were performed with the Calipso set-up,[14] which is an improved version of the ERISS set-up having a base pressure of $2\times10^{-10}$ mbar. All LEIS measurements were carried out using 3 keV $^3He^+$ ions. In this way a high sensitivity to light elements is obtained. The kinetic energy of the ions back-scattered by 145° is analyzed by a double toroidal analyzer and a position-sensitive detector (Figure 2.5). A shower of low-energy electrons during the LEIS measurements prevents charging of non-conducting samples. In order to avoid cross-contamination, only one sample at a time was present in the LEIS UHV analysis chamber. All experiments were carried out under static conditions. This means that the ion and the electron doses were kept sufficiently low to avoid damage of the sample. In order to obtain these static conditions the ion beam was rastered over a sample area of 1.5×1.5 mm. The total ion dose was kept below $3\times10^{13}$ $^3He^+/cm^2$ (typical beam current was

about 0.5 nA, typical measuring time < 200 s, non-destructive 'static' analysis) with good statistics in the spectra. The LEIS spectra were analyzed by the determination of the peak areas after a linear background subtraction with a descending cumulative Gaussian shape.

### 2.5.3 Contact Angles

Advancing contact angles were obtained by means of the sessile drop method, using a Krüss G10 set-up. During the measurement of the advancing contact angles the needle remained inside the drop. The droplet was monitored by a CCD-camera and analyzed by Drop Shape Analysis software (DSA Version 1.0, Krüss). The complete profile of the sessile droplet was fitted by the tangent method to a general conic section equation. The derivative of this equation at the baseline gives the slope at the three-phase contact point and thus the contact angle. In this way angles were determined both at the right and the left side. Reproducibility was within 0.5°.

## 2.6 REFERENCES


[1] Chan, C.-M. *Polymer Surface Modification and Characterization*; Hanser Publisher: Munich, 1994.

[2] Niemantsverdriet, J. W. *Spectroscopy in Catalysis*, VCH Verlagsgesellschaft: Weinheim, 1995.

[3] Graham, R. L.; Bain, C. D.; Biebuyck, H. A.; Laibinis, P. E.; Whitesides, G. M. *J. Phys. Chem.* **1993**, 97, 9456.

[4] Beamson, G.; Briggs, D. *Surf. Interface Anal*. **1998** 26, 343.

[5] Tanuma, S.; Powell, C.J.; Penn, D.R. *Surf. Interface Anal.* **1994**, 21, 165.

[6] Briggs, D. *Surface Analysis of Polymers by XPS and SIMS*, Cambridge University Press: Cambridge, 1998.

[7] Powell, C. J.; Seah, M. P. *J. Vac. Sci. Technol*. **1990**, A8, 735.

[8] Zhuang, H.; Marra, K. G.; Ho, T.; Chapman, T. M.; Gardella, Jr., J. A. *Macromolecules* **1996**, 29, 1660.

[9] Brongersma, H. H.; Mul, P. M. *Chem. Phys. Lett*. **1972**, 14, 380.

[10] Vargo, T. G.; Gardella, Jr., J. A.; Schmitt, R. L.; Hook, K. J.; Hook, T. J.; Salvati, Jr., L. in *Surface Characterization of Advanced Polymers*, 1st edn.; Sabbatini, L., Zambonin, P. G., Eds.; VCH Verlagsgesellschaft: New York, 1993; Chapter 4.

[11] Jacobs, J.-P.; Reijne, S.; Elfrink, R. J. M.; Mikhailov, S. N.; Brongersma, H. H. *J. Vac. Sci. Technol. A* **1994**, 12, 2308.

[12] Van Leerdam, G. C.; Brongersma, H. H. *Surf. Sci*. **1991**, 254, 153.

[13] Brongersma H. H., personal communication.

[14] see *e.g.* the website: www.calipso.nl.

[15] Bertrand, P.; De Puydt, Y. *Nucl. Instrum. Methods. Phys. Res*., *Sect. B* **1997**, 131, 71.

[16] a) Mikhailov, S.N.; Elfrink, R.J.M.; Lacobs, J.-P.; van den Oetelaar, L.C.A.; Scanlon, P.J.; Bongersma, H.H. *Nucl. Instr. Meth.* **1994**, B39, 149. b) Brongersma, H.H.; Carrere-Fontaine, M.; Cortenraad, R.; Denier van der Gon, A.W.; Scanlon, P.J.; Spolveri, I.; Cortigiani, B.; Bardi, U.; Taglauer, E.; Reiter, S.; Labich, S.; Bertrand, P.; Houssiau, L.; Speller, S.; Parascandola, S.; Űnlü-Lachnitt, H.; Heiland, W. *Nucl. Instr. Meth.* **1998**, B142, 377.

[17] Zangwill, A. *Physics at Surfaces* Cambridge University Press: Cambridge, 1988; Chapter 1.

[18] Zisman, W. A. in *Contact Angle, Wettability and Adhesion*, Ed. F. W. Fowkes, ACS Symp. Series, Vol. 43, Washington, DC, 1964.

[19] Wu, S. *Polymer Interface and Adhesion* Marcel Dekker: New York, 1982; Chapter 5.

[20] Kwok, D. Y.; Neumann, A. W. *Adv. Colloid Interface Sci*. **1999**, 81, 167.

[21] Fowkes, F. M. *J. Phys. Chem*. **1962**, 66, 382.

[22] a) Owens, D. K.; Wendt, R. C. *J. Appl. Polym. Sci*. **1969**, 13, 1741. b) Kaelble, D. H. *J. Adhesion* **1970**, 2, 50.

[23] a) Good, R. J.; van Oss, C. J. in *Modern Approaches to Wettabillity*, Schrader, M. E., Loeb, G. I., Eds.; Plenum Press, New York, 1992. b) Van Oss, C. J.; Chaudhury, M. K.; Good, R. J. *Chem. Rev*. **1988**, 88, 927.

[24] Jones, R. A. L.; Richards, R. W. *Polymers at Surfaces and Interfaces*, Cambridge University Press: Cambridge, 1999; Chapter 4.

[25] Scheutjens, J. M. H. M.; Fleer, G. J. *J. Phys. Chem*. **1979**, 83, 1619.

[26] Scheutjens, J. M. H. M.; Fleer, G. J. *J. Phys. Chem*. **1980**, 84, 178.

[27] Fleer, G. J.; Scheutjens, J. M. H. M.; Cohen Stuart, M. A.; Cosgrove, T.; Vincent, B. *Polymers at Interfaces*; Elsevier: London, 1993.

[28] Wheeler, D.R. *J. Vac. Sci. Technol.* **1982**, 20, 226.

[29] Kwok, R. W. M.; http://www.chem.qmw.ac.uk/surfaces/#software.

# Chapter 3

# Quantification of Fluorine in Fluorinated Surfaces


## 3.0 ABSTRACT

*This chapter focuses on the analysis of the chemical composition (fluorine density) of only the outermost atomic layer as studied by low-energy ion scattering (LEIS). After calibration the fluorine signal with a single crystal of LiF (100), absolute quantification of the fluorine concentration at the surface is possible. Such unique information on the chemical composition of the outermost atomic layer may provide a better understanding of the wetting behavior, and of the low surface tension of partially fluorinated materials.*

## 3.1. INTRODUCTION

The surface of materials often plays a central role for their application. Understanding of the physical and chemical properties of surfaces is of paramount importance for the design of novel materials. Fluorinated polymers belong to a class of materials with exceptional properties. These properties originate from the nature of the carbon-fluorine bond and the orientation of the fluorinated tail. Both from a fundamental and commercial point of view it is desirable to gain control over the wetting properties of fluorinated materials. Modern surface analytical methods such as X-ray photoelectron spectroscopy (XPS),[1] time of flight secondary ion mass spectroscopy (TOF-SIMS),[2] atomic force microscopy (AFM),[3] scanning force microscopy (SFM),[4] and near edge X-ray absorption fine structure (NEXAFS)[5] can elucidate many aspects of the chemical composition as well as the structure of fluorinated surfaces. These methods provide useful information on the spatial variation in chemical composition near the surfaces. But none of them can exclusively analyze the outermost atomic layer.

Nevertheless, from the nature of the forces involved, *e.g.* Van der Waals interactions, it is expected that the outermost atomic layer of the surface predominantly determines the wettability. Consequently, the wettability of an organic material is not related to the overall chemical composition, but it rather depends on the chemical nature of the outermost functional groups. Zisman and coworkers[6] observed that the surface free energy decreases depending on the chemical composition of the material in the sequence $–CH_2- > -CH_3 > -CF_2- > -CF_3$. Therefore, knowledge of the interfacial behavior (*e.g.* surface energies) in relation to surface composition will contribute to a better understanding and prediction of adhesion and wetting phenomena. This means that characterization of the chemical composition of the outermost atomic layer is highly relevant. Low energy ion scattering (LEIS) appears to be the only technique that selectively probes the first atomic layer of the surface even when the sample surface is not smooth.[7]

The principles of LEIS for polymers are well documented[8] and summarized in Chapter 2. The technique involves the energy analysis of noble gas ions that are backscattered from the first atomic layer. Such an ion scattering experiment is similar to a 'billiard ball' collision. The information depth of LEIS is limited to one atomic layer because the low-energy inert gas ions have a high neutralization probability in the deeper layers of the surface region. This results in a negligible scattered-ion yield from atoms below the surface. In contrast to *e.g.* static SIMS analyses,[9] there are no matrix effects that distort the interpretation of scattered intensities.

For the quantification of the concentration of a given element, its sensitivity in the LEIS experiments has to be known. Theoretical predictions of the sensitivities, however, are presently not accurate enough to quantify experimental results in an absolute manner. Therefore, when absolute quantification is necessary, reference samples are needed for calibration.

To correlate macroscopic properties like surface tension to atomic composition in the surface, it is necessary to determine the atomic concentration (*e.g.* fluorine) in an absolute way. In this Chapter the absolute fluorine content in the outermost atomic layer is quantified using a single crystal of LiF as a calibration standard. This quantification is verified by analyzing self-assembled monolayers of perfluorinated thiols on gold. Additionally, a molecular interpretation of the surface phenomena of these low surface energy monolayers is given.

## 3.2 EXPERIMENTAL

### 3.2.1 Materials

Single crystals of LiF (100) were purchased from ESCETE Single Crystal Technology B.V. (Enschede, The Netherlands). 1H,1H,2H,2H-perfluorooctanethiol (F6-thiol) and 1H,1H,2H,2H-perfluorodecanethiol (F8-thiol) were purchased from ABCR Germany and used without further purification. Additive-free poly(tetrafluoroethylene) (Teflon) was purchased from Goodfellow and used as received. Methyl methacrylate (MMA, Aldrich, Zwijndrecht, The Netherlands) and 1,1-dihydroperfluoroheptyl methacrylate (F6MA, ACR Technologies B.V. Amsterdam, The Netherlands) were used as received. Deionized water and hexadecane (99+% anhydrous, Aldrich) were used as wetting liquids for the contact angle measurements.

### 3.2.2 Sample Preparation

Gold substrates were prepared by evaporating a gold layer of about 2000 Å thickness on a cleaned silicon wafer covered with a chromate layer of about 100 Å thickness. On placing the gold substrates into a 1 mM thiol solution of absolute ethanol, a monolayer of the perfluorinated thiol spontaneously adsorbed on the gold surface. The gold substrates were immersed in the thiol solution for a period of three hours. Subsequently, the substrates were rinsed thoroughly with absolute ethanol and then spun dry on a spin coater at 5000 rpm for 60 seconds to obtain a surface devoid of any visible film formed during drying.

### 3.2.3 Surface Techniques

The experimental considerations for contact angle measurements and LEIS are described in Section 2.5.

## 3.3 RESULTS AND DISCUSSION

### 3.3.1 LiF (100) Single Crystal

As already mentioned, theoretical predictions for the sensitivity factors are presently not accurate enough for an absolute quantification. Reference samples needed for absolute quantification should have a well-defined elemental density for the required element in the outermost atomic layer. For instance, $B_2O_3$ targets have been used for the quantification of oxygen in the first atomic layer.[10] Here, a LiF (100) single crystal (Figure 3.1) was used as reference sample for the calibration of fluorine.

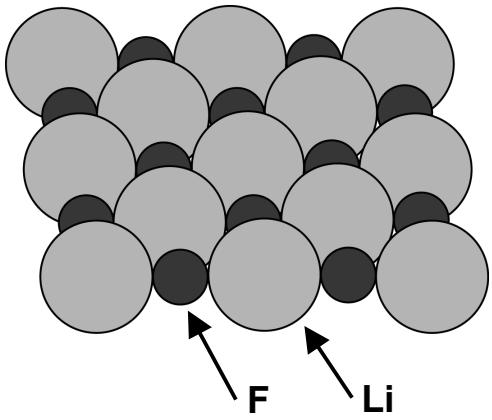


**Figure 3.1** Schematic picture of the top layer of a LiF (100) single crystal.

Figure 3.2 gives the spectrum of the crystal as received as well as the spectra after some cleaning steps. The low signals for the LiF (100) sample as received, indicate a heavy contamination with organic materials. A flux of oxygen reduces the signal for carbon with respect to the baseline due to oxidation of the organics and subsequent evaporation as CO, $CO_2$, and $H_2O$, while a strong fluorine peak becomes visible. The signal for Li is not observed in these spectra as the sensitivity of LEIS for Li is very low and the energy of the ions for backscattering by Li is around 547 eV. Unfortunately, also various inorganic impurities (Na or Mg, K or Ca, Cs or La) are present after the oxidation, and, of course, more oxygen is now present. Sputtering by a high dose of $He^+$ ions partially removes these impurities, but will also

affect the surface structure of the LiF (100). This procedure was, therefore, not believed to produce a reliable surface for calibration of the fluorine.

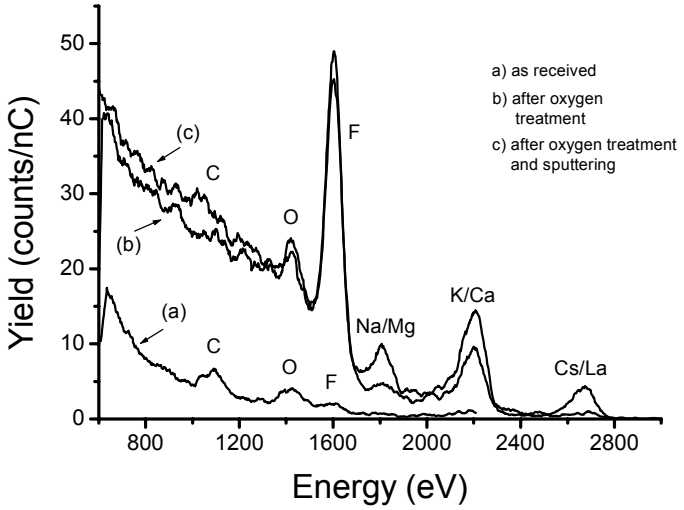


**Figure 3.2** LEIS spectra measured with 3 keV $^3He^+$ ions of (a) a LiF (100) single crystal as received; (b) after oxygen treatment; (c) after oxygen treatment and sputtering with $He^+$ ions.

To avoid contamination problems, while maintaining a well-defined surface, the reference sample was, therefore, cleaved prior to inserting the sample into the setup. Such cleaved surfaces stay atomically clean for prolonged time as known from literature.[11] Following this approach a neat energy spectrum was obtained for LiF showing only fluorine (Figure 3.3). From the crystal structure of LiF (Figure 3.1) it can be derived that the surface density of fluorine in the (100) surface is $1.23*10^{15}$ fluorine atoms/cm$^2$. The LEIS counts (in arbitrary units) can now be converted into a value of fluorine atoms per cm$^2$.

In the following Section, the validity of the LEIS quantification will be evaluated by determining the density of fluorine in the outermost atomic layer of well-defined self-assembled monolayers (SAM) of perfluorinated thiols on gold. Since the electronic structure of the inorganic LiF (100) crystals differs strongly from the organic SAM, this will also be a way to verify the absence of a matrix effect in our LEIS measurements.

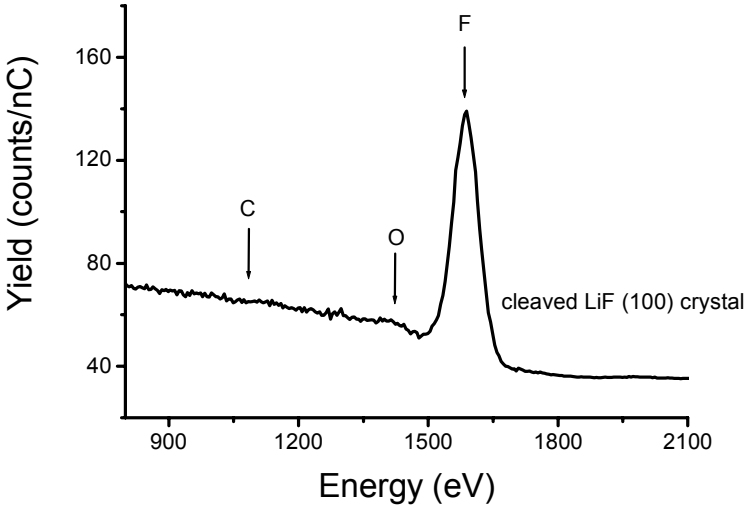


**Figure 3.3** LEIS spectrum measured with 3 keV $^{3}He^{+}$ ions of a freshly cleaved LiF (100) single crystal.

### 3.3.2 Fluorinated Self-Assembled Monolayers

Self-assembled monolayers (SAMs) are ordered molecular assemblies formed by the spontaneous adsorption of molecules on a substrate. The principal driving force for the formation of these films is the interaction between the substrate surface and specific functional groups present in the adsorbed molecules. Besides, a rearrangement of the molecules takes place due to lateral interactions between the adsorbed molecules.

Most investigations have been carried out on SAMs of thiols on Au (111), due to the large variety of functional groups that can be introduced in such monolayers.[12] In the present case monolayers of $F(CF_2)_8CH_2CH_2SH$ (F8-thiol) and $F(CF_2)_6CH_2CH_2SH$ (F6-thiol) on gold substrates were investigated. These monolayers with terminal perfluoro-alkyl chains have been shown by others[3b,c] to be useful models of fluorinated polymer surfaces.

The thiolate monolayers were prepared from 1 mM solutions of the corresponding thiol in ethanol by adsorption at the Au (111) surface plane. To study the wettability of the surfaces, contact angle measurements were carried out with deionized water and hexadecane. The results are given in Table 3.1. It can be seen that the contact angles both for water and hexadecane are slightly lower for the F6-thiol SAM than the F8-thiol SAM. This small difference may be related to the difference in self-organization ability of the thiols.

**Table 3.1** Contact angle results for the SAM of F6- and F8-thiol.

| | Water | | Hexadecane | |
|---|---|---|---|---|
| | $\theta_{adv}$ | $\theta_{rec}$ | $\theta_{adv}$ | $\theta_{rec}$ |
| | | | | |
| F6-thiol | 115.6 | 102.6 | 74.6 | 54.4 |
| F8-thiol | 117.2 | 104.8 | 75.5 | 58.4 |

Figure 3.4 illustrates schematically the packing of the perfluorinated thiols on gold.[3b] The packing and the orientation of the tail group of the thiol are related to the interaction of the sulfur atoms with the Au (111) surface and the characteristics of the tail. Often, the tails are tilted to the surface. The tilt angle is then defined as the angle of the tail with respect to the surface normal.

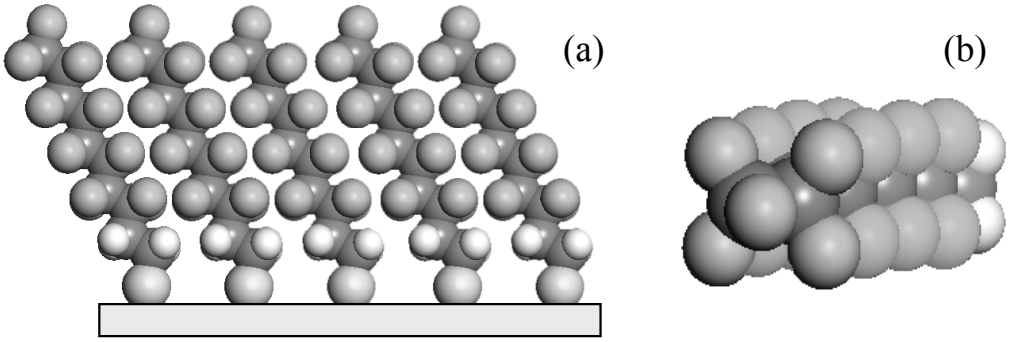


**Figure 3.4** Schematic drawing of an idealized packing of SAM of F8 thiol on Au (111): a) side view and b) top view.

Naud *et al*.[13] studied in detail the tilt angle of perfluorinated thiols on gold by electrochemical capacitance measurements. They found that F8-thiols are able to self-organize, packing with a tilt angle of 22°, whereas the F6-thiols show a tilt angle of 44°. Other authors have reported similar values for the tilt angles.[14]

Figure 3.5 shows the LEIS spectra of the F6 and F8 thiols on gold. In these spectra no sulfur is detected, confirming the orientation of the molecule with sulfur bound quantitatively to the gold. The background in these spectra are due to multiple scattered $He^+$ ions by the underlying gold substrate followed by reionization just before leaving the surface.

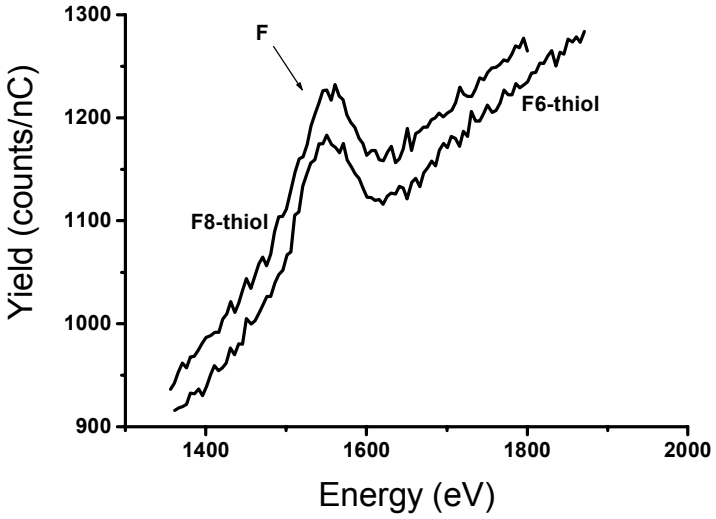


**Figure 3.5** LEIS spectra measured with 3 keV $^3He^+$ ions of SAM of a perfluorinated thiol, $F(CF_2)_nCH_2CH_2SH$ on Au (111) with n=6 and n=8, respectively.

The fluorine densities at the surfaces of thiols were determined by LEIS after background subtraction, using the LiF (100) crystal as calibration. For F8-thiol, F6-thiol, and PTFE the densities are 1.5 * $10^{15}$, 1.4 * $10^{15}$, and 1.2 * $10^{15}$ fluorine atoms/$cm^2$, respectively. These differences in the fluorine density in the surface can be considered as the effect of the tilt angle of the chains (Figure 3.6). An increased tilt angle causes relatively more $CF_2$ groups to be exposed to the surface instead of $CF_3$ groups. This results in a lower fluorine density at the surface. Finally, in the extreme case of PTFE, all $CF_2$ groups lie parallel to the surface, giving rise to the lowest fluorine concentration of all the samples.

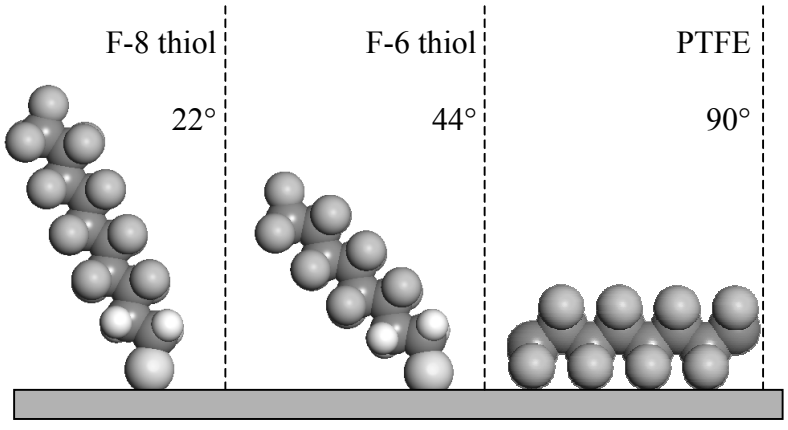


**Figure 3.6** Configuration of F-thiols on gold compared to that of poly(tetrafluoro-ethylene) (PTFE).

The fluorine concentration in the first atomic layer of the F(6,8)-thiol can also be estimated when assuming a closed packed array of $CF_3$ groups in the surface. Taking into account a tetrahedral arrangement around carbon, the covalent radius of fluorine, and the C-F bond length, the calculated molecular area of a $CF_3$ group amounts to 12.8 $Å^2$, corresponding to a fluorine concentration of 2.1 * $10^{15}$ fluorine atoms/$cm^2$. This calculation, however, leads to an overestimation of the fluorine concentration in the outermost atomic layer as the inter-chain spacing between the perfluoroalkyl tail is neglected. For the F8-thiol the inter-chain spacing was determined to be 5.76 Å.[3b,15] Recalculation of the fluorine density based on this value leads to a concentration of 1.0 * $10^{15}$ fluorine atoms/$cm^2$. Barton and others[16] found a molecular area of about 29 $Å^2$/molecule by grazing incident X-ray diffraction of related perfluoroalkyl acid monolayers. The comparative calculation based on this size of molecular area also leads to a surface fluorine concentration of 1.0 * $10^{15}$ fluorine atoms/$cm^2$. In LEIS, however, a higher surface concentration of fluorine of 1.5 * $10^{15}$ fluorine atoms/$cm^2$ was found for the F8-thiol. The LEIS and X-ray results can only be in agreement with each other if LEIS detects more fluorine atoms than solely the -$CF_3$ end-group of the thiol. From space-filling models it follows that an orientation of the thiol in which a plane of four fluorine atoms parallel to the surface is geometrically possible, while it will also be the most energetically favorable configuration (Figure 3.4a). In this conformation two fluorine atoms stem from the terminal –$CF_3$ moiety and the other two fluorine atoms stem from the adjacent –$CF_2$- group while the third fluorine atom of the -$CF_3$ group protrudes out of this plane. The effective fluorine density in LEIS can be estimated using a simple model that includes the shielding by this fluorine atom on top of the plane. In this estimation we assume that the ions are scattered by the nuclei of the fluorine atoms and that the scattered ions are neutralized on their way to the analyzer if they pass through the electron clouds of another atom. From these estimations the two fluorine atoms of the -$CF_2$- are 'visible' for 85%. The shielding of the two fluorine atoms of the -$CF_3$ is somewhat more, since they are closer to the protruded fluorine atom. This results finally in a theoretical fluorine signal of 1.4 ± 0.2 * $10^{15}$ fluorine atoms/$cm^2$, which within the accuracy agrees well with the experimental results. It may thus be concluded that the calibration of the fluorine density in the outermost atomic layer in LEIS using LiF is a reliable procedure.

In the next Chapter a detailed study of the composition of the outermost atomic layer of partially fluorinated polymethacrylates is discussed. These polymers are frequently employed in applications for non-stick coatings and waterproof fabrics. They exhibit low-

energy surfaces due to the orientation of the fluoroalkyl side chains to the air-coating interface.[17-20] The investigations will be directed towards a more detailed understanding of the relationship between the atomic composition in the outermost atomic layer and the wettability of partially fluorinated polymer surfaces.

## 3.4 CONCLUSIONS

The LEIS technique proves to be a very suitable tool to selectively determine the atomic composition of the outermost layer of organic materials. Absolute quantification of fluorine in the outermost layer has been achieved by the use of a freshly cleaved LiF (100) crystal as calibration sample. The reliability of the quantification has been verified by measuring the fluorine concentrations of fluorinated self-assembled monolayers (F6-thiol and F8-thiol). The obtained experimental values compare well to literature data.

## 3.5 REFERERENCES


1 a) Zhang, H.; Gribbin Marra, K.; Ho, T.; Chapman, T.; Gardella Jr., J.A. *Macromolecules* **1996**, 29, 1660. b) Tsibouklis, J.; Stone, M.; Thorpe, A. A.; Graham, P.; Nevell, T. G.; Ewen, R. J. *Langmuir*, **1999**, 15, 7076.

2 Böker, A.; Reihs, K.; Wang, J.; Stadler, R.; Ober, C. K. *Macromolecules* **2000**, 33, 1310.

3 a) Sauer, B. B.; McLean, R. S.; Thomas, R.R. *Langmuir* **1998**, 14, 3045. b) Alves, C. A.; Porter, M. D. *Langmuir*, **1993**, 9, 3507. c) Jaschke, M.; Schönherr, H.; Wolf, H.; Butt, H.-J.; Bamberg, E.; Besocke, M. K.; Ringsdorf, H. *J. Phys. Chem*. **1996**, 100, 2290.

4 a) Sheiko, S.S. *Adv. Polym. Sci*. **1999**, 151, 61. b) Schönherr, H.; Vancso, G. J. *Polymer*, **1998**, 39, 5705. c) Gesquière, A.; Abdel-Mottaleb, M. M.; De Schryver, F. C. *Langmuir* **1999**, 15, 6821.

5 a) Castner, D.G.; Lewis Jr., K.B.; Fischer, D.A.; Ratner, B.D.; Gland, J.L. *Langmuir*, **1993**, 9, 537. b) Genzer, J.; Sivaniah, E.; Kramer, E.J.; Wang, J.; Körner, H.; Xiang, M.; Char, K.; Ober, C.K.; DeKoven, B.M.; Bubeck, R.A.; Chaudhury, M.K.; Sambasivan. S.; Fischer, D.A. *Macromolecules* **2000**, 33, 1882.

6 Zisman, W. A. in *Contact Angle, Wettability and Adhesion*, Fowkes, F. W.; ed., ACS Symp. Series, Vol. 43, Washington, DC, 1964.

[7] Van den Oetelaar, L.C.A.; Nooij, O.W.; Oerlemans, S.; Denier van der Gon, A.W.; Brongersma, H.H.; Lefferts, L.; Roosenband, A.G.; van Veen, J.A.R. *J. Phys. Chem. B* **1998**, 102, 3445.

[8] Vargo, T. G.; Gardella, Jr., J. A.; Schmitt, R. L.; Hook, K. J.; Hook, T. J.; Salvati, Jr., L. in *Surface Characterization of Advanced Polymers*, 1st ed.; Sabbatini, L., Zambonin, P. G., Eds.; VCH Verlagsgesellschaft: New York, 1993; Chapter 4.

[9] Briggs, D. *Surface Analysis of Polymers by XPS and SIMS*, Cambridge University Press: Cambridge, 1998.

[10] Thomas, G. E.; van der Ligt, G. C. J.; Lippits, G. J. M.; van de Hei, G. M. M. *Appl. Surf. Sci*. **1980**, 6, 204.

[11] Winter, H. *Progr. in Surf. Sci*. **2000**, 63, 177.

[12] Ulman, A. *Self-Assembled Monolayers of Thiols*, Academic Press, San Diego, 1998.

[13] Naud, C.; Calas, P.; Commeyras, A. *Langmuir* **2001**, 17, 4851.

[14] Chidsey, C. D.; Loiacono, D. N. *Langmuir* **1990**, 6, 682.

[15] Lui, G.-Y.; Fenter, P.; Chidsey, C. E. D.; Ogletree, D. F.; Eisenberger, P.; Salmeron, M. *J. Chem. Phys*. **1994**, 101, 4301.

[16] Barton, S. W.; Goudot, A.; Bouloussa, O.; Rondelez, F.; Lin, B.; Novak, F.; Acero, A.; Rice, S. A. *J. Chem. Phys*. **1992**, 96, 1343.

[17] Katano, Y.; Tomono, H.; Nakajima, T. *Macromolecules* **1994**, 27, 2342.

[18] Höpken, J.; Möller, M. *Macromolecules* **1992**, 25, 1461.

[19] Kassis, C.M.; Steehler, J. K.; Betts, D. E.; Guan, Z. B.; Romack, T. J.; DeSimone, J. M.; Linton, R. W. *Macromolecules* **1996**, 29, 3247.

[20] Wang, J.; Ober, C. K. *Macromolecules* **1997**, 30, 7560.

[21] Part of this work has been published in: a) Van de Grampel, R. D.; Gildenpfennig, A.; van Gennip, W. J. H; Ming, W.; Laven, J.; Krupers, M.; Thüne, P. C.; Niemantsverdriet, J. W.; Brongersma, H. H.; van der Linde R. *Proc. Fluoropolymers2000 Current frontiers and future trends (ACS)*, ed. D.W. Smith, **2000,** 96. b) Brongersma, H. H.; Gildenpfennig, A.; Denier van der Gon, A. W.; van de Grampel, R. D.; Jansen, W. P. A.; Knoester, A.; Laven, J.; Viitanen, M. M. *accepted in Nucl. Inst. Meth. Phys. Res. Sec. B.*

# Chapter 4

# Fluorinated Polymethacrylates


## 4.0 ABSTRACT

*The surface properties of films of partially fluorinated polymethacrylates were studied as a function of the molar fraction of the fluorinated monomers. Using the acid-base approach the surface tensions of these copolymers were estimated. The introduction of perfluoroalkyl side chain lowers the polymer surface energy significantly. Both angle-dependent X-ray photoelectron spectroscopy (XPS) and low energy ion scattering (LEIS) confirm a higher fluorine concentration in the surface region as compared to the bulk. Angle-dependent XPS measurements revealed that the surface enrichment in fluorine extends over several nanometers in depth. LEIS results point to a linear correlation between the surface energy of thin polymer films and the amount of fluorine atoms in the outermost atomic layer of these films. Evidently, the atoms in the outermost layer primarily determine the surface tension. Ordering phenomena probably causes deviations from this linear behavior at very small and very large fluorine concentrations*.

## 4.1 INTRODUCTION

The understanding of surface properties like wetting, adhesion and friction is of paramount importance for the design of high performance materials for application such as adhesives, biomaterials, and coatings.

Recently, fluorinated surfaces of polymers have attracted much interest because of their advantageous properties, such as low wettability, low adhesion, and low coefficient of friction. In general, non-stick materials are characterized by a low surface tension providing low wettability. It has been observed that the presence of even small quantities of fluorinated material at the surface of conventional materials lowers the surface energy significantly. The surface energy can be even more reduced when the fluorine-containing molecules attain a certain order within the surface layer. For instance, a close-packed, uniformly organized array of trifluoromethyl ($-CF_3$) groups creates a surface with the lowest surface energy ever measured of 6 mN/m.[1]

A wide variety of techniques is nowadays available to study the molecular structures of surfaces. These techniques have been successfully applied to fluorinated surfaces. X-ray photoelectron spectroscopy (XPS) is the most frequently used technique and provides quantitative information on the surface composition. Angle-dependent XPS measurements have revealed surface enrichment of fluorine at the air-polymer interface in many cases.[2-6] The combination of XPS and Secondary Ion Mass Spectroscopy (SIMS) opens the possibility to elucidate the composition of functional groups within the upper 2-10 nm of a polymer layer.[6,7] The application of depth-profiling SIMS has identified gradient[8] and lamellar structures[5] of the fluorinated species perpendicular to the polymer surface. Genzer *et al.*[9,10] performed Near-Edge X-ray Absorption Fine Structure (NEXAFS) measurements to study the molecular orientation of semifluorinated 'fingers' attached to a styrene-isoprene block-copolymer at the surface. An average tilt angle with respect to the surface normal in the range of 29° to 46° was found, depending on the length of the hydrogen-carbon spacer between the perfluoroalkyl side chains and the total length of the side-chain.

The correlation between surface tension and molecular structure of organic systems is a long-standing problem in surface science.[11] Already in 1916 Langmuir[12] anticipated that properties of the surface are in principle determined by the composition and packing of the atoms or groups of atoms in the first atomic layer. Zisman *et al.*[13] reported that the surface tension of hydrocarbon and fluorocarbon materials decreases in the order $-CH_2- > -CH_3 > -CF_2- > -CF_3$. More recently, Mach *et al.*[11c] observed a dramatic change in the surface tension

by a single atom replacement within a sub-molecular surface. Therefore, the understanding of the chemical structure and the surface conformation/composition on molecular scale helps to predict the physical properties of the surface.

This work will focus on the relation between *chemical composition* of fluorinated surfaces and the *surface tension* of these surfaces. When the interactions are short-range, it is expected that the outermost atomic layer of the surface predominately determines the wettability. Therefore, to study the chemical composition of particularly this layer is of great significance. Low energy ion scattering (LEIS) appears to be the only technique that selectively probes the first atomic layer.[14]

The principles of LEIS on polymers are well documented in literature and have been discussed in Chapter 2 of this thesis. Most of the surface characterization studies involving LEIS have been carried out in the field of metals and semiconductors.[15] The application of LEIS towards insulating samples like organic polymer surfaces is limited and requires detection of functional groups of the polymer chain.[16-18] Gardella and Hook[16] showed, for example, that LEIS can distinguish between conformations of stereoregular poly(methyl methacrylate) and random copolymers of methacrylic acid and methyl methacrylate. From these LEIS results, conclusions could be drawn about the polymer chain orientation in the surface. Such information could not have been resolved by XPS or Secondary Ion Mass Spectroscopy (SIMS). Using LEIS it is also possible to follow changes in the surface composition due to segregation, ageing, etc. In this respect Maas *et al*.[18] presented a study of surface modification processes like ageing of polymer surfaces. By combination of LEIS and XPS measurements it was found that ageing is mainly confined to the outermost atomic layer. More recently Ponjée *et al*.[19] used LEIS to study the intermolecular segregation of siloxanes in conjugated polymers. The molecular orientation of these segregated siloxanes on the conjugated polymers resembled that of pure polydimethylsiloxane.

In this Chapter a surface study on partially fluorinated polymethacrylates is presented. Following the approach of Good, van Oss, and Chaudhury,[20] the acid-base characteristics of films of partially fluorinated methacrylates were estimated first. Additionally, the partially fluorinated polymethacrylates were investigated by XPS and LEIS experiments. It will be shown, that the information obtained by LEIS is complementary to the results obtained by XPS and contact angle measurements. Although the relationship between the surface energy (macroscopic structure) and the related properties (wetting, adhesion, etc.) has already been established, there still remains a problem regarding how to correlate the surface energy with

the microscopic and even nanoscopic structure of the surface. A tentative model will be presented to correlate the surface tension with the surface density of fluorine in the outermost atomic layer of partially fluorinated polymethacrylates.

## 4.2 EXPERIMENTAL

### 4.2.1 Materials

Methyl methacrylate (MMA, Aldrich), 2,2,2-trifluoroethyl methacrylate (F1MA, Aldrich) 1,1-dihydroperfluoroheptyl methacrylate (F6MA, ACR Technologies B.V. Amsterdam), and butyl acetate (BuOAc, Aldrich) were used as received. 1H,1H-perfluoroundecane-1-ol (96%, Fluorochem) was sublimed prior to use. Methacrylic anhydride (94%, Aldrich), triethylamine (TEA, 99.5%, Aldrich) and 4-dimethylaminopyridine (DMAP, 99+%, Aldrich) were used as received. Azobisisobutyronitrile (AIBN, Merck) was recrystallized from methanol and stored at in the refrigerator prior to use. All solvents (analytical grade) were used as received.

### 4.2.2 Characterization Techniques

NMR spectra were recorded on a Varian 400 spectrometer at 25 ºC. Operating frequencies were 400.16 MHz for $^{1}H$, 100.63 MHz for $^{13}C$, and 376.49 MHz for $^{19}F$. TMS ($^{1}H$ and $^{13}C$) was used as internal standard and $CFCl_3$ ($^{19}F$) was used as an external reference. Elemental analyses (C, H and F) of the copolymers were carried out at the Microanalytical Department of the University of Groningen. Molecular weights were obtained by means of GPC using four PLGel (Mixed-C) columns (Polymer Laboratories) at 40 °C. The injection volume was 100 µL and THF was used as eluent at a flow rate of 1 mL/min. A Waters 486 UV-detector was applied for detection. Narrow polydispersity polystyrene standards with molecular weights ranging from 580 to 7.1 * $10^6$ g/mol were used to calibrate the GPC set-up. Glass transition temperatures were measured with a Perkin-Elmer Pyris 1 DSC equipment using a scan rate of 10 K/min with sample masses of 5-10 mg. Transition temperatures were taken from the second heating cycle.

### 4.2.3 Monomer and Polymer Synthesis

*Synthesis of 1H,1H-perfluorodecyl methacrylate*

A 250 ml three-neck round bottom flask was charged with 20.2 g (36.7 mmol) of 1H,1H-perfluoroundecane-1-ol and 0.5 g (4.2 mmol) of DMAP, and equipped with a magnetic stirrer, reflux condenser, additional funnel and a septum. With a syringe 100 mL freshly distilled dichloromethane and 22 ml of 1,1,2-trichlorotrifluoroethane was added. After the perfluoroalcohol and the DMAP were dissolved, the solution was cooled with ice. Slowly, 5.3 ml (34.2 mmol) of methacrylic anhydride was added to the cooled solution, followed by the addition of 4.7 ml (38.5 mmol) of TEA. The solution was stirred for 18 h at 30 ºC and subsequently washed with deionized water, diluted hydrochloric acid, saturated sodium bicarbonate solution, and deionized water. After drying the organic phase with anhydrous $MgSO_4$ the solvent was removed, resulting in a yellow liquid. The monomer was further purified by passing it over a short column of neutral aluminiumoxide with dichloromethane as eluent. The solvent was removed under reduced pressure resulting in a white waxy compound which was stored under nitrogen at 4 °C prior to use. Yield: 3 g (45 %); purity > 99.5 % (GC/MS): m/z= 618. $^{1}$H-NMR ($CDCl_3$) δ 2.0 (s, 3H, -$CH_3$), 4.7 (t, 2H, -O-$CH_2$-), 5.7 (s, 1H), 6.2 (s, 1H). $^{13}$C-NMR ($CDCl_3$) δ 18.1 (s, -$\underline{C}H_3$), 60.0 (t, -$\underline{C}H_2$-$CF_2$-), 100-125 (fluorinated carbon region), 127.8 (s, -C=$\underline{C}H_2$-), 134.8 (s, -$\underline{C}$=$CH_2$-), 165.6 (s, -$\underline{C}$=O). $^{19}$F-NMR ($CDCl_3$) δ -126.6 (m, 2F, -$C\underline{F}_2$-$CF_3$), -123.7 (m, 2F, -$C\underline{F}_2$-$CF_2$-$CF_3$), -123.1 (m, 2F, -$C\underline{F}_2$-$CF_2$-$CF_2$-$CF_3$), -122.3 (m, 10F, -$CF_2$-$C\underline{F}_2$-$CF_2$-), 119.8 (m, 2F, -$C\underline{F}_2$-$CH_2$-), -81.2 (m, 3F, -$CF_3$).

Polymerizations and copolymerizations were carried out under ‘starved’ conditions as described Van de Grampel *et. al*.[21]

### 4.2.4 Film Preparation

Thin films of the methacrylic polymers were spin-coated on Si-wafers using solutions of the polymers with concentrations of 100 mg in 1 g of toluene, 1,1,2-trichlorotrifluoroethane, or 1,1,1,3,3,3-hexafluoropropan-2-ol depending on the fluorine concentration. The solutions obtained were filtered through a 0.2 µm Teflon filter prior to spin coating (5000 rpm for 60 s). After spin coating the polymer films were annealed for 2 hours at 125 °C in an oven. By this procedure the silicon wafer was completely covered with the methacrylic polymers resulting in a film free of cracks with a layer thickness of 150-200 nm as determined by Atomic Force Microscopy.

### 4.2.5 Surface Techniques

The experimental considerations for contact angle measurements and LEIS are described in Section 2.5.

### 4.2.6 Surface Tension Calculations

Surface tensions of the polymer films were evaluated using the surface tension component approach (Chapter 2) following the three-liquid Lifshitz-Van der Waals acid- base (LWAB) method,[22] using advancing angles for the calculation.[23] The surface energies of the liquids ($\gamma_{lv}$) used, as well as their Lewis acid components ($\gamma_{lv}^{+}$) and Lewis-base components ($\gamma_{lv}^{-}$) are listed in Table 4.1.

**Table 4.1** Surface tension components for the test liquids used.

| Wetting Liquid | $\gamma_{lv}^{LW}$ (mN/m) | $\gamma_{lv}^{+}$ (mN/m) | $\gamma_{lv}^{-}$ (mN/m) | $\gamma_{lv}^{AB}$ (mN/m) | $\gamma_{lv}$ (mN/m) |
|---|---|---|---|---|---|
| deionized water | 21.8 | 25.5 | 25.5 | 51.0 | 72.8 |
| diiodomethane | 50.8 | 0 | 0 | 0 | 50.8 |
| 1,2-ethylenediol | 29.0 | 1.9 | 47.0 | 19.0 | 48.0 |

## 4.3 SYHTHESIS OF FLUORINATED POLYMETHACRYLATES

### 4.3.1 1H,1H-perfluorodecyl methacrylate (F10MA)

The 1H,1H-perfluorodecyl methacrylate (F10MA) was synthesized using the perfluoroalcohol and methacrylic anhydride as starting materials (Scheme 4.1).[24] The waxy product (mp at 30 ºC) was obtained in good yield and high purity. In the beginning it was also tried to obtain F10MA by using methacrylic chloride in the presence of pyridine at 40 °C. These experiments resulted, however, in the formation of methacrylic anhydride and the overall yield dropped significantly.

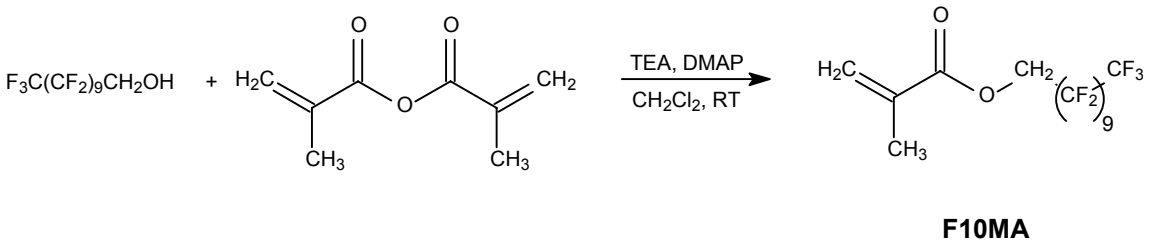


**F10MA**

**Scheme 4.1**

The $^{1}$H-NMR spectrum of purified F10MA, shown in Figure 4.1, corresponds perfectly with the chemical structure. $^{13}$C and $^{19}$F NMR spectra (see Experimental) were also in good agreement with each other. From GC/MS it could be concluded that the final product has a purity of > 99.5 %. The synthesized F10MA, together with the F1MA and the F6MA monomers, were used in free radical homopolymerization and copolymerizations with MMA.

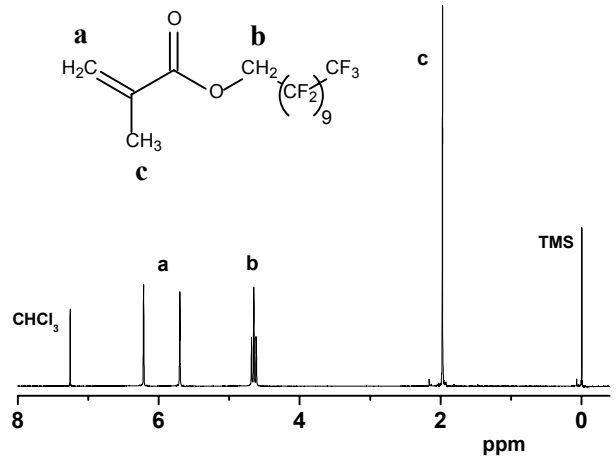


**Figure 4.1** $^{1}$H-NMR ($CDCl_3$) spectrum of F10MA.

### 4.3.2 Partially Fluorinated Polymethacrylates

Homopolymers of MMA, F1MA and F6MA as well as random copolymers of the perfluorinated methacrylates (F1MA, F6MA, and F10MA, see Figure 4.2) with MMA were synthesized by free radical polymerization at 80 °C under nitrogen. As reported in the literature,[21] the copolymerization parameters point to almost 'ideally random' copolymers. Moreover, polymerizations were quenched with methanol after the complete addition of the two monomers in order to minimize any composition drift. This implies a low conversion not exceeding the value of 10%. Note that no precipitation of the polymers in the reaction mixture was observed. Table 4.2 lists the polymer characteristics of the prepared samples. The following notation will be used for the different copolymers. PMMA, PF1MA, PF6MA, and PF10MA are the homopolymers of MMA, F1MA, F6MA, and F10MA, respectively. P(MMA-*co*-F1MA)-50/50 represents a random copolymer of 50 mol% MMA and 50 mol% of F1MA in the monomer feed. Thus P(MMA-*co*-F10MA)-95/5 is a monomer feed with a composition of 95 mol% of MMA and 5 mol% of F10MA. The polymer compositions of the P(MMA-*co*-F6MA) copolymers were determined both by $^{1}$H-NMR and by elemental analyses. The data obtained by both methods are in good agreement. Therefore, for the

determination of the polymer composition for P(MMA-*co*-F1MA) and P(MMA–*co*-F10MA) only $^{1}$H-NMR was used.

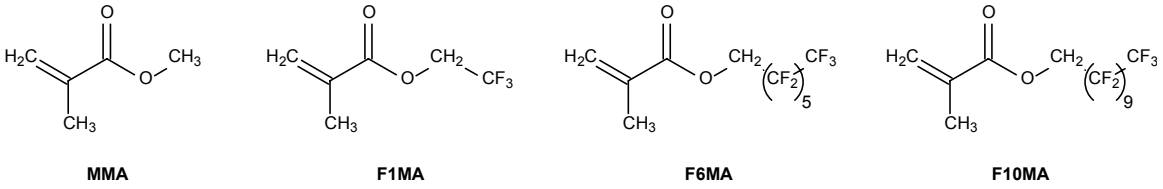


**Figure 4.2** Structures of the methacrylate monomers used in this study.

It is evident that the solubility of the copolymers strongly depends on the composition of the chain and the length of the perfluorinated side-chains. For the polymers soluble in THF, the molecular weight was analyzed by GPC. It has been established[25] that the surface energy of homopolymers depends on its molecular weight according to the relation:

$$\gamma = \gamma_{\infty} - \frac{C_1}{M_n^x} \tag{4.1}$$

where $M_n$ is the number average molecular weight, $\gamma$ is the surface energy of the polymer, $\gamma_{\infty}$ is the surface energy in the limit of very high molecular mass, and $C_1$ is a constant. The exponent $x$ varies from ⅔ for low-molecular weight to 1 for high-molecular weight polymers. In our case all polymers were prepared using similar synthetic procedures in order to ensure the molecular weights of the copolymers to be around 18,000 (Table 4.2). Hence, the surface tension dependence on molecular weight would be minimized. Consequently, differences in surface energies are primarily determined by differences in surface characteristics. The relatively low polydispersity was obtained by precipitating the polymers twice in methanol.

Thermal properties of the polymers synthesized were studied by thermogravimetric analysis and differential scanning calorimetry. It can be seen that the glass transition temperature decreases with increasing content of the perfluorinated monomer, as a result of the plasticizing effect of the perfluoroalkyl side chain (see Table 4.2). It is interesting to note that P(MMA-*co*-F10MA)-75/25 exhibited two endothermic transitions. Next to a glass-transition at 57.1 ºC, a melting transition with an onset temperature of 107.5 ºC was observed. The melting can be explained by side-chain crystallization of the perfluorundecyl side chain

moiety of the F10MA monomer.[26] Decomposition temperatures of the copolymers were found to be around 230 ºC for all polymers.

**Table 4.2** Polymer characteristics of partially fluorinated polymethacrylates.

| Sample ID | molar fraction $F_XMA$[a] (%) | molar fraction $F_XMA$[b] (%) | $T_g$[c] (˚C) | $M_n$ (kg.mol$^{-1}$) | $M_w$ (kg.mol$^{-1}$) | $\frac{M_w}{M_n}$ |
|---|---|---|---|---|---|---|
| PMMA | 0 | 0 | 117.3 | 14.0 | 21.9 | 1.6 |
| | | | | | | |
| P(MMA-*co*-F1MA)-98/2 | 2.6 | - | 113.8 | 18.8 | 24.0 | 1.3 |
| P(MMA-*co*-F1MA)-95/5 | 6.3 | - | 110.9 | 17.2 | 22.3 | 1.3 |
| P(MMA-*co*-F1MA)-90/10 | 12.5 | - | 107.2 | 20.6 | 26.5 | 1.3 |
| P(MMA-*co*-F1MA)-75/25 | 28.9 | - | 100.1 | 20.7 | 26.8 | 1.3 |
| P(MMA-*co*-F1MA)-50/50 | - | - | 90.8 | -[d] | -[d] | -[d] |
| PF1MA | - | - | 74.8 | -[d] | -[d] | -[d] |
| | | | | | | |
| P(MMA-*co*-F6MA)-98/2 | 2.3 | 2.4 | 92.4 | 16.3 | 21.0 | 1.3 |
| P(MMA-*co*-F6MA)-95/5 | 6.4 | 6.7 | 86.6 | 16.6 | 21.9 | 1.3 |
| P(MMA-*co*-F6MA)-90/10 | 14.8 | 14.7 | 81.5 | 15.0 | 21.5 | 1.4 |
| P(MMA-*co*-F6MA)-75/25 | 32.3 | 31.7 | 67.6 | 16.2 | 21.6 | 1.3 |
| PF6MA | - | 100 | 41.9 | -[d] | -[d] | -[d] |
| | | | | | | |
| P(MMA-*co*-F10MA)-99/1 | 1.7 | - | 109.5 | 20.4 | 25.7 | 1.3 |
| P(MMA-*co*-F10MA)-98/2 | 3.0 | - | 108.1 | 16.8 | 21.0 | 1.3 |
| P(MMA-*co*-F10MA)-95/5 | 8.0 | - | 100.4 | 17.9 | 23.2 | 1.3 |
| P(MMA-*co*-F10MA)-90/10 | 14.4 | - | 89.6 | 19.2 | 25.5 | 1.3 |
| P(MMA-*co*-F10MA)-75/25 | - | - | 57.1[e] | -[d] | -[d] | -[d] |

[a] calculated from proton NMR, X = 1, 6 or 10

[b] calculated from elemental analyses

[c] taken at half $C_p$

[d] could not be determined

[e] besides a $T_g$, a melting point transition was found at 107.5 ºC

## 4.4 SURFACE TENSION OF FLUORINATED POLYMETHACRYLATES

To investigate the effect of the incorporated perfluorinated methacrylate monomers on the surface properties of the copolymers, contact angle measurements were performed with deionized water, diiodomethane, and 1,2-ethylenediol as wetting agents. The results are summarized in Table 4.3.

**Table 4.3** Wetting behavior and surface tensions of partially fluorinated polymethacrylates.

| Sample ID | Contact Angle (°) | | | Surface Tension (mN/m) | | | | |
|---|---|---|---|---|---|---|---|---|
| | $H_2O$ | $CH_2I_2$ | EG | $\gamma_{sv}^{LW}$ | $\gamma_{sv}^{+}$ | $\gamma_{sv}^{-}$ | $\gamma_{sv}^{AB}$ | $\gamma_{sv}$ |
| PMMA | 84 | 36 | 52 | 41.5 | 0.0 | 2.9 | 0.6 | 42.1 |
| | | | | | | | | |
| P(MMA-*co*-F1MA)-98/2 | 79 | 41 | 56 | 39.3 | 0.0 | 7.8 | 0.4 | 39.7 |
| P(MMA-*co*-F1MA)-95/5 | 82 | 51 | 59 | 33.9 | 0.0 | 6.7 | 1.0 | 34.9 |
| P(MMA-*co*-F1MA)-90/10 | 84 | 58 | 62 | 29.9 | 0.1 | 6.6 | 1.8 | 31.7 |
| P(MMA-*co*-F1MA)-75/25 | 90 | 64 | 65 | 26.3 | 0.3 | 3.5 | 2.2 | 28.5 |
| P(MMA-*co*-F1MA)-50/50 | 95 | 71 | 68 | 22.6 | 0.6 | 2.1 | 2.2 | 24.8 |
| PF1MA | 100 | 78 | 72 | 18.7 | 0.9 | 1.2 | 2.0 | 20.7 |
| | | | | | | | | |
| P(MMA-*co*-F6MA)-99/1 | 90 | 56 | 62 | 30.8 | 0.2 | 2.7 | 1.4 | 32.4 |
| P(MMA-*co*-F6MA)-98/2 | 95 | 63 | 70 | 26.7 | 0.1 | 2.4 | 1.0 | 27.7 |
| P(MMA-*co*-F6MA)-95/5 | 101 | 77 | 81 | 19.1 | 0.1 | 2.1 | 0.9 | 20.0 |
| P(MMA-*co*-F6MA)-90/10 | 108 | 84 | 86 | 15.4 | 0.3 | 0.5 | 0.9 | 15.3 |
| P(MMA-*co*-F6MA)-75/25 | 113 | 89 | 91 | 13.1 | 0.3 | 0.2 | 0.5 | 13.6 |
| PF6MA | 121 | 97 | 97 | 9.7 | 0.4 | 0.0 | 0.1 | 9.8 |
| | | | | | | | | |
| P(MMA-*co*-F10MA)-99/1 | 97 | 72 | 75 | 21.7 | 0.2 | 2.7 | 1.3 | 23.0 |
| P(MMA-*co*-F10MA)-98/2 | 107 | 82 | 85 | 16.7 | 0.2 | 1.0 | 0.8 | 17.4 |
| P(MMA-*co*-F10MA)-95/5 | 113 | 92 | 92 | 12.0 | 0.3 | 0.5 | 0.7 | 12.7 |
| P(MMA-*co*-F10MA)-90/10 | 117 | 94 | 94 | 11.0 | 0.4 | 0.1 | 0.4 | 11.4 |
| P(MMA-*co*-F10MA)-75/25 | 121 | 98 | 101 | 9.5 | 0.2 | 0.1 | 0.2 | 9.7 |

The advancing contact angles ($\theta$) were used to calculate the surface energies of the copolymers, applying the three-liquid Lifshitz-Van der Waals acid base (LWAB) method[22] (Table 4.3). The data in Table 4.3 clearly show that the perfluoroalkyl side chains lower the polymer surface energy significantly. It can be seen that the contribution of the Lewis acid ($\gamma_{sv}^{+}$) component to the total surface tension of the copolymers is negligible in all cases. Thus $\gamma^{AB}$ is primarily determined by $\gamma_{sv}^{-}$.

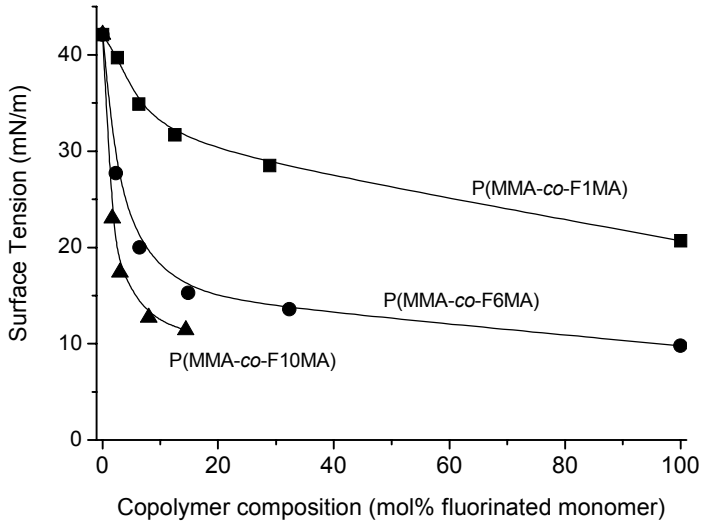


**Figure 4.3** Surface tensions (mN/m) of P(MMA-*co*-F1MA) (■), P(MMA-*co*-F6MA) (●), and P(MMA-*co*-F10MA) (▲) as a function of the molar fraction of the fluorinated monomer.

In Figure 4.3 the influence of the perfluoroalkyl side-chain on the surface tension is depicted. The trend towards lower surface tension with increasing chain length of the perfluoroalkyl side chain is clearly visible. Note that for an incorporation of only 6 mol% of F6MA monomer the surface tension is already comparable to that of poly(tetrafluoroethylene) (20.1 mN/m). A reduction of the surface energy to 9.8 mN/m was reached for the F6MA homopolymer, a value that approaches the value of 6 mN/m for a close-packed array of -$CF_3$ groups in the surface.[1] The sharp decrease in surface energy of the copolymers points to the enrichment of the perfluoroalkyl side chains in the polymer-air interface. Similar trends have been observed for copolymers using styrene and fluoroalkyl modified styrene.[27] However, the results found in the present study are much more pronounced.

Differences in surface energies of the components within a polymer or in polymer blend systems have a large influence on the surface composition, in such a way that the lower surface energy segments reside at the polymer–air interface. Jones and Kramer[28] showed that

the magnitude of the surface excess is determined by the surface energies and the interaction parameters of the constituent segments.

## 4.5 SURFACE COMPOSITION

### 4.5.1 X-Ray Photoelectron Spectroscopy (XPS)

To prove the preferential adsorption of the perfluoroalkyl moieties at the surface and to gain a better understanding of the microscopic surface composition, a detailed study of the surfaces of these films was carried out via angle-dependent XPS. In the spectral analysis, we focused on signals from the 1s-orbital of carbon ($C_{1s}$), as discussed in Chapter 2 of this thesis. Spectra were obtained at two different angles: 0° (XPS-0) and 60° (XPS-60) with respect to the surface normal. The information depth corresponding to these angles are 7.3 and 3.8 nm, respectively (see Eq. 2.2).

XPS-60 $C_{1s}$ spectra for a series of P(MMA-*co*-F6MA) copolymers with varying bulk compositions are shown in Figures 4.4. The $C_{1s}$ spectral region shows a pattern of peaks over a range of approximately 15 eV. The two peaks at 291.4 ± 0.1 eV ($CF_2$ group) and 293.6 ± 0.1 eV ($CF_3$ group) are due to the F6MA monomer; their intensities increase with increasing content of F6MA.

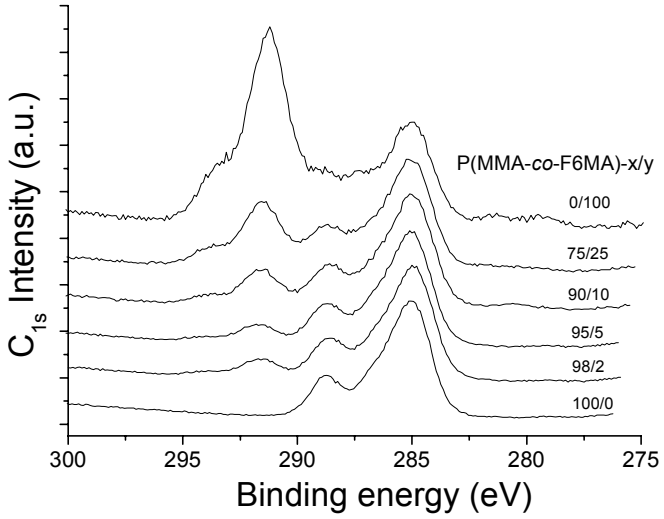


**Figure 4.4** XPS window spectra of the $C_{1S}$ region of the P(MMA-*co*-F6MA) copolymers as measured at an angle of 60º relative to the surface normal. Charge correction and normalization were based on the aliphatic carbon at 285.0 eV.

To obtain quantitative data, all $C_{1s}$ spectra were fitted with the 5 peaks belonging to the aliphatic part (1), -$\underline{C}H_2O$ (2), -$\underline{C}OO$ (3), -$\underline{C}F_2$- (4) and -$\underline{C}F_3$ (5) as shown in Figure 4.5 for the PF6MA homopolymer as an example. The areas of all peaks were quantified using a

Gaussian Lorentzian fitting procedure. These areas are interpreted as relative concentrations of the atoms involved. Peaks 1 to 3 originate from the aliphatic part in the copolymer, and could hence be fitted as one group given that the areas of these peaks have an internal ratio of 3:1:1, according to the stoichiometry of the backbone. The F6MA monomer contains a fluorinated side chain, which means that peak 4 and 5 can be fitted as one group with an internal ratio of 5:1. In this way the ratio between, for example, the -COO and -$CF_3$ peak is a direct measure for the concentration of fluorinated side-chains in the near-surface region of the copolymer. Note that the quantification of the data gave no indication for chain branching of the perfluoroalkyl side chain, contrary to what was observed by Kassis *et al*.[2] This was also confirmed by $^{19}$F-NMR.

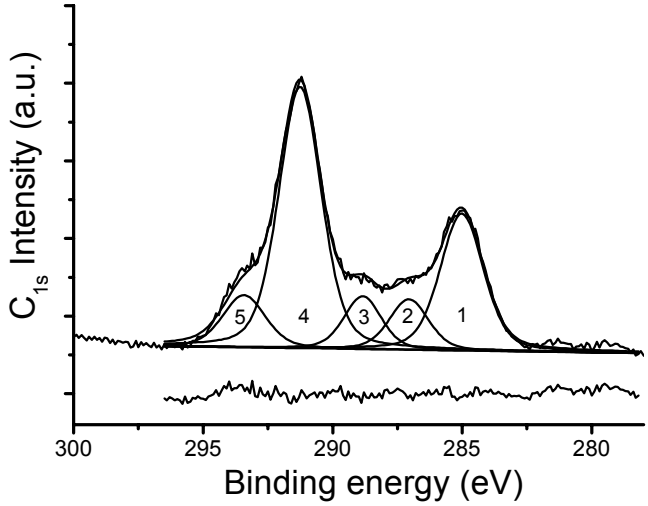


**Figure 4.5** XPS spectrum of the $C_{1s}$ region of the homopolymer of F6MA showing the carbon atoms at different environments. The peaks were assigned to the aliphatic part (**1**), -$CH_2O$ (**2**), -COO (**3**), -$CF_2$- (**4**) and -$CF_3$ (**5**).

The quantitative results in Figure 4.6 indicate that the experimentally determined amount of fluorine over a sampling depth of 7.3 nm almost equals the amount of fluorine calculated for the bulk within the experimental error of XPS. The lower values obtained by XPS-0 compared to the theoretical bulk is probably due to small degradation of the surface due to the electron flow. An enrichment of the fluorine content is observed when going from 7.3 nm to 3.8 nm depth, indicating that the near-surface region of the copolymer is enriched in fluorinated side chains. The perfluoroalkyl chain induces a lower surface tension and therefore tends to migrate to the surface (intra-molecular segregation).

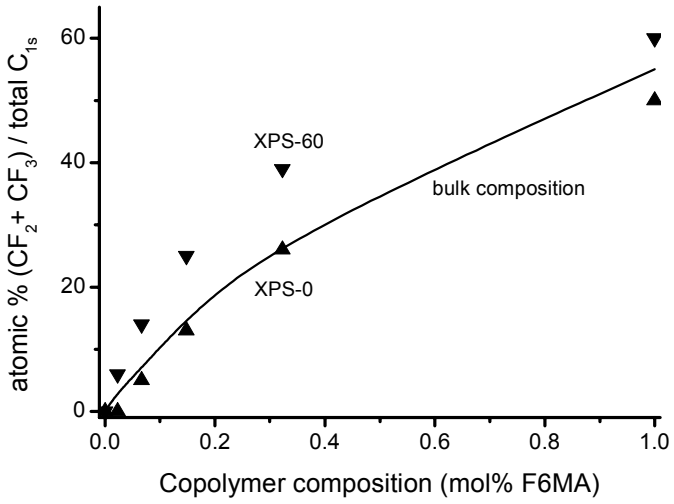


**Figure 4.6** Atomic% ($CF_2$ + $CF_3$)/total $C_{1s}$ as a function of F6MA content in the P(MMA-*co*-F6MA) copolymer as found by XPS. Angle relative to the surface normal of 60º (▼) and 0º (▲); (—) represents the composition of the bulk.

### 4.5.2 Low Energy Ion Scattering (LEIS)

As mentioned previously it can be expected from short-range interactions that the outermost atomic layer in the surface predominantly determines the wettability. To study the outermost atomic layer is ambitious indeed. High-resolution XPS measurements have penetration depths of around 2-10 nm. Low-energy ion scattering measurements (see Chapter 2) were employed to study the composition in exclusively the outermost atomic layer.

The technique is based on the measurement of the energy losses of noble gas ions scattered by atoms in the surface. Since the mass and the energy of the probing ion, and the scattering angle are fixed in the LEIS experiment, there is a direct correlation between the mass of the target atom and the energy of the back-scattered ion. The energy spectra can thus directly be interpreted as mass spectra of the surface

LEIS measurements were conducted on thin films (150-200 nm) of the polymers listed in Table 4.2. All measurements were carried out with $^3He^+$ ions having an incident energy of 3 keV. Figure 4.7 shows the LEIS spectra for the P(MMA-co-F1MA) copolymers.

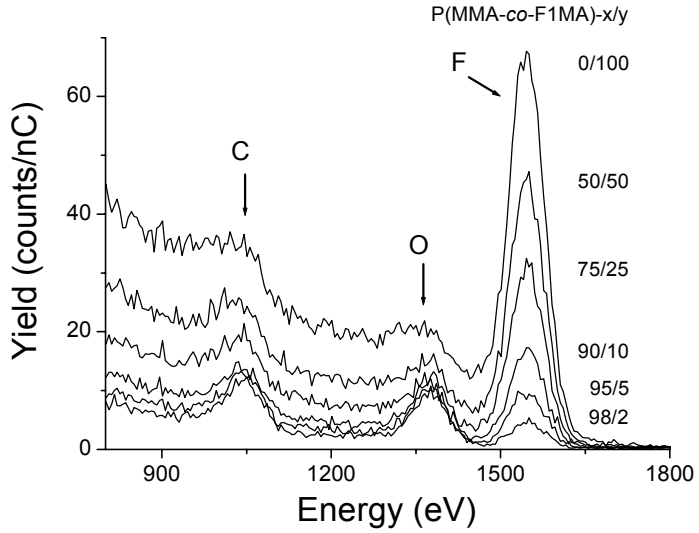


**Figure 4.7** LEIS energy spectra measured with 3 keV $^{3}He^{+}$ ions on P(MMA-*co*-F1MA) copolymer with increasing molar fraction of F1MA in the copolymer.

Three peaks, representing carbon, oxygen, and fluorine can be distinguished in the energy spectra. The high-energy onsets of these peaks agree with the theoretical values of 1178, 1498, and 1572 eV, respectively. Hydrogen is not visible in the spectra, since conservation of momentum excludes backscattering of atoms that are lighter than the probing ion.

The background signal of the spectra increases for the polymers with a higher fluorine content. Two effects are responsible for the increase of the background. Firstly, neutralized projectile particles that collide with target atoms below the surface can be re-ionized when they leave the surface and contribute to the background. Secondly, to some extent at low energies in the spectra, charged atoms or fragments may be sputtered from the surface and reach the detector thus contributing to the background. Since both types of background are very smooth, they can be easily separated from the relevant peaks in the spectrum.

A comparison of the LEIS spectra of the P(MMA-*co*-F1MA) copolymers shows, as expected, a gradual increase of the fluorine signal with increasing fluorine content. More interesting is the observation that for low fluorine concentrations of F1MA in the copolymer (P(MMA-co-F1MA)-98/2, P(MMA-co-F1MA)-95/5, and P(MMA-co-F1MA)-90/10, and P(MMA-*co*-F1MA)-75/25, the carbon and the oxygen signals are not only clearly visible, but also the ratio C/O remains almost constant. At higher F1MA content the carbon and oxygen peaks are still visible, but their ratio changes with changing concentration. All these observations point to a simple surface-model in which fluorine-containing tails are present on

a matrix of PMMA. At low contents of F1MA the original PMMA surface is still visible with the LEIS technique, whereas at higher F1MA content this surface is more shielded by the tails. This results in low-intensity peaks for carbon and oxygen with C/O.

One may expect that a longer perfluoroalkyl side-chain length results in more effective shielding. This means that for a longer perfluorinated side-chain in the copolymer, the carbon-oxygen matrix of PMMA becomes hidden by the fluorine-containing tails at a lower content than observed for P(MMA-*co*-F1MA) copolymers. The LEIS spectra for the F6MA-MMA (Figure 4.8) and F10MA-MMA (Figure 4.9) copolymers are in full accordance with this supposition. In the case of F10MA copolymers the oxygen peak cannot be discerned at all from the background scattering when the amount of F10MA is as low as 1%.

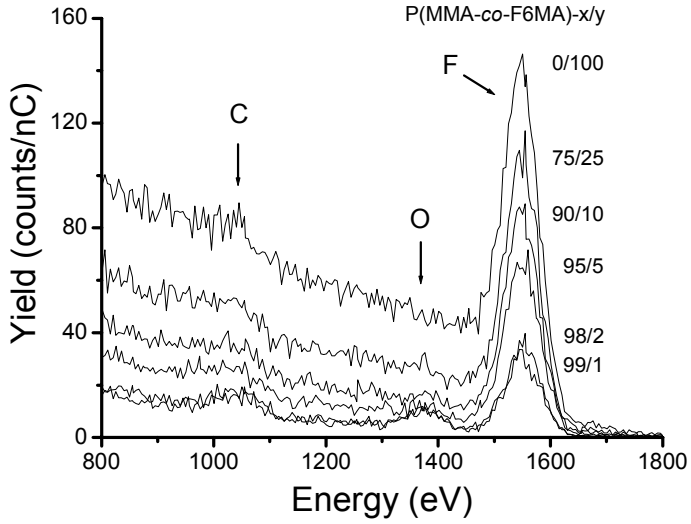


**Figure 4.8** LEIS energy spectra measured with 3 keV $^{3}He^{+}$ ions on P(MMA-*co*-F6MA) copolymers with increasing molar fractions of F6MA in the copolymer.

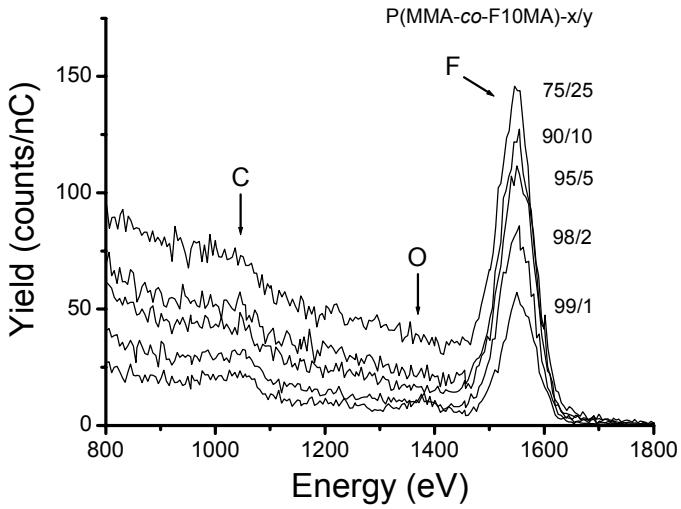


**Figure 4.9** LEIS energy spectra measured with 3 keV $^{3}He^{+}$ ions on P(MMA-*co*-F10MA) copolymers with increasing molar fractions of F10MA in the copolymer.

## 4.6 DISCUSSION

The question arises whether the surface-model as proposed in the foregoing also fits to macroscopic properties as surface tension. To answer this question the fluorine concentration in the first atomic layer, as found by LEIS, was plotted versus the corresponding surface tension for all FMA-MMA copolymers. This plot (Figure 4.10) can be divided into three parts: a low-concentration region where the surface tension rapidly decreases with increasing fluorine concentration; a concentration region from about 35 mN/m to 13 mN/m in which the surface tension is linearly related to the fluorine concentration in the outermost atomic layer; and a high-concentration region starting at about 11 mN/m where the surface tension hardly decreases with increasing fluorine concentration. The linear region implies that for increasing fluorine content each additional fluorinated tail at the surface replaces a certain amount of MMA unit. It is important to realize such a linear relationship between observed number of fluorine atoms and surface tension is only seen when LEIS is used to determine the surface composition. When using other surface analytical techniques, such as XPS, the information depth is too high and contributions from deeper layers obscure the results. The deviations from linearity below 13 and above 35 mN/m might be ascribed to a different packing density at the surface. For the region with the highest fluorine concentration it is known that ordening has been observed. For instance, the F10MA-25 copolymer exhibits crystalline behavior with

a melting point of 107.5 ºC. None of the fluorinated (co)polymers reaches the value 6 mN/m, being the surface tension for a close-packed array of $-CF_3$ groups in the surface.

For the highest surface tensions, a very small amount of fluorine in the outer surface leads to a strong decrease in surface tension. A possible explanation is that there is some degree of ordering in the PMMA at the surface, while this is disturbed by the presence of some fluorinated tails.

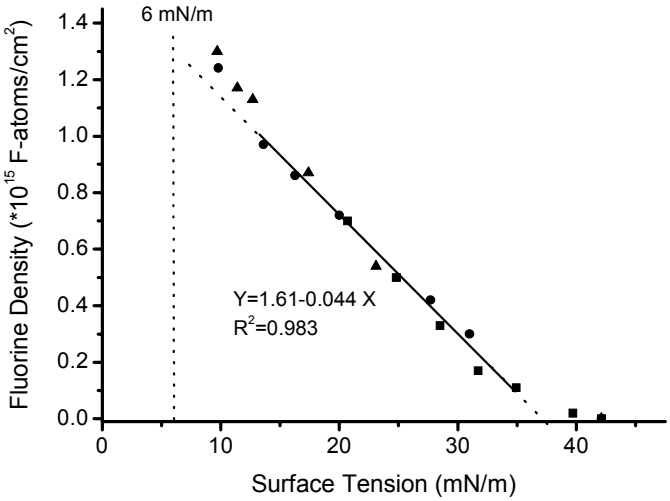


**Figure 4.10** Surface tension dependence of P(MMA-*co*-F1MA) (■), P(MMA-*co*-F6MA) (●), and P(MMA-*co*-F10MA) (▲) as a function of the fluorine density in the outermost atomic layer of the surface. The solid line represents the best fit for the data points in the region 35-13 mN/m.

It has to be stressed that the discussion given so far only holds for a class of copolymers where one of the monomers remains the same (here MMA) whereas the other comonomer has a predominant influence on the surface tension. It would be therefore very interesting to investigate other copolymer systems, in order to verify a similar linear correlation between the content of the copolymer and the surface tension.

As mentioned in the Experimental Part, the surface tension data were calculated by the acid-base method. Since systematic errors can be introduced by this method of calculation, all data were recalculated by the method of Owens and Wendt.[29] Again a similar linear relationship was found between the concentration of fluorine at the uppermost layer (LEIS) and the surface tension. This similarity clearly suggests that the linear dependence is a real physical phenomenon.

It is known that the roughness of the surface influences the repellency towards polar and non-polar solvents.[30] If the surface is microscopically rough but not rough enough to form

voids at the solid-liquid interface, the relation between the actual contact angle $\theta_W$ and the Young contact angle $\theta_Y$ can be given by the Wenzel equation:

$$\cos \theta_W = r \cos \theta_Y \tag{4.2}$$

In this equation $r$ is the roughness factor and defined as the ratio of the true surface area versus the projected surface area. As $r$ is always larger than 1, roughness effects will increase the wetting of the surface for $\theta$ values smaller than 90˚, whereas repellency is increased for $\theta$ values larger than 90˚. For the closely related (co)polymers considered in this Chapter, it can be expected that macroscopic roughness effects for all the polymers are equal or almost equal. This means that in a comparison of the copolymers roughness effects play a minor role.

Figure 4.10 clearly shows that there is a linear correlation between the fluorine concentration (chemical composition) in the outermost atomic layer and the surface tension. Despite our investigations on the molecular contribution to the surface tension, a complete understanding of the origin of the surface tension is still absent and only a tentative answer can be given. In this respect, surface geometry and the topography on an atomic scale are likely to play a role and have to be considered. This is especially true for the region at low surface energy where the surface tension of the copolymers is presumably influenced by conformational changes in the surface caused by the association of the perfluorinated side-chains. It is not clear in literature wether a surface with high length scale roughness, as used in the Wenzel relation, also have nano-scale topographies superimposed on these larger features.

The results described in this Chapter combined with investigations on related systems with different polymer architectures (block copolymers, random copolymers, and end-capped polymers) could eventually lead to a control in surface and interfacial phenomena.

Segregation or preferential orientation of the fluorinated side chains has been described as a thermodynamically controlled process.[31] This means that at higher temperature the entropic contribution of the Gibbs free energy will overcome the enthalpic contribution, resulting in a lower segregation for fluorine. However, *in situ* LEIS measurements at different temperatures did not show any significant difference in the intensities of the fluorine signal. Presumably, the effects are too small to be observed. The present findings are in contrast to recent studies of Ming *et al.*[32] where *in-situ* LEIS is used for end-capped polymer blend systems. In those studies it was found that above a certain temperature the fluorine signal does decrease with increasing temperature. It could even be shown that this process was reversible

in nature. These results can lead to a better understanding of the thermodynamics and the kinetics of segregation.

## 4.7 CONCLUSIONS

The combination of LEIS, XPS, and contact angle measurements has proven to be a powerful method for the investigation of surfaces and has given a better insight into surface phenomena (wetting, adhesion) for partially fluorinated polymers. Incorporation of perfluoroalkyl moieties into a polymethacrylate reduces the surface tension of the polymer significantly, pointing to a preferential orientation of the perfluorinated alkyl side chain to the air-polymer interface. Angle-dependent XPS measurements reveal a surface enrichment of fluorine over several nanometers in depth. Using LEIS analysis it is possible to determine the fluorine composition of the first atomic layer of thin polymer films under static conditions *i.e.* without damaging the surface. The results confirm that for a wide variety of compositions the surface tension is linearly dependent on the fluorine concentration in the outermost atomic layer. Deviations from this behavior for the very small and very large fluorine concentrations are believed to be due to ordering phenomena leading to a different packing density in the surface region.

## 4.8 REFERENCES


[1] Zisman, W. A. *Contact Angle, Wettability, and Adhesion,* Advances in Chemistry Series 43, Am. Chem. Soc., Washington DC, 1964.

[2] Kassis, C. M.; Steehler, J. K.; Betts, D. E.; Guan, Z.; Romack, T. J.; DeSimone, J. M.; Linton, R. W. *Macromolecules* **1996**, 29, 3247.

[3] Takahashi, S.; Kasemura, T.; Asano, K. *Polymer* **1997**, 38, 2107.

[4] Bongiovanni, R.; Beamson, G.; Mamo, A.; Priola, A.; Recca, A.; Tonelli, C. *Polymer*, **2000**, 41, 409.

[5] Böker, A.; Reihs, K.; Wang, J.; Stadler, R.; Ober, C. K *Macromolecules* **2000**, 33, 1310.

[6] Affrossman, S.; Bertrand, P.; Hartshorne, M.; Kiff, T.; Leonard, D.; Pethrick, R. A.; Richards, R. W. *Macromolecules* **1996**, 29, 5432.

[7] Thomas, R. R.; Anton, D. R.; Graham, W. F.; Darmon, M. J.; Sauer, B. B.; Stika, K. M.; Swartzfager, D. G. *Macromolecules* **1997**, 30, 2883.

[8] Van de Grampel, R. D.; van Gennip, W. J. H.; Wassing, B.; Krupers, M. J.; Laven, J.; Niemantsverdriet, J. W.; van der Linde, R. *Pol. Mater. Sci. Eng. (ACS)* **2000**, 305.

[9] Genzer, J.; Sivaniah, E.; Kramer, E. J.; Wang, J.; Körner, H.; Xiang, M.; Char, K.; Ober, C. K.; DeKoven, B. M.; Bubeck, R. A.; Chaudhury, M. K.; Sambasivan. S.; Fischer, D. A. *Macromolecules* **2000**, 33, 1882.

[10] Genzer, J.; Sivaniah, E.; Kramer, E. J.; Wang, J.; Körner, H.; Xiang, M.; Char, K.; Ober, C. K.; DeKoven, B. M.; Bubeck, R. A.; Fischer, D. A; Sambasivan. S. *Langmuir* **2000**, 16, 1993.

[11] a) Chaudhury, M. K.; Whitesides, G. M. *Science* **1992**, 255, 1230. b) Olbris, D. J.; Ulman, A.; Shnidman, Y. *J. Chem. Phys*. **1995**, 102, 6865. c) Ulman, A. *Thin Solid Films*, **1996**, 273, 48. d) Mach, P.; Huang, C. C.; Nguyen, H. T. *Phys. Rev. Lett*. **1998**, 80, 732. e) Fadeev, A. Y.; McCarthy, T. J. *Langmuir* **1999**, 15, 3759. f) Castner, D. G.; Lweis, Jr., K. B.; Fischer, D. A.; Ratner, B. D.; Gland, J. L. *Langmuir* **1993**, 9, 537. g) Lüning, J.; Stöhr, J.; Song, K. Y.; Hawker, C. J.; Ionidice, P.; Nguygen, C. V.; Yoon, D. Y. *Macromolecules*, **2001**, 34, 1128.

[12] Langmuir, I. *J. Am. Chem. Soc*. **1916**, 38, 2221.

[13] Hare, E. F.; Shafrin, E. G.; Zisman, W. A. *J. Phys. Chem*. **1954**, 58, 236.

[14] Brongersma, H. H.; Mul, P. M. *Chem. Phys. Lett*. **1972**, 14, 380.

[15] a) Viitanen, M. M.; Jansen, W. P. A.; van Welzenis, R. G.; Brongersma, H. H.; Brands, D. S.; Poels, E. K.; Bliek, A. *J Phys. Chem. B* **1999**, 103, 6025. b) Jansen, W. P. A.; Ruitenbeek, M.; Denier van de Gon, A. W.; Geus, J. W.; Brongersma, H. H. *J. Catal.* **2000**, 196, 379.

[16] Hook, T. J.; Schmitt, R. L.; Gardella, Jr., J. A.; Salvati, Jr., L.; Chin, R. L. *Anal. Chem.* **1986**, 58, 1285.

[17] Hook, K. J.; Gardella, Jr., J. A.; Salvati, Jr., L. *Macromolecules*, **1987**, 20, 2112.

[18] Maas, A. J. H.; Viitanen, M. M.; Brongersma, H. H., *Surf. Interface Anal*. **2000**, 30, 3.

[19] Ponjée, M. W. G.; Reijme, M. A.; Denier van der Gon, A. W.; Brongersma, H. H.; Langeveld-Vos, B. M. W.; *Polymer* **2002**, 43, 77.

[20] a) Good, R. J.; van Oss, C. J. in *Modern Approaches to Wettabillity*, Schrader, M. E., Loeb, G. I., Eds.; Plenum Press, New York, 1992. b) Van Oss, C. J.; Chaudhury, M. K.; Good, R. J. *Chem. Rev*. **1988**, 88, 927

[21] Van de Grampel, R. D.; van Geldrop, J.; Laven, J.; van der Linde, R. *J. Appl. Polym. Sci.* **2001**, 79, 159.

[22] Van Oss, C. J.; Chaudhury, M. K.; Good, R. J. *Chem. Rev*. **1988**, 88, 927.

[23] Kwok, D. Y.; Neumann, A. W. *Adv. Colloid Interface Sci*. **1999**, 81, 167.

[24] Krupers, M.; Slangen, P.-J.; Möller, M. *Macromolecules*, **1998**, 31, 2552.

[25] LeGrand, D. G.; Gaines Jr., G. L. *J. Colloid Interface Sci*. **1969**, 31, 162.

[26] Pittman, A. G.; Ludwig, B. A. *J. Polym. Sci. A* **1969**, 7, 3053.

[27] Bouteiller, V.; Garnault, A.M.; Teyssié, D.; Boileau, S.; Möller, M. *Polym. Int.* **1999**, 48, 765.

[28] Jones, R. A.; Kramer, E. J. *Polymer* **1993**, 34, 115.

[29] Owens, D. K.; Wendt, R. C. *J. Appl. Polym. Sci*. **1969**, 13, 1741.

[30] Wu, S. *Polymer Interface and Adhesion*; Marcel Dekker: New York, 1982; Chapter 1.

[31] Su, Z.; Wu, D.; Hsu, S.L.; McCarthy, T.J. *Macromolecules* **1997**, 30, 840.

[32] Ming, W. *et al*. to be published.

[33] Part of this work has been published in: a) Van de Grampel, R. D.; Gildenpfennig, A.; van Gennip, W. J. H; Ming, W.; Laven, J.; Krupers, M.; Thüne, P. C.; Niemantsverdriet, J. W.; Brongersma, H. H.; van der Linde R. *Proc. Fluoropolymers2000 Current frontiers and future trends (ACS)*, ed. D. W. Smith, **2000,** 96. b) Van de Grampel, R. D.; Gildenpfennig, A.; van Gennip, W. J. H; Ming, W.; Laven, J.; Krupers, M.; Niemantsverdriet, J. W.; Brongersma, H. H.; van der Linde R. accepted in *Prog. Org. Coat.*

# Chapter 5

# The Influence of Polymer Architecture on Surface Structure


## 5.0 ABSTRACT

*A molecular-level self-consistent-field theory is used to analyze physical and thermodynamic properties of partially fluorinated poly(methylmethacrylate) chains in the vicinity of the polymer-vapor interface. The molecules are described on a united atom level in which the methyl ester and perfluoroalkyl esters are linked onto a C-C backbone, whereas the vapor is modeled as free volume. Replacing -$OCH_3$ groups by –$OCH_2C_6F_{13}$ groups was used to vary the chain composition/architecture. In agreement with experimental data, the degree of fluorination of the polymer chains influences the surface tension in a non-linear way; a small fraction of fluorinated groups leads to a relatively large drop of the surface tension. The surface characteristics also depend on various polydispersity effects. The effects of chain length, blockiness, and degree of incorporation of the fluorinated monomer were systematically analyzed. It was found that both the surface tension and surface structure are very sensitive to the degree of blockiness, leading in special cases to microphase separation of the bulk. For these microphase-separated systems a completely ordered bulk with lamellae parallel to the surface was observed.*

## 5.1 INTRODUCTION

Wettability, low adhesion to the surface, and friction resistance of polymeric coatings are material properties that are controlled by the composition of the outermost surface layer. Such coatings may contain several constituents, one or a few of which may adsorb preferentially at the surface. It follows from the classical Gibbs adsorption law that in these multi-component systems the surface concentration differs from that in the bulk. Typically, the surface is enriched with the component with the lowest surface tension. Surface segregation phenomena have, for example, been observed in polymer blends,[1] solutions,[2] and block copolymers.[3] This surface enrichment can be useful to design an 'ideal' coating system that combines the best bulk properties with the optimized surface properties.

The driving force for surface segregation in these systems is related to the lowering of the free energy. When the surface area is fixed, *e.g.*, by the macroscopic dimensions of the system, the excess free energy of the surface per unit area (the surface tension $\gamma$) is the only parameter that is left to minimize the free energy of the system.

It is known that the surface tension of a random copolymer melt is, in many cases, almost linearly related to the molar fraction of its monomer units.[4] Recently, surface segregation phenomena have been observed in mono-component polymer systems containing pendant perfluoroalkyl side groups, comparable to what was found with polymer blends. In such cases only part of the polymers, *viz.* the fluorinated side groups, are preferentially adsorbed at the coating-air interface.[5-10] These surface anisotropic conformations lead to a relatively low free energy density at the surface when incorporating only small amounts of fluorinated moieties. This has been confirmed by X-Ray Photoelectron Spectroscopy (XPS)[11], Secondary Ion Mass Spectroscopy (SIMS)[12], Forward Recoil Spectroscopy (FRES)[13], Near-Edge X-Ray Absorption Fine Structure (NEXAFS)[14], and the highly surface sensitive Low-Energy Ion Scattering (LEIS)[15]. The quantitative analysis of the surface structure, however, is still a matter of extensive research.[16]

It is of interest to complement chemical-physical measurements as described in Chapter 4 by appropriate theoretical modeling. In this chapter a detailed self-consistent field (SCF) theory will be used for this purpose. Self-consistent field (SCF) theories are known to be applicable to dense polymeric systems because the excluded-volume correlations are screened to a large extent.

Although polymer blend systems are studied extensively, relatively little work on 'neat' copolymer systems has been published. In this chapter a detailed study of surface

segregation effects in a well-defined system of copolymers is presented. The SCF method enables surface composition and surface tension to be determined. Additionally, the effects of chain length, chemical variations, and molecular architecture on surface composition and surface tension are considered. All these aspects can be included in a molecular model in which the size and the shape of the molecule up to the level of monomer units are accurately accounted for.

The remainder of this chapter is organized as follows. Firstly, a short introduction to molecular modeling of polymer systems will be given, followed by a review of the basic concepts of the SCF technique. In this review a compact formalism is given for branched polymers[17] within the SCF method of Scheutjens and Fleer.[18,19] Additionally, the molecules and the parameters used in the model are described. Subsequently, the results of the SCF analyses will be presented and compared to available experimental data as obtained in Chapter 4. Conclusions are summarized in the last section.

## 5.2 MOLECULAR MODELING

Molecular modeling of the surface properties of polymer materials may be used to understand the regularities found in these systems *viz*. to obtain detailed conformational results on an atomic level. In molecular dynamics simulations one uses essentially Newton's law, $F = ma$, to trace the molecules and atoms in space and time. There are commercially available software packages in which molecules can be defined in full molecular detail, including the hydrogen atoms. Typically this approach can be used to answer questions about materials, related to the nm length scale and ns timescale domains. Changes in chain conformations, surface reorganizations, and the exchange of surface active molecules with less surface active molecules take place on much larger timescale, thus for such purpose an all-atom MD technique cannot be used due to computational limitations. One option is *to coarse grain* the simulations and probe on a larger length and time scale. One of the problems is to find appropriate interaction parameters and the corresponding time scales in these reduced approaches. If dynamical information is only used to investigate the degree of equilibration, one can also use the Monte Carlo (MC) technique to sample the conformational properties in the system. This technique becomes very efficient if molecules are placed on a lattice, such as in the bond fluctuation model (BFM). The BFM technique has been used frequently to study polymer blends and polymer surfaces.[20]

In simulations one can in principle account for all possible excluded-volume correlations. The positions of all segments in the system are known at any moment. However, the struggle with the statistical accuracy is always there and especially for large systems wherein the polymer chains are densely packed, the equilibration is very time demanding. Moreover, it is very difficult to 'measure' the appropriate thermodynamic parameters, such as the surface tension, in a simulation.

Thermodynamic properties are readily available if the partition function of the system is known. The only types of partition functions that can be solved are those in which mean field approximations are used. In polymer physics the mean-field approach is based upon the Edwards diffusion equation:[21]

$$\frac{\partial G(r,N)}{\partial N} = \frac{1}{6}\nabla^2 G(r,N) - u(r)G(r,N) \qquad (5.1)$$

where *G(r,N)* denotes the probability distribution of finding the end segments *N* of a polymer chain at coordinate *r*.

This equation features the behavior of a test chain in an average self-consistent potential field *u(r)*. This potential field is a function of the local density of the various segments. The exact analytical solution of the Edwards equation is known only for very few systems. Typically these equations have to be solved numerically. A discretisation scheme, as first suggested by Scheutjens and Fleer[18,19] in the context of polymer adsorption, is utilized in this Chapter. This approach has successfully been used in a wide range of interfacial systems, *e.g*. polymer surfactant adsorption, solid/liquid interfaces, polymeric melts, polymeric solutions, self-assembly of copolymers and surfactants and polymeric brushes.[22] Recently, also transitions between adsorbed chains and so-called flowers have been analyzed.[23] Leermakers[24] used the approach to model the self-assembly of lipid molecules in bilayer membranes. The lipid molecules consist of branched chains in which the united atoms concept, *i.e.* segments such as $CH_2$, $CH_3$, is used. Polar, apolar and even charged entities can be descibed. This model will be applied here to deal with the partially fluorinated copolymer systems.

In a SCF calculation, the calculations are course-grained such that degrees of freedom on the monomer length scale are ignored. Indeed, the classical approach is to replace one or more monomeric building blocks by one statistical segment.[25] Such an approach is of interest

to investigate universal effects in these systems and will be used below when the dependence of the interfacial free energy on the degree of polymerization of the polymer chains will be discussed. However, when the main interest is in the structure of the interfacial layer on the (sub) monomeric length scale, it is important to include the structural characteristics on the segment scale. In this chapter the detailed structure of the polymer chains will be included. The conformational characteristics of interfacial molecules on the sub-segment level will be predicted.

## 5.3 THEORY

### 5.3.1 Discretization Scheme for Branched Systems within the Scheutjens-Fleer Theory

The Edwards equation (5.1) needs to be generalized to account for (i) the presence of more than one segment type along the chain, *i.e.* not all segments feel the same self-consistent potential, and (ii) for the nontrivial chain connectivity (branched chain architecture). Both generalizations are possible and documented in the literature. However, a short review of these extensions is useful. We will introduce a compact formalism which is suitable both for linear as well as for branched chains.

Within the framework of the Scheutjens-Fleer model, the continuous differential equation (Eq. 5.1) transforms into a discrete propagator formalism. Within this formalism, it is important that the segments of molecule *i* have fixed segment ranking number, $s = 1, 2,.., N$. Subsequently, it is necessary to know the segment type of each segment. A composition operator $\delta_{i,s}^{x}$ is introduced, which assumes the value unity when segment *s* of molecule *i* is of type *x* and zero otherwise. This operator will be used to select the appropriate weighting factor in the propagators defined below.

The start is to define the Boltzmann weight that accounts for the self-consistent field felt by segment *s* of molecule *i*:

$$G_i(z,s) = \sum_x G_x(z)\delta_{i,s}^{x} \tag{5.2}$$

where the segment type dependent Boltzmann weights are given by:

$$G_x(z) = \exp\{-u_x(z)\} = \exp\left\{-\left[u'(z) + \sum_y \chi_{xy}\left(\langle\varphi_y(z)\rangle - \varphi_y^{\beta}\right)\right]\right\} \tag{5.3}$$

This equation defines the dimensionless (scaled by *kT*) self-consistent segment potential $u_x(z)$ felt by a segment of type *x* at coordinate *z* along the z-axis. This potential is normalized with respect to a reference phase indicated by the superscript $\beta$. By way of normalization, the weighting factors $G_x(z)$ are defined to be unity in this reference phase. Here the vapor phase will be used, which is (extremely) dilute in polymer, as the reference. Alternatively, it would be possible to choose a homogeneous polymer-rich phase as the reference phase. This choice is problematic as soon as the polymer system becomes structured on microscopic length scales. Apart from these obvious problems, there is no important consequence for the choice of the reference system.

As can be seen in Eq. (5.3), the segment potential contains two terms. The first quantity on the right hand side of Eq. (5.3), $u'(z)$, is a Lagrange field (a hard-core potential) coupled to the constraint $\sum_x \varphi_x(z) = 1$ in each layer. Here the volume fractions that refer to a particular segment type are computed from corresponding molecule type and ranking-number dependent quantities:

$$\varphi_x(z) = \sum_i \sum_{s=1}^{N_i} \varphi_i(z,s) \delta_{i,s}^x \tag{5.4}$$

These ranking-number dependent volume fractions are calculated with the propagator formalism.

The second term in the segment potential Eq. (5.3), $\sum_y \chi_{xy} \left( \langle \varphi_y(z) \rangle - \varphi_y^\beta \right)$, accounts for the nearest-neighbor contact interactions felt by segment of type *x* in layer *z*. It is a summation over all segment types *y*, including the free volume component, *i.e.*, with *y* = *V* (vacuum). In this contribution the Flory-Huggins interaction parameters, $\chi_{xy}$ occur. Below these parameters will be discussed in more detail. The angular brackets in Eq. (5.3) denote a three-layer average of the segment density:

$$\langle \varphi(z) \rangle = \frac{\varphi(z-1) + \varphi(z) + \varphi(z+1)}{3} \tag{5.5}$$

The composition of the reference phase is fully specified by the volume fractions of all the components: $\varphi_x^\beta = \sum_i \sum_s \frac{\varphi_i^\beta}{N_i} \delta_{i,s}^x$. In principle, it is thus possible to compute the segment potentials from the segment volume fraction profiles. In the SCF approach the reversed action (calculating the volume fractions from the potentials) is also defined.

To compute the segment density profiles from the potentials, it is necessary to first specify uniquely how the segments in the chain are connected to each other. The number of segment-segment bonds is always one less than the number of segments. Let denote the bonds with bond ranking numbers $t$ = 1,…, $N$–1. It is necessary to know the segment ranking numbers that are on both sides of a given bond. These two segments can be specified by sub and superscript: $t_{s_1}^{s_2} = t_{s_2}^{s_1}$. A segment can be involved in one (chain end), two (middle segment), three or four (branched segment) bonds. Let $t_s$ be the set of bonds connected to segment $s$.

In the following first of all the appropriate Green function $G$ will be introduced, which is the quantity that collects the overall statistical weight of all possible and allowed conformations of particular chain fragments. This quantity is rather complicated in this case because the chains are branched. Then a discussion will be given how one can compute these functions starting from the chain ends and propagating along the chain. Finally it is shown how these functions can be used to obtain the observable segment density profiles.

The Green function, which may be referred to as the end-point distribution function, is defined as $G_i(z,s,t_s^{s'})$. It reflects the statistical weight of that part of the polymer molecule in which $s$ is the 'end-point' segment $s$; the bond $s$-$s'$ is not yet connected. In other words, this quantity contains the combined statistical weights of (complete, *i.e.* propagated from chain ends) chain fragments that contain segment $s$ at coordinate $z$ with the extra requirement that fragments are not connected to segment $s$ from the side of bond $t_s^{s'}$. This means that this bond $t_s^{s'}$ is available for the next propagator step. A branched polymer has more than two chain ends. Each chain end has only one bond. Such a chain end can also operate as an 'end-point'. If the walk is started at such an end-point, the starting condition is:

$$G_i(z,s,t_s^{s'}) = G_i(z,s) \tag{5.6}$$

where $s'$ is again the segment following to the end-segment $s$, where the walk is started.

Having defined the end-point distribution of a chain-end, the segment adjacent to the chain-end will be considered as the end-point *s*. The corresponding end-point distribution function will be defined. In this case the propagator step in the direction of the free bond can now be expressed by:

$$G_i\left(z,s,t_s^{s'}\right)=G_i\left(z,s\right)\prod_{t_s\neq t_s^{s'}}\left\langle G_i\left(z,s'',t_{s''}^{s}\right)\right\rangle \tag{5.7}$$

Here the angular brackets indicate a three-layer average as before. The multiple product goes over all bonds in which segment *s* is involved except the one between *s'* and *s*. Actually, Eq. (5.7) is a general expression that is applicable to all segments for propagating along a linear chain, but also for propagating along a chain with branch points.

The segment densities of a particular segment along the chain is found by a generalized composition law:

$$\varphi_i(z,s)=C_iG_i(z,s)\prod_{t_s}\left\langle G_i(z,s',t_s^{s'})\right\rangle \tag{5.8}$$

This equation computes the segment densities for all segments in the chain, *i.e.* for chain ends (which have only one bond), middle segments (which have two bonds) and branches.

The normalization constant $C_i$ is chosen such that the integral over the density profile is equal to the known number of molecules in the system. Once this constant is known, it is possible to compute the volume fraction of the polymer in the reference system, $C_i=\varphi_i^{\beta}/N_i$. The distribution of free volume is found by:

$$\varphi_V(z)=\left(1-\sum_{i\neq V}\varphi_i^{\beta}\right)G_V(z) \tag{5.9}$$

The above set of equations is closed and is routinely solved by a computer. In the solution, the segment densities both *determine* the segment potentials and *follow from* the segment potentials. In addition the space filling constraint (volume fractions including the free volume add up to unity) is obeyed in each coordinate. Typically, the density profiles are obtained with

seven or more significant digits. From the self-consistent solution, it is possible to compute all thermodynamic properties, including the interfacial tension.

### 5.3.2 Evaluation of the Surface Tension

The evaluation of the surface tension is intrinsically difficult, because it involves the difference between two large contributions, *i.e.* the difference between the overall free energy and that of the bulk. Only those contributions that are in excess of the bulk have to be accounted for. However, in the SCF theory the evaluation of the grand potential per unit area, *i.e.* the dimensionless surface tension $\tilde{\gamma}$ is evaluated straightforwardly from the segment density- and the potential profile:

$$\tilde{\gamma} = -\sum_{z=1}^{M}\left[\sum_{i}\frac{\varphi_i(z)-\varphi_i^{\beta}}{N_i}+\sum_{A}u_A(z)\varphi_A(z)-\frac{1}{2}\sum_{A,B}\chi_{AB}\left[\varphi_A(z)\left\langle\varphi_B(z)-\varphi_B^{\beta}\right\rangle-\varphi_A^{\beta}\left\langle\varphi_B(z)-\varphi_B^{\beta}\right\rangle\right]\right] \qquad (5.10)$$

#### *5.3.2.1 The surface tension of a molecularly homogeneous bulk in equilibrium with a vapor.*

It should be clear from the above that the SCF calculations are done on closed systems, in systems where the temperature $T$, the volume $V$, and the number of molecules $n$ are fixed. In this system the conformations and density profiles are adjusted such that the Helmholtz energy is minimal.

Calculations are typically carried out on a discrete set of coordinates (a lattice). It is common that gradients in densities develop that are not negligible on the discretisation length scale (strong segregation limit). Then so-called lattice artifacts may occur. These problems are best shown when the interface is shifted with respect to the discretisation points (lattice). Typically, it will be observed that the chemical potentials as well as the surface tension become functions of the position of the interface. One way to view these artifacts is that there exists some stress in the system as long as the interface is not placed optimally with respect to the grid. This stress can be viewed upon as a type of lattice pressure $\Delta p$. Then the chemical potentials of the molecules are given by:

$$\mu_i = \mu_i^{FH} + N_i \Delta p \qquad (5.11)$$

where $\mu^{FH}$ is the chemical potential as given by the Flory-Huggins theory, corresponding to the binodal value. The Gibbs-Duhem relation for interfacial systems reads:

$$\partial\gamma = -\sum_i n_i \partial\mu_i \tag{5.12}$$

from which it is seen that the surface tension in the system is a function of the position of the interface as well. Only when the lattice pressure vanishes, *i.e.* when $\mu = \mu_i^{FH}$ (binodal), the Helmholtz energy is minimal. This provides a straightforward way to compute the optimal position of the interface and therefore the unperturbed surface tension.

There exists an alternative method to find a good estimate of the artifact-free surface tension. In this method the interface is shifted in small steps over a distance of one lattice site. As a result a quasi-sinusoidal variation of the interfacial tension is obtained. The artifact-free point is found when the average of these interfacial tensions is computed, *i.e.* halfway the period of the oscillation.

*5.3.2.2 The surface tension for a system wherein the bulk is micro-phase segregated*

Next the case will be considered, that the bulk is no longer completely homogeneous in density. Indeed it is possible that the bulk has some structure on the molecular scale. This is called micro-phase separation. The calculation of the interfacial tension of the system in which the polymer phase is micro-phase separated cannot proceed along the same lines as specified in Section 5.3.2.1. The reason is that the Flory-Huggins theory does not give direct access to the chemical potentials that should be used to find the point with a vanishing lattice pressure. Therefore it is necessary to perform separate calculations to investigate the equilibrium properties of the micro-phase separated bulk phase.

It must be true that a macroscopic amount of the micro-phase segregated system has no interfacial tension associated with the presence of the local density variations. In the calculations, it is not possible to impose this constraint directly onto the calculations. However, it is possible to investigate the 'unit cell' properties of the system in the SCF approach systematically. In such a particular calculation it is necessary to assume the volume of the small system under investigation, *i.e.* it is necessary to fix the length of the unit cell. This length can be referred by the variable *M*. Reflecting boundary conditions on both sides of the small system implies that the unit cell is copied on either side of the system boundaries. The amount of polymer, and thus the amount of free volume, is varied until the grand potential of the system vanishes (again, Eq. 5.10 may be used to find the interfacial tension in

the small system). Of course it is necessary to vary the system size $M$ and to repeat the calculations. Of interest is the Helmholtz energy density, *i.e.* $f(M) = F(M)/(M)$. The optimal unit cell length $M^*$ corresponds to the minimum of $f(M)$. The chemical potential of the polymers that occurs at the optimal unit cell size, $\mu^*$, is, of course, available from such analysis.

From this point on, it is possible to follow the procedure discussed above to obtain the surface tension of the polymer-vapor interface. Now the chemical potential of the optimized bulk $\mu^*$ takes the role of the $\mu^{FH}$ (binodal). The optimal position of the interface, *i.e.* for which the polymer bulk is fully relaxed (where there is no lattice pressure), occurs when the chemical potential of the polymers equals $\mu^*$. The grand potential per unit area of this system corresponds to the requested artifact-free surface tension.

### 5.3.3 The Molecules

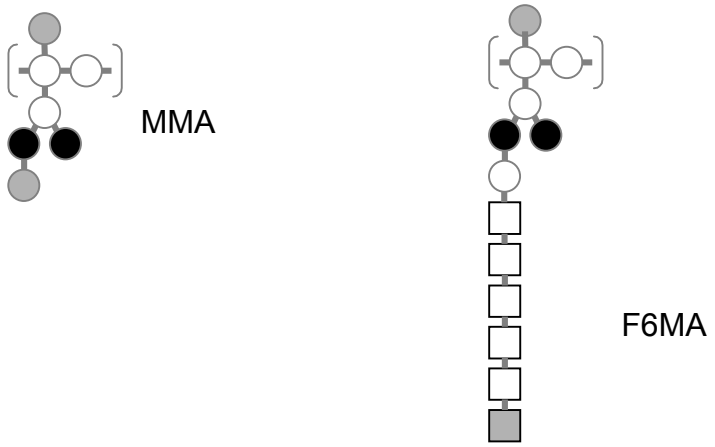


**Figure 5.1** A representation of the building blocks of the molecules, used in this study. On the left the methyl methacrylate monomer unit (MMA) and on the right 1,1-dihydroperfluoroheptylmethacrylate (F6MA) unit are depicted. The open circles represent the $CH_x$ groups (x = 0, 1, or 2), the black circles are oxygens, the gray circle is the $CH_3$ group, the open squares is a $CF_2$, and the gray square is the $CF_3$ unit.

The structure of a particular polymer chain is defined by the sequence of MMA and F6MA units. The following notation will be used. A regular or block copolymer will be represented by *r* or *b*, respectively. Thus *r*-$(MMA)_{55}$($F6MA)_5$ is a regular copolymer of 55 units of MMA and 5 units of F6MA, whereas *b*-$(F6MA)_5(MMA)_{55}$ is a block structure. Typically, the sequence of monomer units in the regular copolymer *r*-$(MMA)_{55}$($F6MA)_5$ is that each unit of F6MA is followed by 11 MMA units. In another example, *r*-

$(MMA)_{50}(F6MA)_{10}$, every unit of F6MA is followed by 5 units of MMA. Furthermore, *r*-$(MMA)_{30}(F6MA)_{30}$ is an alternating copolymer of units of MMA and F6MA. The number of units of MMA between two units of F6MA is represented by *m*.

Note the difference between *b*-$(MMA)_{27}(F6MA)_5(MMA)_{28}$ and *b*-$(MMA)_{55}(F6MA)_5$. Both copolymers have the same overall composition, but the sequence of five F6MA units is in the first case positioned in the center of the molecule, whereas in the latter the F6MA units are at one of the chain ends.

In order to get a realistic description of the system it is important to accurately account for the size and shape of molecules**,** *i.e.* for the chain architecture. Moreover, information is required about parameters that specify how the various parts of the molecule interact. Here it is important to mention that a lattice gas model is applied in which the system with volume M*L is incompletely filled with polymer units. The unoccupied lattice sites are denoted by the letter V (vacancies or free volume). These two aspects will be discussed in somewhat more detail because of their importance later on.

The molecules are considered to be fully flexible and are allowed to return to previously occupied sites according to the discretised Edward's equation using a first-order Markov approximation. A united atom description is used to represent the molecules (Figure 5.1). As mentioned previously the lattice sites can be filled by either x = V, $CH_2$, $CH_3$, O, $CF_2$, $CF_3$. For all solutions of the SCF equations the volume fractions obey the constraint: $\sum_x \varphi_x(z) = 1$ for each layer z. This means that the polymers cannot visit the same sites too often, because otherwise the density of the polymers will exceed unity.

### 5.3.4 The Parameters

The interactions in the system are parameterized by the well-known Flory-Huggins (FH) parameters $\chi_{xy}$. The values of the parameters must be chosen in such a way that they represent the system as accurately as possible. Because there are 6 different 'units' there are 6*5/2 = 15 different segment pairs, where the $\chi$*'s* should be found from comparison with experiments. However, the ideal situation that all parameters are known accurately is not yet reached and 'educated guesses' for the Flory-Huggins interaction parameters have to be made. In this respect it is important to realize that the parameters should be consistent with the level of detail that is chosen for the description of the structure of the monomeric building blocks. From the fitting of the phase behavior of the alkane-vapor system, Schlangen[26] recommends

$\chi_{V,CH_2}$ = 1.6. Unless otherwise specified, the same value has been taken for $\chi_{V,CH_2}$. This point is used as a reference for the other FH values for interaction with unoccupied sites. For example, because the oxygen is more polarizable it will have a higher FH value and therefore a value of $\chi_{V,O} = 2$ was taken. The effect will be that the hydrocarbon units prefer the polymer vapor interface above the oxygen atoms. The fluorinated groups on the other hand are poorly polarizable and therefore have a relatively low $\chi$ value. Again, fitting appropriate phase diagrams will result in better guesses for these units. Here a value of $\chi_{V,CF_3} = \chi_{V,CF_2} = 1.2$ was taken. Although not optimized, this set of parameters seems reasonable and will probably reflect the trends of the system qualitatively correct. Fine-tuning the parameter set is possible but this is not attempted in this work.[27]

All SCF calculations were performed, unless mentioned otherwise, for polymer chains consisting of sixty 'monomer' units (remember that each monomer is composed out of several united atoms). The short-range interactions, expressed by the Flory-Huggins interaction parameters, are listed in Table 5.1.

**Table 5.1** Short-range interaction parameters.

| $\chi$ | V | $CH_x$ | O | $CF_2/CF_3$ |
|---|---|---|---|---|
| V | 0 | 1.6 | 2 | 1.2 |
| $CH_x$ | 1.6 | 0 | 1 | 0.5 |
| O | 2 | 1 | 0 | 2 |
| $CF_2/CF_3$ | 1.2 | 0.5 | 2 | 0 |

## 5.4 RESULTS

As outlined in the introduction the macroscopic relationship between the surface tension and properties such as wetting and adhesion is well established. However, the correlation with the microscopic molecular structure of the surface is less well documented. Nevertheless, it is generally accepted that the surface tension is predominantly determined by the compositions in the first atomic layer of the film.[28] Our SCF analyses involve no *a priori* assumptions about the molecular properties of the surface and near surface layers. Therefore,

it is very interesting to compare the outcome of the theoretical analysis with experimental surface data, like contact angle data and angle-dependent XPS, conducted on these systems. These and related aspects will be considered in the following sections.

First the surface tensions of regular copolymers of MMA and F6MA, as obtained by our SCF model, will be considered.

### 5.4.1 Surface Tensions

In this section the polymer-vapor interface for regular copolymers of MMA and F6MA is discussed. The interfacial tension ($\tilde{\gamma}$) of a polymer-vapor interface is one of the key properties and results from the density and potential profiles of the segments according to Eq. (5.10). In order to investigate the liquid-vapor interface within the SCF theory, the amount of molecules in the system is chosen such that the two phases coexist. The densities of these coexisting phases follow directly the Flory-Huggins theory. As explained above in the SCF calculations of the surface tension, lattice artifacts are eliminated by adjusting the number of molecules (for shifting the position of the interface) until the volume fractions of the coexisting bulk phases equals those calculated with the Flory-Huggins theory. Within this theory the surface tension of the lattice fluid is dimensionless. To convert this value to units of N/m it has to be multiplied by the area of a lattice site and divided by $k_BT$:

$$\tilde{\gamma} = \frac{\gamma b^2}{k_B T} \tag{5.13}$$

where $\tilde{\gamma}$ is the dimensionless surface tension, $T$ the absolute temperature, $k_B$ Boltzmann's constant and $b$ is the lattice parameter of the cubic lattice.

In Figure 5.2 the calculated surface tension is given as a function of the molar fraction of F6MA. It can be seen that a small increase of the F6MA content in the copolymer results in a significant reduction of the surface tension of the random copolymer. This is consistent with the results obtained experimentally for these systems using contact angle data[15] (also shown in Figure 5.2).

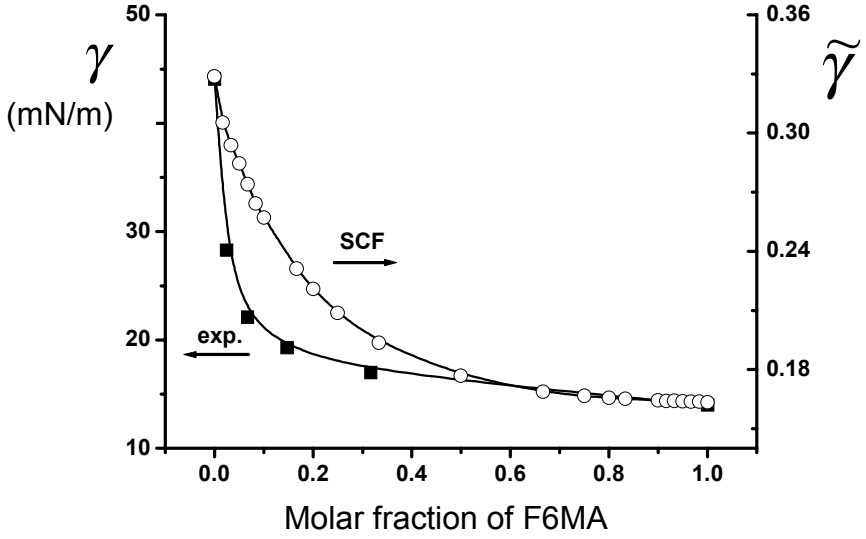


**Figure 5.2** Surface tensions for regular MMA/F6MA copolymers for different molar fractions of F6MA. Calculated SCF results (open points) are compared to experimental data for random copolymers[15] (solid points).

However, the surface tension as a function of molar fraction of F6MA for the experimental data on random copolymers shows more curvature than for the SCF analyses of regular copolymers, in particular for regions with low content of F6MA. This cannot be explained by the short-range FH interactions between the different segments in the molecules, *e.g.* changing the $\chi_{V,CF_3}$ value from 1.2 to 1 did not affect this difference. From polymer blend studies it is well known that several other factors influence the polymer-polymer phase and interface behavior as well. Examples are the nature of the monomers, the molecular architecture, composition, and the molecular size of the polymers.[29] The influence of all these factors on the SCF results will be studied systematically and the results will be discussed in more detail later on in this Chapter. The next section will deal with the general features of the surface structures of these regular copolymers.

### 5.4.2 The Structure of the Surface

One of the main interests of surfaces is the microscopic molecular structure of regular polymers in the polymer-air interface. From a given SCF solution, not only thermodynamic information (surface free energy) is readily obtained, it is also possible to evaluate structural information, *i.e.*, density profiles of the different segments. Generally, the surface tensions of polymer melts are largely determined by the bulk behavior of the fluid. However, surface conformations of functional groups (such as fluorinated tails orienting themselves in arrays)

may be pivotal to the minimization of the surface tension. Therefore the conformation of the polymer chain near the interface was studied in detail. Some typical density profiles for *r*-(MMA)$_{57}$(F6MA)$_3$ are given in Figure 5.3. Figure 5.3a shows the segmental density of $CF_2$ + $CF_3$ ($\overline{\varphi}_F$) as scaled with $\varphi_F$ in the bulk of the polymer phase. In the liquid-vapor interface, enrichment in the density of fluorine is observed, pointing to a preferential presence of the perfluorinated alkyl side chains at the boundary of the interface. A depletion zone, as a natural consequence, follows this fluorine-enriched layer. Angle dependent XPS measurements on these systems (see Chapter 4) did not reveal this depletion layer, probably because of the limited depth sensitivity in these measurements. The minimum of depth resolution is 5 nm for by angle dependent XPS measurements. Moreover, the intensity of an XPS signal falls off exponentially with the depth.[15]

From the density profiles of fluorine it is clear that the enriched top layer is very thin, typically 1-2 nm. This thin layer is a segregation layer rather than a stratified layer of phase separated bulk material. Such thin layers have been observed for systems by others using neutron reflection experiments.[10]

The scaled segmental density profiles for carbon ($\overline{\varphi}_C$) and oxygen ($\overline{\varphi}_O$) at the boundary of the coexisting phases (Figure 5.3b and 5.3c, respectively) show features that differ from that of $\overline{\varphi}_F$. Both atoms are repelled from the surface and a relatively small maximum is found at the location where $\varphi_F$ shows a depletion zone.

Finally, the location of the scaled segmental density of the $CF_2$ and $CF_3$ at the boundary of the coexisting liquid-vapor phases was considered. Figure 5.4 reveals that the chain ends of the fluorinated side chains have the highest preference for the 'contact zone' with the vapor, *i.e.*, in the outer surface region the $CF_3$ moieties are preferred over the $CF_2$ segments. This is in agreement with melt surface tension studies of poly(hexafluoropropene oxide) and Cahn-Hilliard density gradient studies, suggesting that the $CF_3$ side groups are oriented to the surface.[30] In SCF calculations for the liquid-vapor boundaries of n-alkanes this chain end effect has also been observed and can be explained as follows. Firstly, when chain ends are exposed to the vapor boundary side of the interface, the number of unfavorable segment-vacancy contacts is smaller. Secondly, the conformation entropy of a chain molecule in the interfacial region is larger when a chain end is pushed out of the interface instead of a string of segments. For our system the origin of the difference is only due to conformation entropy, because both the $CF_2$ and $CF_3$ segments were given the same FH-interaction parameter.

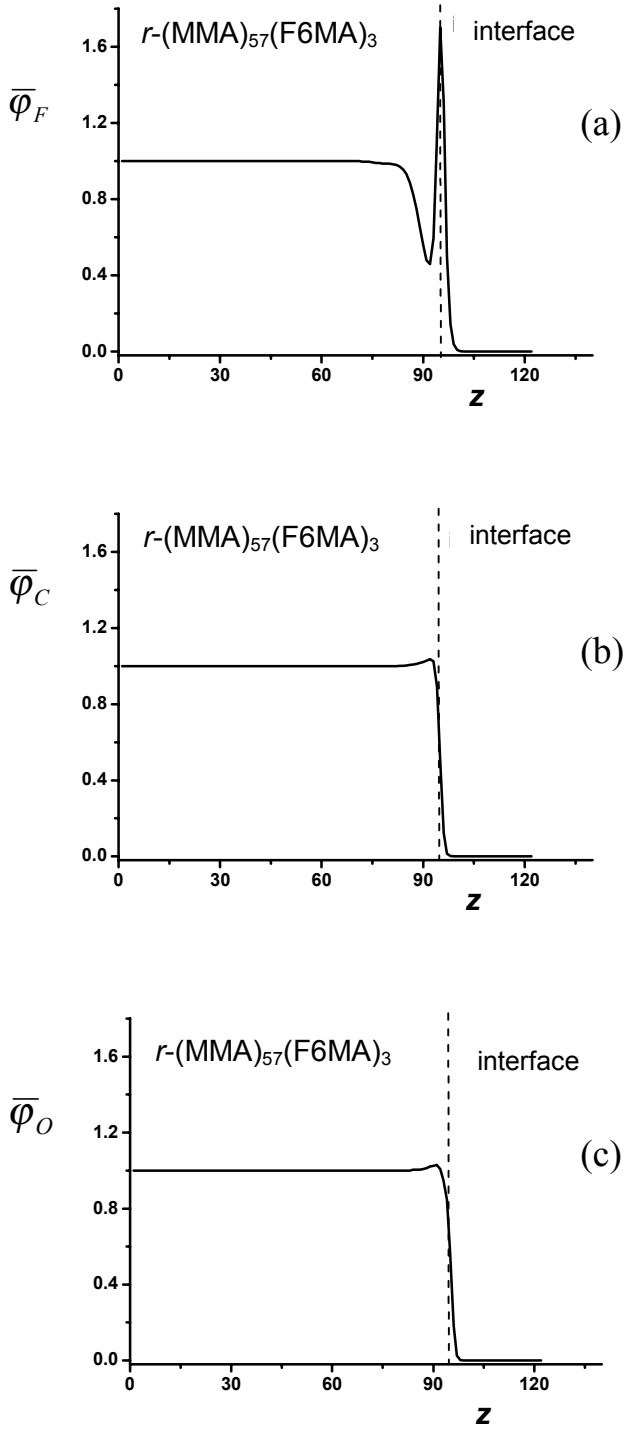


**Figure 5.3** Scaled segment density profiles of (a) $CF_2$ + $CF_3$ ( $\overline{\varphi}_F$ ), (b) $CH_2$ + $CH_3$ ( $\overline{\varphi}_C$ ), and (c) O segments ( $\overline{\varphi}_O$ ), in the liquid-vapor interface film of polymer *r*-$(MMA)_{57}(F6MA)_3$.

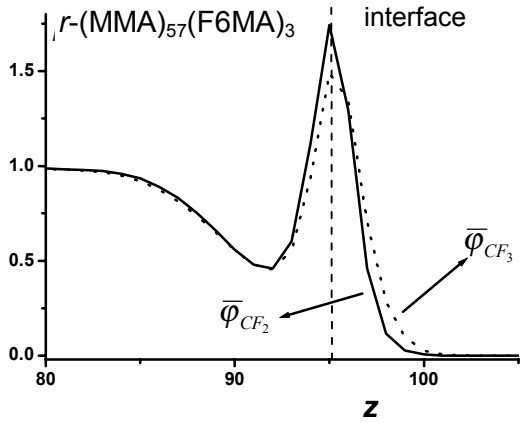


**Figure 5.4** Scaled volume fraction of the $CF_2$ ($\overline{\varphi}_{CF_2}$) and the $CF_3$ ($\overline{\varphi}_{CF_3}$) segments at the liquid-vapor interface for polymer *r*-$(MMA)_{57}(F6MA)_3$.

From Figure 5.3a it can be seen that there is enrichment in fluorine at the boundary of the coexisting liquid-vapor phases. Depending on the molar concentration of F6MA in the regular copolymer, a secondary and sometimes also a third maximum or higher order maximum is observed. The distance between the first and the second maximum is defined as the depletion thickness:

$$d = z_1 - z_2 \tag{5.11}$$

where $z_1$ and $z_2$ refer to the position of the primary and secondary maximum, respectively. This depletion thickness decreases with increasing number of units of F6MA in the copolymer. This effect can be seen in Figure 5.5 where the scaled segment density of $CF_3$ plus $CF_2$ moieties near the surface are plotted as a function of $z - z_1$.

Within a chain of *r*-$(MMA)_{60-x}(F6MA)_x$ the ratio of the number of units of MMA over F6MA ($m$) is a function of $x$ according to $m + 1 = 60/x$. When $m$ is larger than unity the physical interpretation of $m$ is the number of MMA units between two F6MA units along the chain. It is interesting that the depletion layer thickness appears to be proportional to the square root of $m$ in the case of *r*-$(MMA)_{60-x}(F6MA)_x$ molecules (Figure 5.6). The depletion zone will be enriched with the MMA units particularly for values of $m > 1$. Gaussian statistics implies that the length scale associated with a MMA fragment of length $m$, is given by the square root of $m$. This length scale dictates the depletion layer thickness. Structurally, this region is expected to be composed of loops and bridges of length $m$. The loops are chain

fragments that return to the same fluorine region from which they depart and bridges are chain fragment that cross over from one fluorine-rich region to the other. The relative importance of loops vs. bridges is presently not clear. Further inspection of Figure 5.6 reveals that the depletion layer thickness is proportional to the square root of *m* even in the region where *m* is smaller than unity. The picture of loops and bridges cannot explain this. In this regime, the surface enrichment indicates that the backbone of the molecules at the surface is predominantly laying parallel to the surface. This alignment is expected to improve for smaller values of *m.* Fluctuations in the backbone positions increase the depletion layer thickness. Hence, it is not unreasonable to have a square root dependence in the range $m \leq 1$. Extrapolation to $m = 0$ gives a depletion layer thickness of approximately 6 lattice units. The dimensions of the perfluoroalkyl side chains must determine this separation. As the length of the side chains is comparable to this limiting depletion layer thickness, it is concluded that the fluorinated side chains are strongly stretched (brush).

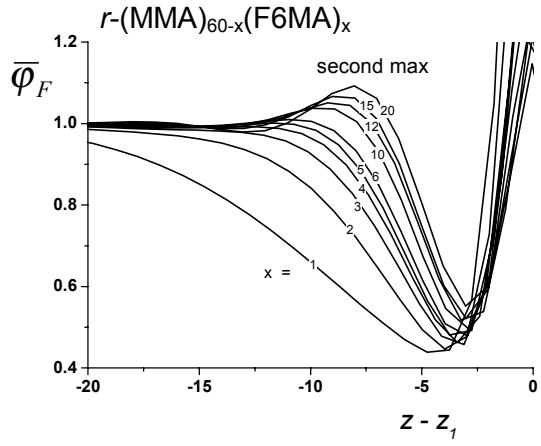


**Figure 5.5** Scaled segmental density profiles of $\overline{\varphi}_F$ fluorine in the subsurface region for *r*-$(MMA)_{60-x}(F6MA)_x$ with x = 1, 2, 3, 4, 5, 6, 10, 12, 15 and 20. The position of the primary maximum is defined as $z_1$.

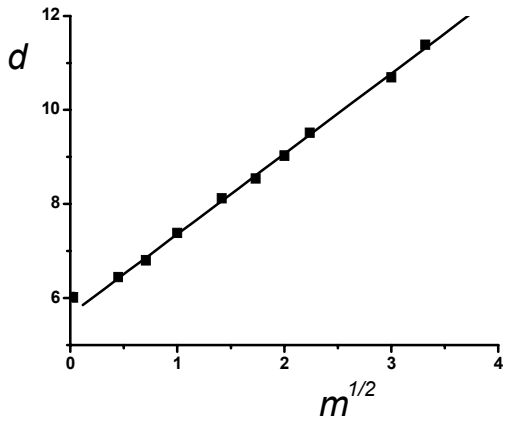


**Figure 5.6** Depletion layer thickness as a function of the square root of the length of the MMA block between two F6MA units in the *r*-$(MMA)_{60-x}(F6MA)_x$ molecules.

### 5.4.3 Chain Length Dependence

As shown in Figure 5.2, the experimental surface tension decreases much steeper with the addition of small amounts of F6MA than that predicted by the SCF simulations. Therefore, it is interesting to analyze the effect of molar mass on the surface tension and to compare these results with experimental data.

The LeGrand-Gaines relation describes the molecular weight dependency of a homologous series of polymers on the surface tension:[31]

$$\gamma = \gamma_\infty - C_1 M_n^{-x} \tag{5.12}$$

where $M_n$ denotes the number-average molecular mass, $\gamma_\infty$ is the surface tension at infinite molar mass, and $C_1$ is a semi-empirical parameter. The exponent $x$ varies from ⅔ for low molecular weight species to 1 for high-molecular weight polymers.

Experimentally, this empirical relation has been found to be valid for n-alkanes, perfluoroalkanes, polysiloxanes and polystyrenes. However, the theoretical interpretation of these results is still a matter of considerable discussion. Poser and Sanches,[32] who follow the Cahn-Hilliard theory,[33] have suggested that the primary contribution arises from the variation of the density of a polymer system with molecular weight. De Gennes[34] and Theodorou[35] suggested that chain conformation entropy causes lower molecular weight components to be preferentially at the surface. Recently, Kumar and Jones[36] found, using mean field treatments, that density effects are dominating, except in special cases where chain ends are strongly attracted or repelled from the surface. This is in line with the results of Koberstein and coworkers for end-functionalized polydimethylsiloxanes.[37]

To show that the SCF theory applied in this study can be used to evaluate the surface tension of the melt as a function of the molecular weight, first a simplified system was considered. This system is defined as a homopolymer composed of spherical segments of A in a monomeric solvent S with only one FH parameter, *viz.* $\chi_{A,S}$ = 1. This approach enables to deal with large molecular weights. Extrapolation to infinitive molar mass leads to a value of $\tilde{\gamma}_\infty$ =0.01375. In Figure 5.7a $\log(\tilde{\gamma}_\infty - \tilde{\gamma})$ is plotted as a function of $\log(M)$. In accordance with the LeGrand-Gaines relation a slope of –1 is found for high molar mass. Going to lower molecular weight a gradual deviation of this slope to a lower value is observed, reaching finally a value of order –2/3. It should be mentioned that this value is not found over a large range of molecular mass, and therefore it cannot be considered as a scaling law result. An

additional complication is that $\tilde{\gamma}$ at these low molar masses vanishes due to the appearance of a critical point.

A similar analysis has been carried out for the MMA-F6MA copolymer system. In this case it is necessary to increase the molecular weight at a fixed overall MMA-F6MA composition to exclude composition fluctuation effects. As repeating unit $(MMA)_2(F6MA)_1(MMA)_2$ block was chosen. Because of the higher molecular detail in this system the calculations are limited to shorter overall chain lengths. Nevertheless an estimation of $\tilde{\gamma}_\infty$ could be made and the corresponding results are given in Figure 5.7b. It can be seen that the results in Figure 5.7b show a similar behavior as the simplified homopolymer system. The slope at high molecular weight tends to be slightly smaller than –1. This is most likely due to the inaccuracy in the determination of $\tilde{\gamma}_\infty$.

In summary, it is observed that the maximum reduction of surface tension that can be reached with chain length variation (at constant composition) is only of order $10^{-3}$ in $\tilde{\gamma}$, corresponding to $10^{-4}$ in $\gamma$. This effect is too small to explain the much larger deviations between the experiments and theoretical predictions (Figure 5.2). Therefore it can be concluded that the polydispersity in chain length is not responsible for the deviation.

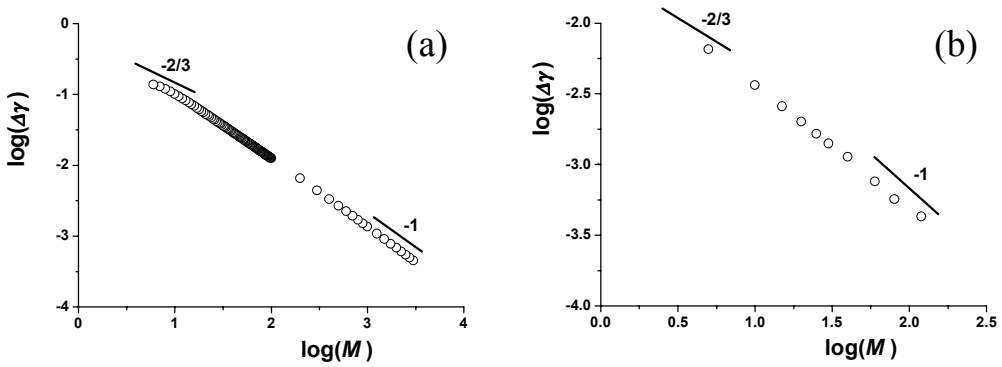


**Figure 5.7** Surface tension dependency on the chain length. Plotted is $\log(\Delta\gamma) = \log(\tilde{\gamma}_\infty - \tilde{\gamma})$. At high $M$ a slope of $x$ =-1 and at low $M$ a slope of $x$ = -⅔ was calculated: a) for an A-S system and b) for the detailed MMA-F6MA system.

### 5.4.4 Chemical Composition Variation

As mentioned before not only polydispersity in chain length but also polydispersity in chain composition can influence the surface tension. Polydispersity in chain composition implies that some chains contain more fluorinated moieties then others. Consequently, in such a case a mixture is considered, for which it can be expected that the surface will be enriched

with the component with lower surface tension, *i.e.*, the one with the higher fraction of F6MA.

Surface segregation phenomena have been studied extensively in the past for both miscible and immiscible blends. In these calculations the interest was focused on the determination of the surface excess of one component without considering the change in surface tension of the system. Here, the effect of polydispersity in composition on the surface free energy was explored for a blend system of *r*-$(MMA)_{59}(F6MA)_1$ and *r*-$(MMA)_{58}(F6MA)_2$ with molar fractions of $\varphi_1$ and $\varphi_2$, respectively.

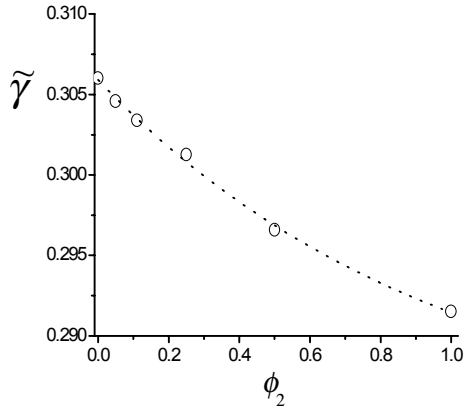


**Figure 5.8** The influence of blend composition on the surface energy as analyzed by the SCF model.

From Figure 5.8 it can be seen that the surface tension $\tilde{\gamma}$ gradually decreases with increasing amount of $MMA_{58}F6MA_2$ in the blend (open circles). The points at $\varphi_2 = 0$ and $\varphi_2 = 1$ represents monodisperse systems but all point at intermediate values of $\varphi_2$ represent polymers that are polydisperse in composition. In Figure 5.2 the dotted line through the SCF results represents the dependence of $\tilde{\gamma}$ for regular polymers, mono-disperse in composition. It appears that the dotted line from Figure 5.8 perfectly overlaps with the line through the monodisperse polymers in Figure 5.2. This suggests that slight polydispersity in composition for regular copolymers do not lead to drastic reduction in surface tension.

### 5.4.5 Chain Architecture

As seen in the previous sections the influence of both polydispersity of molecular weight and chemical composition is not large enough to account for the differences between the SCF analyses and the experimental data in the surface tension at low F6MA content in the

polymer. Generally, random copolymers are hetero-disperse in composition. Moreover, the sequence of monomer units along the chain may not be ideally random; any composition drift along the chain will give the copolymer, to some extent, the character of a pseudo-block copolymer.

In the SCF analysis so far only regular copolymers were considered. In this section the influence of non-regularity of the distribution of the F6MA monomers along the chain will be investigated, *viz*. the influence of blockiness. Two parameters of blockiness will be studied (i) the length of the block and (ii) the position of the block in the polymer chain. The first F6MA unit in the block defines the position in the chain. Thus in the polymer *b*-$(MMA)_8(F6MA)_5(MMA)_{47}$ the block of 5 F6MA units starts at position 9 of the polymer chain.

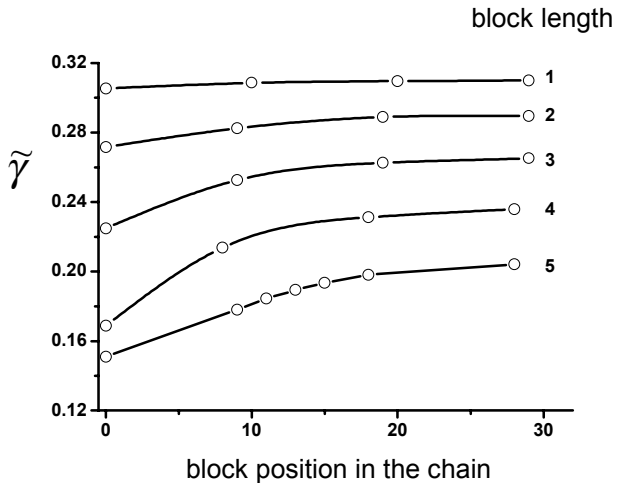


**Figure 5.9** Influence of the size and chain position of blockiness on the surface tension of the polymer melt.

A dramatic effect on the surface tension is observed when blockiness is introduced into the polymer chain (Figure 5.9). Upon changing the chain architecture from r-$(MMA)_{55}(F6MA)_5$ to b-$(MMA)_{55}(F6MA)_5$ a reduction in $\tilde{\gamma}$ was observed from 0.264 (Figure 5.2) to 0.151.

When analyzing the effect of blockiness in more detail (Figure 5.9) we observe that upon changing the block position for each block from the end to the middle, a gradual increase in $\tilde{\gamma}$ occurs. Furthermore it can be seen that increasing the block length leads to a decrease of the surface tension. The effects of polydispersity in architecture on the surface tension of the polymer melt can therefore well explain the difference between the SCF and experimental data as shown in Figure 5.2.

It is shown that the surface conformation of the partially fluorinated polymethacrylates is dominated by the large affinity of fluorine towards the liquid-vapor interface. In Figure 5.10 the density profiles are given for three different polymer architectures with the same overall composition. It can be seen that three morphology transitions can be observed. A single fluorine enriched layer in the liquid-vapor interface is found for the polymer *r*-$(MMA)_{55}(F6MA)_5$. The enrichment is followed by a depletion zone similar as was observed for *r*-$(MMA)_{57}(F6MA)_3$ in Figure 5.3. When the five F6MA segments are grouped together in the middle of the polymer chain an interesting oscillatory density profile is found. These oscillations arise from the preference of the fluorinated moieties for the surface. In this density profile the tendency towards surface-induced ordering of a lamellar phase is already very strong. Moreover, the surface ordering suggests that the system is close to a microphase separation transition (MST). Indeed, microphase separation in the bulk can be observed when the fluorinated block is placed at the end of the polymer chain (Figure 5.10c). Here a completely ordered bulk with lamellae parallel to the surface is visible.

## 5.5 DISCUSSION

The SCF theory predicts a non-linear dependence of the surface tension of a polymer melt as a function of the degree of fluorination of the chains. When the perfluoroalkyl side chains are regularly distributed along the chain, it was found that the theory strongly underestimated this non-linearity as compared to experimental data. It is noteworthy that for all regular compositions the polymer melt remains homogeneous. A significant change in physical behavior is observed when the fluorinated units were grouped together forming a blocky molecule. This change is seen both in the surface tension as well as in the (surface) structure. Already at a low degree of fluorination (small blocks) the surface tension is significantly reduced as compared to the regular case. On top of this, it was found that the polymer melt does not necessarily remain homogeneous. These two aspects are of interest both from a theoretical as well as a practical point of view. The effect of blockiness may explain the disparity between the theoretical and experimental data for the surface tension as a function of the amount of perfluoroalkyl side chains in the molecule. In random copolymers it should be expected that some type of blockiness exists, and therefore the surface tension in the experimental systems is probably strongly affected by the preferential

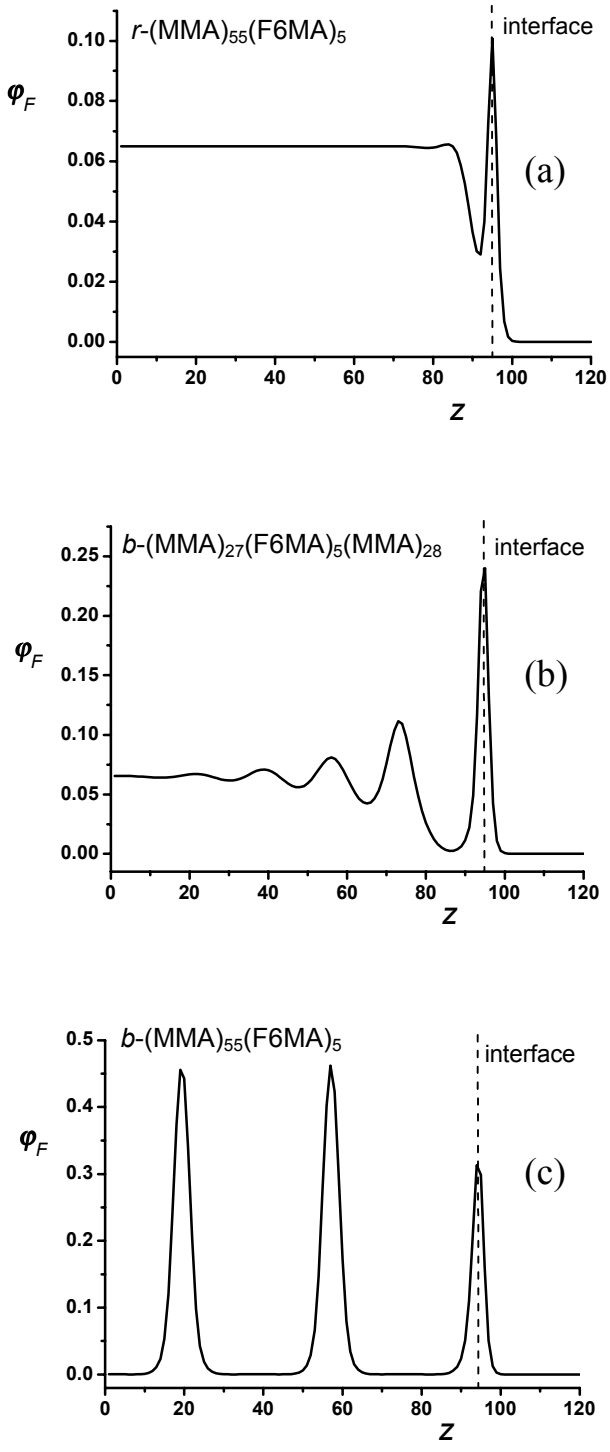


**Figure 5.10** Density profiles of $\varphi_F$ for the polymers, (a) *r*-$(MMA)_{55}(F6MA)_5$, (b) *b*-$(MMA)_{27}(F6MA)_5(MMA)_{28}$, and (c) *b*-$(MMA)_{55}(F6MA)_5$, respectively.

adsorption of a chain with a blocky-nature. The results also show that there is a non-monotonous effect on the stability of the melt with respect to microphase segregation on the length of the fluorine block. Both for very small blocks as well as for very long blocks the bulk will remain homogeneous, whereas for intermediate cases an inhomogeneous bulk may be found.

From a practical point of view the results are of interest to translate the phenomena described above into ways of making useful structures in polymer thin films. In this respect the use of surface-driven phase separation seems to be an attractive strategy to make coatings, whose surface properties are different from those of the bulk. The final result will then be a stratified film where the fluorinated species have formed a layer facing the coating-air interface. The design of such self-stratifying coatings offers some principal advantages. The first is the economic advantage of effectively applying two coatings in one operation and minimize the necessary amount of expensive perfluorinated materials to create a fluorinated surface. Secondly, the intercoat adhesion is supposed to be improved. The ultimate goal is to make an ideal coating that combines the best bulk properties with the optimized surface properties. Both in Chapter 6 and Chapter 7 this strategy has been employed in an epoxy formulation and a liquid oligoester system, respectively.

## 5.6 CONCLUSIONS

In this Chapter a molecular-level self-consistent-field theory was used to analyze physical and thermodynamic properties of partially fluorinated methacrylate chains in the vicinity of the polymer-vapor interface. A general formalism was developed for branched polymer systems within the SCF model of Scheutjens-Fleer, which was applied to polymer melt-vapor interfaces. Calculations showed that introduction of the perfluorinated side-chain leads to a significant reduction of the surface tension. However, for random copolymers the calculated reduction in the surface tension is less pronounced than that observed experimentally.

A number of polymer parameters were investigated to study their influence on the surface tension. Chain length variations, obeying the empirical LeGrand-Gaines relationship, as well as polydispersity in chemical composition were found to have only a small effect on the SCF results. However, the influence of chain architecture on surface properties appeared to be substantial. Blocky arrays of F6MA units reduce the surface tension to a large extent. Strong effects of the position of the block (end or middle) and the size of the block could be

observed. Introduction of blockiness also plays a significant role in the surface composition of these polymers, leading in extreme cases to microphase separation of the bulk with lamellae parallel to the surface.

From the scaled density profiles of the regular copolymers it was observed that the fluorinated tail is located predominantly at the boundary of the interface. For reasons of conformational entropy, the $CF_3$ segments are preferably present in the interface compared to the $CF_2$ segments. Furthermore, it was found that the depletion layer thickness was linearly related to the square root of *m* (the ratio of the number of units of MMA over F6MA), showing the Gaussian characteristics of the MMA fragment between two F6MA units.

The SCF analyses for partially fluorinated polymethacrylates can be improved by considering flexibility constraints as a function of the grafting density for comb-like polymer chains. Some of these aspects have been described previously showing a preferred enrichment of the 'stiffer' chains in blends of polymer melts, which has been explained by entropic effects: the stiffer polymers lose less entropy when adsorbing at the interface than the flexible ones.[38]

## 5.7 REFERENCES


1 a) Pan, D. H.; Prest, J. W. M. *J. Appl. Phys*. **1985**, 28, 8621. b) Bhatia, Q. S.; Pan, D. H.; Koberstein, J. T. *Macromolecules* **1988**, 21, 2166. c) Jones, R. A. L.; Norton, L. J.; Kramer, E. J.; Bates, F. S.; Wiltzius, P. *Phys. Rev. Lett***. 1991**, 66, 1326.

2 a) Siow, K. S.; Patterson, D. *J. Chem. Phys.* **1973**, 74, 356. b) Ober, R.; Paz, L.; Taupin, C.; Pincus, P.; Boileua, S. *Macromolecules* **1983**, 16, 50.

3 a) Shull, K. R.; Kramer, E. J. *Macromolecules* **1990**, 23, 4769. b) Shull, K. R.; Kramer, E. J.; Hadziioannou, G.; Tang, W. *Macromolecules* **1990**, 23, 4780. c) Liebler, L. *Macromol. Chem., Macromol. Sym*. **1988**, 16, 1.

4 Wu S. *Polymer Interface and Adhesion*; Marcel Dekker: New York, 1982; Chapter 3.

5 Krupers, M.; Slangen, P. J.; Möller, M. *Macromolecules* **1998**, 31, 2552.

6 Höpken, J.; Möller, M. *Macromolecules* **1992**, 25, 1461.

7 Pospiech, D. U.; Jehnichen, D.; Häußler, L.; Voigt, D.; Grundke, K.; Ober, C.; Körner, H.; Wang, J. *Polym. Prepr. (ACS)* **1998**, 39, 882.

8 Bouteiller, V.; Garnault, A. M.; Teyssié, D.; Boileau, S.; Möller, M. *Polym. Int*. **1999**, 48, 765.

[9] Schmidt, D. L.; Coburn, C. E.; DeKoven, B. M.; Potter, G. E.; Meyers, G. F.; Fischer, D. A. *Nature* **1994**, 368, 39.

[10] Elman, J. F.; Johs, B. D.; Long, T. E.; Koberstein, J. T. *Macromolecules* **1994**, 27, 5341.

[11] Kassis, C. M.; Steehler, J. K.; Betts, D. E.; Guan, Z.; Romack, T. J.; DeSimone, J. M.; Linton, R. W. *Macromolecules* **1996**, 219, 3247.

[12] Thomas, R. R.; Anton, D. R.; Graham, W. F.; Darmon, M. J.; Sauer, B. B.; Stika, K. M.; Swartzfager, D. G. *Macromolecules* **1997**, 30, 2883.

[13] Iyengar, D. R.; Perutz, S. M.; Dai, C-A.; Ober, C. K.; Kramer, E. J. *Macromolecules* **1996**, 29, 1229.

[14] Genzer, J.; Sivaniah, E.; Kramer, E. J.; Wang, J.; Körner, H.; Char, K.; Ober, C. K.; DeKoven, B. M.; Bubeck, R. A.; Fischer, D. A.; Sambasivan, S. *Langmuir* **2000**, 16, 1993.

[15] Chapter 4 of this thesis.

[16] Lüning, J.; Stöhr, J.; Song, K. Y.; Hawker, C. J.; Iodice, P.; Nguyen, C. V.; Yoon, D. Y. *Macromolecules* **2001** *34,* 1128; and references therein.

[17] Van der Linden, C. C.; Leermakers, F. A. M.; Fleer, G. J. *Macromolecules* **1996**, 29, 1000.

[18] Scheutjens, J. M. H. M.; Fleer, G. J. *J. Phys. Chem*. **1979**, 83, 1619.

[19] Scheutjens, J. M. H. M.; Fleer, G. J. *J. Phys. Chem*. **1980**, 84, 178.

[20] Binder, K. *Monte Carlo and Molecular Dynamics in Polymer Science*; Oxford University Press: Oxford, 1995.

[21] a) Edwards, S. F. *Proceedings of the Physical Society, London* **1965**, 85, 613. b) Dolan, A. K.; Edwards, S. F. *Proceedings of the Royal Society, London, A* **1974**, 337, 50.

[22] Fleer, G. J.; Scheutjens, J. M. H. M.; Cohen Stuart, M. A.; Cosgrove, T.; Vincent, B. *Polymers at Interfaces*; Elsevier: London, 1993.

[23] Leermakers, F. A. M.; van Male, J.; Skvortsov, A. M. *Macromolecules* **2001**, 34, 8294.

[24] Leermakers, F. A. M.; Scheutjens, J. M. H. M. *J. Phys. Chem*. **1988**, 89, 3264.

[25] Theodorou, D. N. *Macromolecules*, **1988**, 21, 1391.

[26] Schlangen, L. J. M.; Koopal, L. K.; Lyklema, J. *J. Phys. Chem. B* **1996**, 100, 3607.

[27] It will influence details and it will keep the physical interpretation of the phenomena observed and described intact *e.g.* it is well know that $CF_3$ is more surface active than $CF_2$.

[28] Zisman, W. A. *Contact Angle, Wettability, and Adhesion*; American Chemical Society; Washington DC, 1964.

[29] Bates, F. S. *Science*, **1991**, 251, 898.

[30] Sauer, B. B.; Dee, G. T. *J. Colloid Interface Sci*. **1994**, 162, 25.

[31] LeGrand, D. G.; Gaines Jr., G. L. *J. Colloid Interface Sci*. **1969**, 31, 162.

[32] Poser, C. I.; Sanchez, I. C. *J. Colloid Interface. Sci*. **1979**, 69, 539.

[33] Cahn, J. W.; Hilliard, J. E. *J.Chem. Phys*. **1958**, 28, 258.

[34] De Gennes, P. G.; *Acad, C.R. Acad. Sci. II* **1988**, 307, 1841.

[35] Theodorou, D. N. *Macromolecules* **1988**, 21, 1411.

[36] Kumar, S. K.; Jones, R. L. *Adv. Colloid Inter. Sci*. **2001**, 94, 33.

[37] Jalbert, C.; Koberstein, J. T.; Yilgor, I.; Gallagher, P.; Krukonis, V. *Macromolecules* **1993**, 26, 3069.

[38] Yethiray, A.; Kumar, S.; Hariharan, A.; Schweizer, K.S. *J. Chem. Phys*. **1994**, 100, 4691.

# Chapter 6

# Fluorinated Epoxy Films


## 6.0 ABSTRACT

*A route towards low surface tension films in epoxy-amine coatings is described. Low surface tension could be obtained by the incorporation of small quantities of perfluorinated species, which become enriched in the coating-air interface after application. The fluorinated species are covalently bonded to the epoxy matrix due to their epoxy functionality. As the amount of the fluorinated species increases, the surface tension decreases and values as low as 9.3 mN/m can be reached depending on the chain-length of the perfluorinated epoxide. These low surface tensions indicate a highly ordered structure in the surface of the perfluoroalkyl tails perpendicular to the substrate. The surface enrichment was verified by angle-resolved XPS showing an enrichment in fluorine of more than an 80 fold excess compared to the theoretical bulk concentration.*

## 6.1 INTRODUCTION

In the past several practical approaches have been explored for the modification of polymer surfaces, including chemical reactions, graft copolymerizations, blending, plasma treatments, corona discharge treatments, grafting reaction, and the adsorption of block-copolymers.[1] In particular, fluorinated surfaces have gained considerable interest because of the advantageous surface properties induced by the fluorine, as known for polytetrafluoroethylene (PTFE). A drawback of conventional perfluorinated polymers is their poor solubility in common organic solvents, which renders them intractable materials. An example is the use of polytetrafluoroethylene (PTFE) in coatings formulations.[2] Despite the high inertness and the low surface energy, the application is limited to aqueous PTFE dispersions and fusion at high temperatures. When PTFE is added to a coating system as a powder the surface of the coating will not be completely covered with PTFE, leading to regions with different surface tensions. Because of these heterogeneities in the surface many advantageous properties of fluorinated polymers are not attained to a full extent.[3] Besides, the reduced friction coefficient and surface energy of such a coating material is temporary since the material is only *physically* covered by the PTFE particles.

In this Chapter a new coating system based on a conventional epoxy resin is described. Epoxy resins have been extensively used in paints, electronic parts, composite materials, and adhesives.[4] Blending the epoxy matrix with high-performance thermoplastics like polyetherimides,[5] polyethersulfones,[6] and poly(methyl methacrylate),[7] has been carried out to obtain materials with improved mechanical properties. Peroxides are often added to coating formulations to improve adhesion.[8]

Here an interesting concept of surface modification is explored by introducing small amounts of fluorinated species with an epoxy functionality into a chemically curing epoxy-amine coating system. After film application the lower-energy species will migrate towards the coating-air interface due to the low surface tension of the fluorinated epoxy. This system is not only interesting from a fundamental point of view but also technologically attractive: an inexpensive bulk material with a fluorinated surface can be provided in an easy way.

The surface enrichment of these fluorinated epoxides has been characterized by several techniques including contact angle measurements and X-ray photoelectron spectroscopy. Subsequently, we monitored the curing reactions by Raman spectroscopy and reactive rheology in order to discriminate whether the surface modification by the fluorinated species was thermodynamically driven or kinetically controlled.

The strategy to use small molecules to realize a permanent surface modification is related to the concept of surface modification described by Torstensson *et al*.[9] and others.[10,11] These researchers introduced small photo-polymerizable perfluorinated surfactants into a photo-crosslinkable matrix to ensure a permanent surface modification.

## 6.2 EXPERIMENTAL

### 6.2.1 Materials

A diglycidyl ether of bisphenol-A (DGEBA, Epikote 828, epoxy equivalent weight (EEW) ≅ 187) was used as epoxy resin and supplied by Shell, Amsterdam, The Netherlands. As curing agent a propyleneoxide diamine [Jeffamine D230, Huntsmann, amine-hydrogen equivalent weight (AHEW) = 60] was used. The reagents (2,2,3,3,4,4,5,5,6,6,7,7,7-tridecafluoroheptyl)oxirane (EP-F6), [2,2,3,3,4,4,5,5,6,7,7,7-dodeca-fluoro-6-(trifluoromethyl)heptyl]oxirane (EP-F7), (2,2,3,3,4,4,5,5,6,6,7,7,8,8,9,9,9-heptadecafluorononyl)oxirane (EP-F8), 2,2,3,3,4,4,5,5,6,6,7,7,8,9,9,9-hexadecafluoro-8-(trifluoromethyl)nonyl]oxirane (EP-F9), and (2,2,3,3,4,4,5,5,6,6,7,7,8,8,9,9,10,10,11,11,11-heneicosafluoroundecyl)oxirane (EP-F10) were purchased from Aldrich and used as received. The chemical formulas of the perfluorinated epoxides are given in Figure 6.1.

### 6.2.2 Sample Preparation

Fluorinated epoxides (Figure 6.1) were mixed in various weight ratios with Epikote-828. Firstly, a fluorinated prepolymer was prepared by reacting Jeffamine-230 (a known excess) with a small amount of fluorinated epoxide at 100 °C. In this step the fluorinated epoxide was chemically bonded to the Jeffamine-230 as confirmed by $^{1}$H-NMR and IR. Subsequently, the fluorinated prepolymer, Epikote-828 and Jeffamine-230 (ratio epoxy/NH was kept at 1:1) were mixed together with 10 wt% of toluene. This mixture was exposed to ultrasound for five minutes to remove air that may otherwise result in bubbles during epoxy solidification. Finally, the mixture was cast on aluminum panels with a 100 μm wet thickness and cured immediately for two hours at 100 °C. Under these conditions smooth transparent films with a layer thickness between 50-60 μm were obtained.

The direct addition of the fluorinated epoxide to an Epikote-828/Jeffamine formulation appeared to be less successful, as the cured films exhibited a large amount of surface defects.

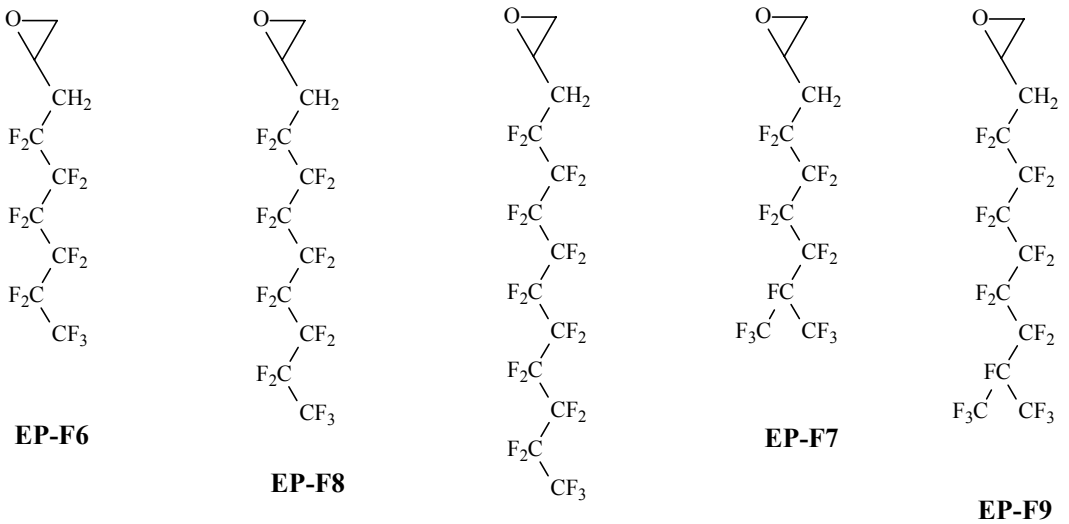


**Figure 6.1** Chemical structures of the fluorinated epoxides used.

### 6.2.3 Surface Techniques

The experimental considerations for contact angle measurements and XPS are described in Section 2.5.

### 6.2.4 Surface Tension Calculations

The surface tensions of the modified epoxy films were determined by the geometric mean method of Owens and Wendt,[12] using the advancing angles of the wetting liquids.[13] The surface tensions of the wetting liquids ($\gamma_{lv}$) used as well as their polar ($\gamma_{lv}^{p}$) and dispersive components ($\gamma_{lv}^{d}$) are listed in Table 6.1.

**Table 6.1** Surface tension components for the wetting liquids used

| Wetting Liquid | $\gamma_{lv}^{t}$ (mN/m) | $\gamma_{lv}^{p}$ (mN/m) | $\gamma_{lv}^{d}$ (mN/m) |
|---|---|---|---|
| deionized water | 72.8 | 51.0 | 21.8 |
| diiodomethane | 50.8 | 2.3 | 48.5 |

### 6.2.5 Atomic Force Microscopy

Cured epoxy coatings were examined by using tapping mode AFM on a Digital Instrument Nanoscope III Scanning Probe Microscope, with NT-MDT non-contact ultra sharp silicon cantilevers coated by gold (Digital Instruments, Inc., Santa Barbara, California). These probes have a stiffness of 11 N/m and a resonance frequency in the range of 200-230 kHz. During the measurements, the tip goes over the surface with the cantilever vibration near the resonance frequency. Height, amplitude and phase images were recorded simultaneously in every scanning circle.

### 6.2.6 Raman Spectroscopy

The epoxy-amine reaction was on-line monitored by Raman Spectroscopy, using a Dilor Labram Raman spectrometer, equipped with a Milennia II doubled Nd:$YVO_4$ laser (Spectra Physics) with an excitation wavelength of 532 nm and operating at a power of 0.2 W. The spectrometer was equipped with a 1800 grooves/mm holographic grating. Combined with a 1024×256 pixel CCD detector resolutions (spectral spacing) of 0.14 nm (approximately 1.5 $cm^{-1}$) were realized. For the measurements, a 10× magnification (Olympus) was used. The spectra were locally corrected with a staight baseline and further analyzed in an in-house developed LabVIEW program.[14] The extent of the curing reaction, $E$, during the network formation can be derived from the ratio of the integrated Raman intensities of the epoxy band $I_e$ and a reference band $I_r$ according to:

$$E = 1 - \frac{I_e(t) I_r(t_0)}{I_r(t) I_e(t_0)} \tag{6.1}$$

## 6.3 RESULTS AND DISCUSSION

### 6.3.1 Surface Tension of Starting Materials

To achieve surface segregation, a difference in surface tension of the components is necessary. From the classical Gibbs adsorption law it follows that in multi-component systems the surface will be preferentially enriched with the component with the lowest surface tension. This principle also applies to the epoxy-amine system.

The surface activity of the monomers is dependent on their amphiphilic structure and in particular on the balance of hydrophobic-hydrophilic groups. In order to give an indication of the surface activity of the different monomers, their surface tensions were determined using

the Wilhelmy plate method. In addition also an estimation of the surface tension was made by the so-called group contribution theory (Parachor method).[15] The experimental determined values of the surface tensions of Epikote-828, Jeffamine-230, and EP-F8 were found to be 46.0, 32.7, and 16.7 mN/m, respectively (Table 6.2). Both the experimental determined surfaces tensions as the theoretical estimated values by the Parachor method are in good agreement with each other.

The prepolymer was prepared by reacting the fluorinated epoxide with a large, but known, excess of Jeffamine-230. The excess is very important to ensure that still NH groups are available for the cross-linking reaction. The 'prepolymer' prepared by EP-F8 epoxide showed a decrease of the surface tension with an increasing amount of wt% EP-F8 (Table 6.3). Adding only 0.14 wt% of EP-F8 the surface tension decreases by more than 3 mN/m.

**Table 6.2** Surface tension of the components used at 20 °C.

| | Epikote-828 (mN/m) | Jeffamine-230 (mN/m) | EP-F8 (mN/m) |
|---|---|---|---|
| Wilhelmy Plate | 46.0 | 32.7 | 16.7 |
| Parachor estimation | 46.6 ± 3.0 | 34.3 ± 3.0 | 17.0 ± 3.0 |

The same trends in surface tension, as shown in Table 6.2 and 6.3, can be expected for the other epoxides, EP-F6, EP-F7, EP-F9 and EP-F10. Having established a difference in surface tension for the modified Jeffamine-230, the surface segregation of fluorinated species was investigated by making formulations with the modified Jeffamine-230.

**Table 6.3** Surface tension of the different prepolymers based on EP-F8.

| wt % of EP-F8 | 0 | 0.14 | 0.21 | 0.65 | 1.01 | 2.13 | 3.04 | 4.09 |
|---|---|---|---|---|---|---|---|---|
| Surface Tension (mN/m)[a] | 32.7 | 29.5 | 28.7 | 26.8 | 26.0 | 25.0 | 24.6 | 24.4 |

[a] measured by the Wilhelmy plate at 20 °C

### 6.3.2 Surface Tension of the Epoxy Films

Interesting results were obtained for the wetting behavior of Epikote-828 epoxy films containing EP-F8 and EP-F10 in various concentrations in the epoxy matrix (Figure 6.2a,b). The advancing contact angle data for deionised water clearly points to hydrophobic surfaces

that are completely different from the film of pure Epikote-828 with an advancing contact angle of water of 76°. When the fluorinated epoxides were added, the wettability of the cured film decreased gradually with increasing fluorinated epoxide concentration. It is remarkable that only a relatively small difference (3.2 mN/m) in surface tension of the components (see Table 6.3) can already lead to a significant fluorine-enrichment in the surface of the cured films.

The dependence of $\theta_{H_2O}$ on the amount of EP-F8 for the modified Epikote-828 is depicted in Figure 6.2a. It can be seen that at a fluorine concentration of about 1.5 wt% the $\theta_{H_2O}$ value reaches a plateau at about 108°, which corresponds to a surface tension of 15.6 mN/m. This value is lower than *e.g.* the surface tension of polytetrafluoroethylene (20.1 mN/m).[16] Higher concentration of EP-F8 (> 3 wt%) leads to severe dewetting in the film. On parts of the film, where the film is still intact a second plateau of $\theta_{H_2O}$ values was found. This sudden increase in the contact angle suggests a different phase behavior at the surface *i.e.* a significant reorganization occurs in these surfaces leading to serious dewetting in the film. On the other hand the dewetted areas were found to be not completely dewetted as indicated by the large contact angle of 106°. This seems to parallel the spreading of a liquid drop on a non-mixing liquid for which it is possible to have lenses and monolayers together in one surface.[17]

At the second plateau contact angles were determined for EP-F8 to be as high as 117.8º and surface tensions as low as 9.3 mN/m. The lowest surface tension obtained for the modified epoxy systems is very close to values of a close-packed perfluoroalkyl surface, which exhibit surface tensions less than 8 mN/m.[18] Although the contact angle data give insufficient information to draw any firm conclusion with respect to orientation of the fluorinated species at the solid-air interface the reduction in the surface tension from 44 to 9.3 mN/m with increasing concentration of the fluoro-epoxide suggests that the perfluoroalkyl chains may be orientated to some extent perpendicular to the surface. Nevertheless, it can be concluded that the introduction of a small amount of perfluorinated epoxide in an epoxy-amine formulation results in a significant modification of the surface.

Dewetting in the Epikote-828 films modified by EP-F10 occurred at about a concentration of 1 wt% of EP-F10. Just before dewetting took place the surface tension of the modified epoxy film was 14.2 mN/m. After dewetting a plateau is reached with a $\theta_{H_2O}$ value corresponding to a surface tension of 9.3 mN/m, similar as for the EP-F8 epoxide.

A comparison of the Figures 6.2a and 6.2b shows that the curve for Epikote-828 modified by EP-F10 exhibits a steeper initial slope than that in the case of EP-F8 modified epoxy films. This suggests that the wetting is also influenced by the chain length of the fluorinated tail.[19] It is interesting to note that the branched epoxide EP-F9 (Figure 6.1), which has a comparable chain length with EP-F8, induces an almost identical dependence of the $\theta_{H_2O}$ values with the concentration of the fluorinated epoxide as EP-F8 does (Figure 6.2c). Also the occurrence of a second plateau at about 120° resembles the behavior of EP-F8. The fact that the $\theta_{H_2O}$ values in the case of EP-F9 are slightly higher than for EP-F8 may be ascribed to the number of $CF_3$ groups per chain at the surface.[20]

In Figure 6.2d fluorinated epoxides of shorter chain length, EP-F6 and EP-F7 (Figure 6.1) are compared to EP-F8. It can be clearly seen that the compounds containing 6-7 fluorocarbons exhibit a completely different behavior. First, the relation between the advancing angles of water and the concentration of the fluorinated epoxide is less pronounced than for EP-F8. In the second place, EP-F6 does not exhibit higher values for $\theta_{H_2O}$ than about 100°, whereas for EP-F7 the plateau value of $\theta_{H_2O}$ (about 108˚) can only be reached at much higher epoxide concentrations than for EP-F8. However, a second plateau for EP-F6 and EP-F7 is not observed. This behavior can possibly be correlated with the smaller tendency to form ordered structures at the solid-air interface, as it is known that the organization of perfluoroalkyl groups at the surface improves with increasing chain length.[19] Similar to the case of EP-F9, the influence of the EP-F7 concentration on the advancing angle of water is more pronounced than for EP-F6, which can also be ascribed to the difference in the number of $CF_3$ groups per perfluoroalkyl chain.

It is important to prove that the perfluorinated epoxides are chemically incorporated into the epoxy-amine network. This was verified by rinsing some of the epoxy films with acetone and 1,1,2-trifluoro-trichloroethane and measuring the wettability of these coatings before and after rinsing. It was found that the differences in contact angles before and after rinsing were negligible (within 1 degree), suggesting that the films are stable and the surface modification is permanent in nature.

The changes introduced into the composition and structure of the surface layer of the epoxy films by adding successively increasing amounts of the fluorinated epoxides can be compared with the behavior of surfactant molecules spreading on a water surface in a Langmuir-Blodgett balance. At low concentrations the surfactant molecules are separate and

move independently in the surface layer, but a decrease in surface area finally results in the formation of an insoluble two-dimensional monolayer of surfactant molecules. If the surface area is further compressed, the surfactant molecules in the monolayer become more closely packed together and coherently orientated towards the surface. Finally, no further compression is possible and the monolayer collapses.

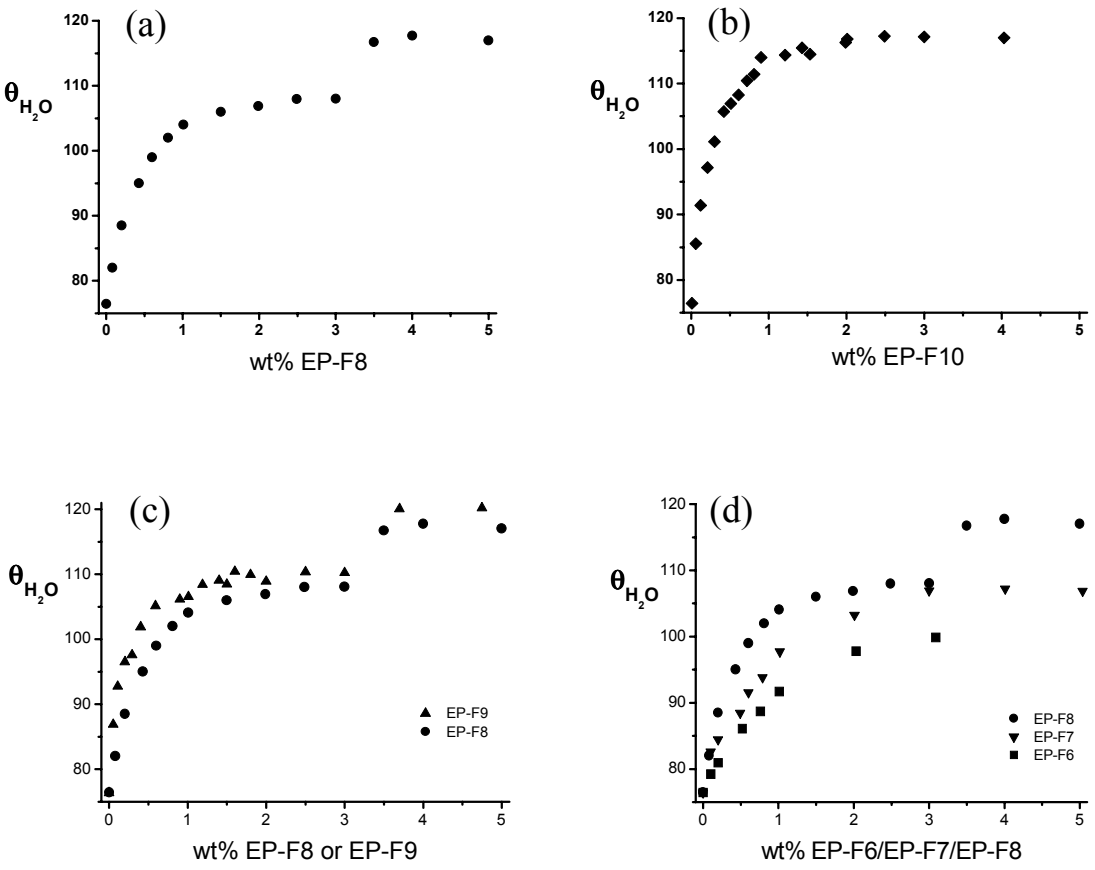


**Figure 6.2** Advancing contact angles (°) of deionized water as function of the amount (wt%) of fluorinated epoxide in the epoxide matrix a) EP-F8 (●); b) EP-F10 (♦); c) EP-F8 (●) and EP-F9 (▲); d) EP-F6(■), EP-F7 (▼) and EP-F8 (●).

From a molecular perspective it could be expected that micro-heterogeneity in the surface is present due to the different nature of the fluorinated tails and the hydrocarbon matrix.[21] However, the interpretation of only advancing contact angles must be taken with care according to Johnson and Dettre.[22] They analyzed the advancing and receding angles on a model heterogeneous surface with water and concluded that relatively small domains of low surface energy species would result in relative high advancing angles accompanied with

relatively low receding contact angles. The contribution of the individual areas of the two surface components is given by the Cassie equation:[23]

$$\cos\theta = f_1 \cos\theta_1 + f_2 \cos\theta_2 \qquad (6.2)$$

where $\theta$ denotes the contact angle of a liquid on the heterogeous surface, $\theta_1$ and $\theta_2$ are the contact angles on each of the components, and $f_1$ and $f_2$ are their respective surface fractions. To study the existence of fluorine enriched domains (micro-heterogeneity) in the surface tapping-mode AFM measurements were conducted.

### 6.3.3 Surface Structures

Tapping mode AFM employs very low contact forces and gives an indirect chemical mapping of the surface with different domain topologies with high lateral resolution.[24] The contrast comes usually from different local stiffness variations of domains at the surface. Sauer *et al.*[25] observed a very fine network of fluorine-rich domain in crosslinked partially fluorinated polyacrylate system. Light domains in the phase images were ascribed to fluorine-rich regions and dark domains to fluorine poor regions. Imaging such domains requires very high lateral resolution, which results from combined effects of sharp tips, low deformation, and high spring-constant cantilevers. Recently, Ming *et al.*[26] observed similar small fluorine-rich domains in the surfaces of partially fluorinated isocyanate-oligoester cured coatings.

Light-tapping force AFM images for the EP-F8 epoxide at different concentration in the epoxy matrix, however, did not show any small domains in the coating-air interface. No significant contrast was observed in both height and phase images indicating that the fluorinated species are relative uniformly distributed at the surface.

### 6.3.4 Surface Composition

The surface enrichment in fluorine of the modified epoxy films was confirmed by XPS results. All spectra were collected at an angle of 0° with respect to the normal to the surface. As a result, the information obtained pertains to regions located within a range of 7.3 nm from the surface. The spectra of the $C_{1s}$ for modified epoxy films with different concentrations of EP-F8 are shown in Figure 6.3. In the spectra of the modified epoxy films, two additional peaks appear around 292 eV and 294 eV. These peaks correspond to carbon atoms bound to fluorine. The peak intensity at 293.6 ± 0.1 eV ($CF_3$ group) and 291.4 ± 0.1 eV

($CF_2$ group) increases at higher concentration of EP-F8 in the coating formulation. Relatively high fluorocarbon signals for the samples with more than 1 wt% of EP-F8 strongly suggest high levels of surface enrichment in perfluorinated species. This important point is addressed further in Figure 6.4. This Figure shows an 80-100 fold surface excess of fluorine compared to theoretical bulk levels. Moreover, the curve has the same shape as that of the contact angle plot in Figure 6.2. This again emphasizes that wettability clearly is correlated to the fluorine concentration in the surface (see also Chapter 4).

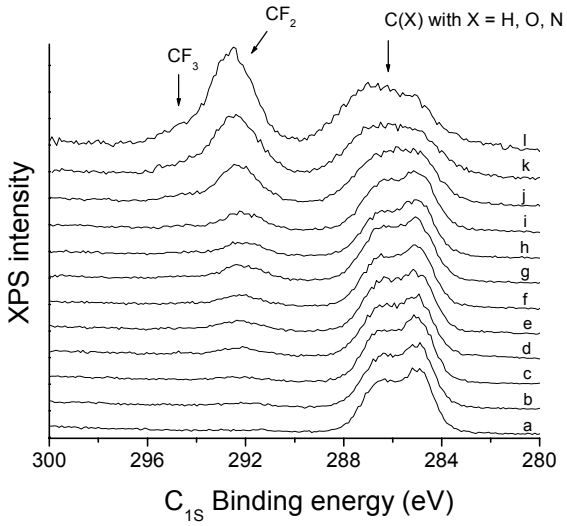


**Figure 6.3** Compositional dependence of the $C_{1s}$ region, as measured by XPS, for a series of epoxy films containing various ratios of the fluorinated epoxide EP-F8. a) 0.0 wt%, b) 0.1 wt%, c) 0.2 wt%, d) 0.4 wt%, e) 0.7 wt%, f) 0.8 wt%, g) 1.0 wt%, h) 2.0 wt%, i) 3.0 wt%, j) 3.5 wt%, k) 4.0 wt%, and l) 5.0 wt%.

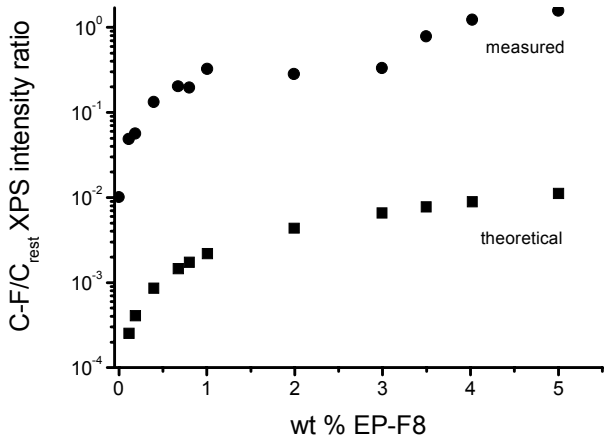


**Figure 6.4** Intensity ratios of $(CF_3 + CF_2)/C_X$ (x = H, O, and N) of $C_{1s}$ XPS spectra of cured epoxy films as a function of the amount (wt%) of EP-F8. ■ represents the theoretical value based on a homogeneous distrubution of EP-F8 in the cured film; ● represents the experimental value.

Figure 6.5 shows the results for angular-resolved XPS experiments on an epoxy film containing 1 wt% of the fluorinated epoxide EP-F10. Six different angles were used, giving access to compositional information over depths from 3.8 to 7.3 nm. These data show that the fluorine concentration is highest at the coating-air interface. Secondly, the profile strongly supports a gradient structure where the fluorine concentration increases going from the bulk to the surface.

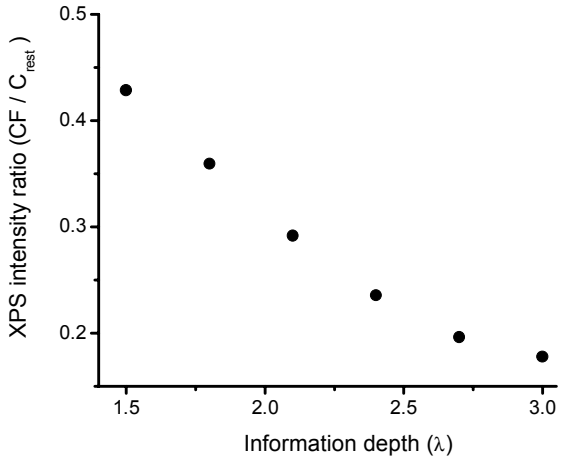


**Figure 6.5** Intensity ratio ($CF_3$ + $CF_2$) / $C_x$ (x = H, O, N) of $C_{1s}$ XPS spectra of cured epoxy films with 1 wt% of EP-F10 as function of information depth ($\lambda$).

### 6.3.5 Network Formation

The epoxy-diamine reaction includes mainly a two-step pathway as given in Scheme 6.1. First, the reaction of the primary amine with the epoxy group leads to the formation of a secondary amine. In the second, rate-determining step the secondary amine reacts with another epoxy group to form a tertiary amine. The third step represents the etherification of an epoxy with a hydroxy group. This etherification reaction can be neglected in the presence of a slight excess of amine.

During the curing process of the epoxides at elevated temperatures, the system changes from a low-molecular weight liquid to a highly crosslinked network. The mobility of the fluorinated epoxides in the systems, therefore, decreases as the curing reaction proceeds, which influences the surface segregation of fluorinated species. This may result in insufficient time for the surface-active epoxide to migrate through the bulk towards the surface. However, the increased rate of diffusion at higher temperature may compensate for this shorter time-period.

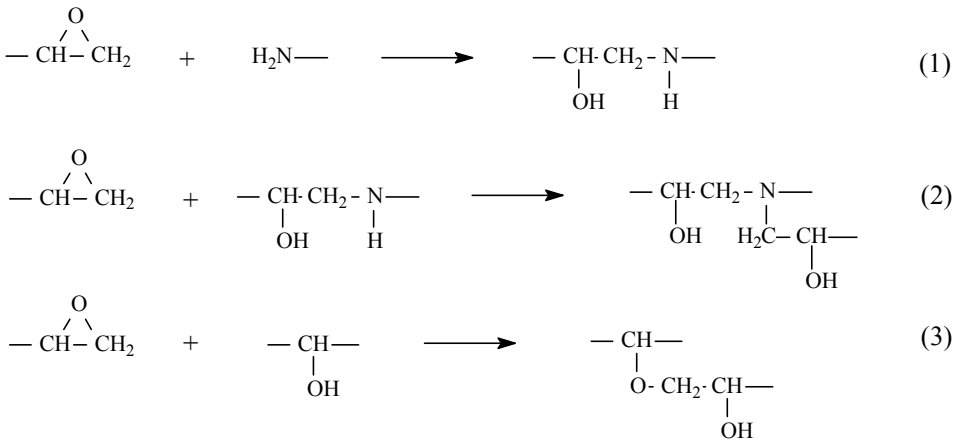

**Scheme 6.1**

To study the influence of the two opposite effects on the surface enrichment with fluorine, curing reactions were carried out at three different temperatures: 80, 100, and 120 ºC. The conversion of the curing reaction and the development of the change in viscosity was followed online by Raman spectroscopy and viscosity measurements, respectively.

For the determination of the conversion of the epoxy-amine reaction, the integrated area of the stretch vibration of the epoxy at 1270 $cm^{-1}$ was monitored in time.[27] As internal standard the aromatic ring vibration at 1610 $cm^{-1}$ was chosen.[28] Figure 6.6 shows the conversion as a function of the cure time at three different temperatures for stoichiometric Epikote-828/Jeffamine-230 formulations. Increasing the curing temperatures by twenty degrees results in an increase in the final conversion of more than 10 %. More interesting is the observation that the crosslinking reaction proceeds very rapidly in the first 5-10 min, with the highest reaction rate between the epoxides and the amines at 120 °C. As a direct consequence, the viscosity of the system became very high in a short period of time when compared to the case where a curing temperature of 80 °C was used. This can also be observed in Figure 6.7, where the dependence of the steady state viscosity ($\eta$) during isothermal curing reactions with a stoichiometry between epoxide and amine is shown. It can be seen that the viscosity of the system increases strongly in time, due to the change of the molecular weight of the system. From Figure 6.7 it can be determined that the viscosity increases by orders of magnitude within about 2 minutes. This corresponds with a conversion less than 10 % as found by Raman spectroscopy. Therefore it is very unlikely that diffusion of the fluorinated epoxide towards the surface takes place during curing *i.e.* the results suggest that the surface enrichment of the fluorinated species takes places already shortly after application. Contact angle measurements of water of the cured films confirm this statement

because the advancing angle remained unaffected by the different curing temperatures. The combined effects show that the diffusion of the surface-active fluorinated epoxide is apparently high.

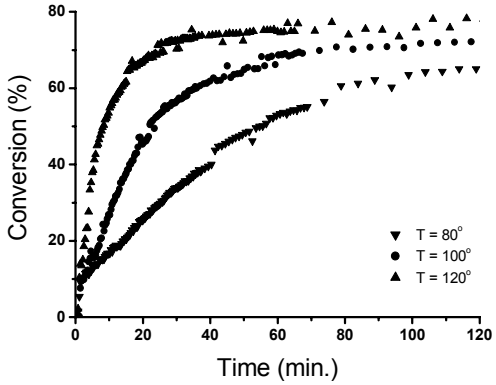


**Figure 6.6** Epoxy conversion (%) as a function of curing time at T = 80, 100, and 120 ◦C for stoichiometric Epikote-828/Jeffamine-230 formulations followed by Raman spectroscopy.

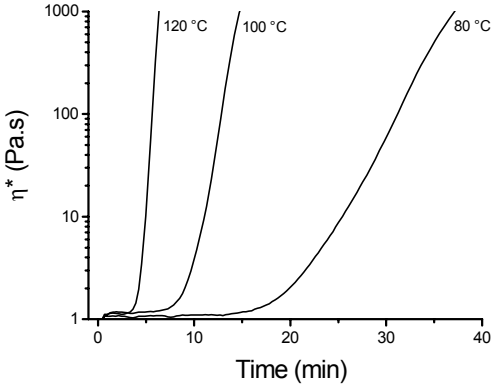


**Figure 6.7** Steady shear viscocity $\eta$ (Pa.s) (1Hz) as a function of curing time at T = 80, 100, and 120 ◦C for stoichiometric Epikote-828/Jeffamine-230 formulations.

## 6.4 CONCLUSIONS

The route described in this Chapter opens an interesting way to a permanent surface modification with very small amounts of fluorinated epoxides. The perfluorinated epoxides can easily be incorporated into a thermally cured, epoxy/amine coating system. Before being incorporated into the epoxy matrix, the perfluorinated epoxides are able to enrich the air-coating interface significantly. This segregation at the air-coating interface is confirmed by contact angle data and XPS measurements. Through a judicious choice of the fluorinated components it is possible to control the surface tension of the final cured epoxy film. By varying not only the type of fluorine epoxides but also their amounts, a large variety of low surface tension epoxy films can be obtained. The covalently bonded fluorinated species in the coating-air interface reduce the surface energy of the material tremendously, while keeping the bulk properties unchanged as observed by angle-resolved XPS data on the films.

As stated by Thomas *et al*.[29] the surface excess of fluorine and the gradient normal to the surface determine the ultimate repellency and durability of coatings. It is therefore expected that these modified epoxy coatings would have excellent properties as packing materials for (micro)electronic components.

## 6.5 REFERENCES


[1] Chan, C-M. *Polymer Surface Modification and Characterization*; Hanser Publisher: Munich, 1994.

[2] Livigni, R. A.; Melby, E. G.; Hargis, I. G.; Vitus, F. J. *US Pat.* US5543200.

[3] Anton, D. *Adv. Mater*. **1998**, 10, 1197.

[4] Wick, Jr., Z. W.; Jones, F. N.; Pappas, S. P. in *Organic Coatings; Science and Technology*, 2nd edn., Wiley-Interscience, New York, 1999.

[5] Vanderbosch, R. W. *Processing of Intractable Polymers using Reactive Solvents* PhD Thesis, Eindhoven University of Technology, 1995.

[6] Bucknall, C. B.; Partridge, I. K. *Polymer* **1983**, 24, 639.

[7] Jansen, B. J. P. *Toughening of Glassy Amorphous Polymers via Chemically-induced Phase Separation* PhD thesis, Eindhoven University of Technology, 1998.

[8] Bratychak, M.; Brostow, W. *Polym. Eng. Sci*. **1999**, 39, 1541.

[9] Torstensson, M.; Rimby, B.; Hult, A. *Macromolecules* **1990**, 23, 126.

[10] Schnurer, A. U.; Holcomb, N.R.; Gard, G. L.; Castner, D. G.; Grainger, D. W. *Chem. Mater*. **1996**, 8, 1475.

[11] Ameduri, B.; Bongiovanni, R.; Malucelli, G.; Pollicino, A.; Priola, A. *J. Polym. Sci.: Part A: Polym. Chem*. **1999**, 37, 77.

[12] Owens, D. K.; Wendt, R. C. *J. Appl. Polym. Sci*. **1969**, 13, 1741.

[13] Kwok, D. Y.; Neumann, A. W. *Adv. Colloid Interface Sci*. **1999**, 81, 167.

[14] Van den Brink, M.; Pepers, M.; Van Herk, A. M.; German, A. L. *Polym. React. Eng*. **2001**, 9, 101.

[15] Van Krevelen, D. W. *Properties of Polymers: Their Estimation and Correlation with Chemical Structure*; Elsevier: Amsterdam, 1976; Chapter 8.

[16] Wu, S. *Polymer Interface and Adhesion* Marcel Dekker: New York, 1982; Chapter 3.

[17] Murrel, J. N.; Jenkins, A. D. *Properties of Liquids and Solutions* John Wiley & Sons: Chichester, 1982; Chapter 12.

[18] Chaudhury, M. K.; Whitesides, G. M. *Langmuir* **1991**, 7, 1013.

[19] Corpart, J.-M.; Girault, S.; Juhué, D. *Langmuir* **2001**, 17, 7237.

[20] Zisman, W. A. *Contact Angle, Wettability, and Adhesion,* Advances in Chemistry Series 43, Am. Chem. Soc., Washington DC, 1964.

[21] Rabolt, J. F.; Russell, T. P.; Twieg, R. J. *Macromolecules* **1984**, 17, 2786.

[22] Johnson, R. E., Jr.; Dettre, R. H. in *Wettability* Berg, J. C., Ed.; Marcel Dekker: New York, 1993; Chapter 1.

[23] Cassie, A. B. D. *Discuss. Faraday Soc*. **1948**, 3, 11.

[24] Schönherr, H.; Hruska, Z.; Vancso, G. J. *Macromolecules* **1998**, 31, 3679.

[25] Sauer, B. B.; McLean, R. S.; Thomas, R. R. *Langmuir* **1998**, 14, 3045

[26] Ming, W. *et al*. to be submitted to *Macromolecules*.

[27] Chike, K. E.; Myrick, M. L.; Lyon, R. E.; Angel, S. M. *Appl. Spectr*. **1993**, 47, 1631.

[28] Lin-Vien, D.; Colthup, N. B.; Fateley, W. G.; Grasselli, J. G. *The Handbook of Infrared and Raman Characteristics Frequencies of Organic Molecules*, Academic Press: San Diego, 1991.

[29] Thomas, R. R.; Anton, D. R.; Graham, W. F.; Darmon, M. J.; Sauer, B. B.; Stika, K. M.; Swartzfager, D. G. *Macromolecules* **1997**, 30, 2883.

[30] Part of this work has been published in: Van de Grampel, R. D.; van Gennip, W. J. H.; Wassing, B.; Krupers, M.J.; Laven, J.; Niemantsverdriet, J. W.; van der Linde R. *Polym. Mater. Eng. Sci. (ACS)* **2000**, 83, 305.

# Chapter 7

# Fluorinated Oligoesters


## 7.0 ABSTRACT

*In this Chapter the synthesis of two kinds of liquid oligoesters, linear and three-armed, is described. The oligoesters were synthesized by direct esterification of a mixture of diacids and a diol, and a triol in the case of 3-armed oligoesters. The molecular weights of these oligoesters are in the range of 800 – 1000. Linear oligoesters have a single melting point between -5 to 0 °C while a single glass transition temperature at about -60 °C was found for three-armed oligoesters. The oligoesters were partially end-capped with a perfluoroalkyl group by reacting with perfluoroalkyl acid chloride. Films were prepared from homogeneous mixtures of normal and fluorinated oligoesters and a liquid polyisocyanate crosslinker, and cured at elevated temperatures. As the fluorine content in the films increases from 0 to about 1.4 wt%, the surface tension of the film surface decreases by as much as 20 mN/m, indicating that the surface is mainly occupied by the fluorine-containing species. The surface enrichment with fluorine-containing species is confirmed by X-ray photoelectron spectroscopy (XPS) investigations. The fluorine level of the top 5 nm is about 20-80 fold above its stoichiometric level, whereas the fluorine level at the surface becomes almost saturated at the fluorine content of about 1 wt%. Thus, a fluorine-rich surface with low surface energy can be readily obtained based on solventless liquid oligoester systems.*

## 7.1 INTRODUCTION

Organic polymer films have found wide applications for coating materials. Typical applications include passivation layer, corrosion protection, adhesives, and decorative paints. Due to the large variety of applications, many different coating systems have been developed, for example, acrylic polymers, polyesters, urethanes, alkyds, and epoxy systems.[1] In many applications, it is desirable to modify the surface while maintaining proper bulk properties.

Lowering the surface tension of a coating can result in desirable properties like water and oil repellency, low coefficient of friction, and non-wettable surfaces. Fluorinated polymers can provide a surface with low surface energy.[2-19] This renders fluorine-containing materials very attractive in coatings applications. The fluorine can be incorporated into the main polymer chains,[7-10] or as pendant perfluoroalkyl side chains.[2,4,5,13-20]

However, most of these systems involve the use of solvents, *i.e.*, polymers were synthesized in solution and most of the films were prepared using solvents. The use of organic solvents not only increases application costs, but also gives off volatile organic compounds (VOCs) or hazardous air pollutants (HAPs). Furthermore, some of the synthetic methods employed require more difficult polymerization techniques.[15-20] Additionally, relative high concentrations of fluorinated substances were used.

This work describes an easy approach to prepare oligoesters[21] that are partially end-capped with a perfluoroalkyl group. A thin fluorine-rich top layer can be formed through surface segregation of the fluorinated species at the coating-air interface. The solventless liquid oligoesters can be crosslinked with a polyisocyanate agent, without dealing with any potential problem associated with organic solvents. In addition, the fraction of fluorinated substances for surface modification is not necessarily large. The occurrence of fluorine enrichment in the top surface of the films was examined by contact angle measurements and X-ray photoelectron spectroscopy (XPS). The ultimate goal is to make an ideal coating that combines optimal bulk properties with optimal surface properties.

## 7.2 EXPERIMENTAL

### 7.2.1 Materials

Adipic acid (>99%), glutaric acid (>99%), azelaic acid (about 88%), 1,4-butanediol (>98%), and 1,1,1-trimethyloylpropane (TMP, >99%) were purchased from Merck and used as recieved. Butylchlorotindihydroxide with trademark of FASTCAT 4101 (Atofina, France) was used as catalyst for direct esterification. Perfluoroalkyl agents, like

pentadecafluorooctanoic acid (PFOA, 97%) and perfluorooctanoyl chloride (PFOC, 97%), were purchased from Fluorochem and used as received. A polyisocyanate crosslinker, under the trademark Desmodur N3300 (Bayer AG, Germany) and consisting of isocyanurate trimers of hexamethylene diisocynate, was used as received. Aluminum panels (0.6 × 76 × 152 mm) were purchased from Q-Panel Co, and cleaned with ethanol and acetone prior to use.

### 7.2.2 Synthesis of Oligoesters

Linear oligoesters were synthesized by direct esterification between a mixture of diacids with a diol. A typical synthesis for a liquid oligoesters is given below. For the synthesis of 3-armed oligoesters, an additional triol (TMP) was used.

Linear Oligoester (Oligo-II, see Figure 7.1): To a 500 mL 4-neck flask equipped with a mechanical stirrer, Dean-Stark trap, reflux condenser, thermometer and nitrogen inlet, a mixture of diacids (adipic acid, glutaric acid, and azelaic acid, 0.12 mol each), 1,4-butanediol (0.48 mol), and FASCAT 4101 (0.1 % of total weight of reactants) was added. The temperature was gradually heated to 140 °C, raised further to 200 °C over a period of 3 hours, and then kept at 200 °C until the amount of water collected in the Dean-Stark trap reached 95% of the theoretical amount.

The three-armed oligoester (Oligo-III, see Figure 7.1), based on TMP was prepared in a similar way. The starting mixture consists of 0.1 mol of TMP, 0.3 mol of 1,4-butanediol, and three diacids of 0.1 mol each.

### 7.2.3 Synthesis of Partially Fluorinated Oligoesters

The partially fluorinated oligoesters were prepared by reacting the previously synthesized oligoesters (in excess) with perfluoroalkyl acid (PFOA) or the corresponding acid chloride (PFOC). For example, the three-armed fluorinated oligoester (Oligo-III-F, see Figure 7.1) was prepared by reacting 20 g (about 0.08 mol of hydroxyl groups) of Oligo-III with 5.69 g (0.013 mol) of PFOC. PFOC was added dropwise to Oligo-III in a period of about 3 hours with the temperature rising from 90 to 120 °C. A stream of nitrogen was purged through the reaction mixture to remove HCl that was formed during the reaction. The obtained fluorine content after partial fluorination is 14 wt% as estimated from end group titration (theoretical value is 14.7 wt%).

### 7.2.4 Characterization Techniques.

NMR-spectra were recorded on a Varian 400 spectrometer at 25 ºC, operating at 400.162 MHz for proton, 100.630 MHz for carbon, and 376.487 MHz for fluorine, respectively. $CDCl_3$ was used a solvent and as an internal standard for proton and carbon NMR, $CFCl_3$ was used as an external standard for fluorine NMR.

The hydroxyl number, *i.e.*, the number of mg potassium hydroxide equivalent to the hydroxyl groups in 1 g of material, was determined according to the test method, TM-2432, developed by DSM Resins. In brief, the hydroxyl groups in the oligoester are first acetylated with a known amount of acetic anhydride. The excess anhydride is decomposed with water, and the formed acetic acid is titrated with a methanolic potassium hydroxide solution. The average molecular weight of oligoesters could be deduced from the hydroxyl numbers since chain ends in the oligoesters are hydroxyl groups.

Size Exclusion Chromatography (SEC) analyses were carried out using four Plgel (Mixed-C) columns (Polymer Laboratories) at 40 ºC with a Waters 510 pump. The injection volume was 100 μL using THF as eluent at a flow rate of 1 mL/min. A Waters 410 differential refractometer was applied for detection. Narrow distributed polystyrene standards (Polymer Laboratories) with molecular weights ranging from 580 to $7.1 \times 10^6$ were used to calibrate the SEC setup.

MALDI-TOF MS measurements were preformed on a Voyager-DE Pro (PerSpective Biosysytems, Framingham, MA, USA) instrument equipped with a 337 nm nitrogen laser. Positive-ion spectra were acquired in reflection mode. α-Cyano-4-hydroxycinnamic acid was chosen as the matrix. Oligomer samples were dissolved in tetrahydrofuran (THF) at 2 mg/mL and the matrix at 20 mg/mL; matrix and oligomer solution were mixed afterwards. The MALDI system was calibrated with polythiophene oligomer standards of known molecular weight. The mass accuracy is within ± 0.05 %.

The experimental considerations for contact angle measurements and XPS are described in Chapter 2.5.

### 7.2.5 Film Preparation

A small amount of fluorinated oligoester was mixed with non-fluorinated oligoester at 40 ºC under magnetic stirring. A stoichiometric amount of Desmodur N3300 was added to keep the OH/NCO molar ratio at 1. Subsequently, the mixtures were applied on aluminum

panels with a block applicator and immediately cured at 80 ºC for 30 minutes, resulting in transparent films (layer thickness 20-40 μm).

## 7.3 RESULTS AND DISCUSSION

### 7.3.1 Synthesis and Characterization of Oligoesters

To eliminate the use of organic solvents in preparing coating formulations, one strategy is to synthesize oligoesters by direct esterification between diols or triols and diacids. To ensure that the oligoester is in a liquid state at ambient temperatures, its molecular weight will be targeted at around 1000. Moreover, to reduce the regularity of the ester backbone and, consequently the crystallinity of the resulting oligoester, a mixture of diacids has been used. All the chain ends are hydroxyl groups (see Figure 7.1), which will enable the further cross-linking of oligoester with polyisocyanate. The degree of condensation is controlled stoichiometrically. For example, with a targeted degree of condensation of 3 for Oligo-II, the HO/COOH molar ratio in the starting raw materials would be 4/3 (see Experimental Section).

The partially fluorinated oligoesters were synthesized by dropwise addition of perfluoroalkyl acid chloride to the normal oligoester. The reaction temperature is slightly below the boiling point of the acid chloride agent. It is noteworthy that a fast purging of dry nitrogen is required to remove the produced HCl. The largely excessive amount of normal oligoester and the very slow addition of acid chloride allow to prepare the structure with at most one perfluoroalkyl end group per oligoester molecule. In the case of the fluorinated oligoester based on diol, the linear oligoester molecules will then have on average far more than one hydroxyl group left after partial fluorination. For three-armed oligoester based on triol, at least two hydroxyl groups would remain. In both cases, the remaining hydroxyl groups will react with the isocyanate group during the film formation to ensure that the perfluoroalkyl groups are connected to the cross-linked network.

At the very beginning, it has been also tried to introduce the fluorine into oligoester by using perfluoroalkyl diacids or diols. In these approaches the perfluoroalkyl groups are located inside the main chain of the oligoester. It was found that for these systems the surface tension decrease is much less pronounced than that for the perfluoralkyl end-capped oligoesters. This may be due to two factors: perfluoroalkyl end groups are more efficient in reducing the surface energy than those located in the middle of the chain, and the $CF_3$ group could contribute even more in the decrease of surface tension than the $–CF_2-$ groups.[23]

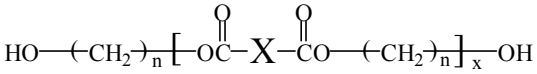

**Oligo-II**

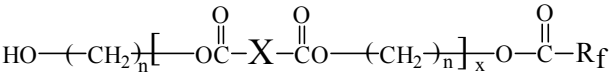

**Oligo-II-F**

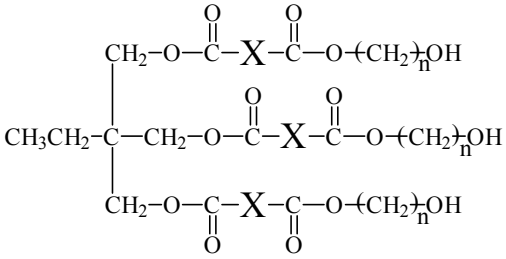

**Oligo-III**

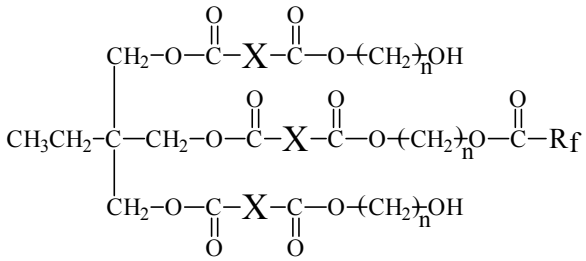

**Oligo-III-F**

n = 4, 6
X = mixture of $(CH_2)_3$, $(CH_2)_4$, and $(CH_2)_7$
$R_f = (CF_2)_mCF_3$

**Figure 7.1** Chemical structures of the synthesized oligoesters

The $^1$H-NMR spectra for Oligo-II and its fluorinated counterpart (Oligo-II-F, see Figure 7.1) are shown in Figure 7.2. The peak at 4.1 ppm corresponds to the protons ($H_\beta$) in the methylene group connected to the ester group (-C$\underline{H_2}$-O-CO-), while the peak at 3.7 ppm is attributed to the proton ($H_\alpha$) in the methylene next to the hydroxy group (-C$\underline{H_2}$-OH). The degree of condensation, $d_C$ ($x$) can be calculated from the peak area ratio of $H_\alpha$ and $H_\beta$.[21]

$$d_C = \frac{area(H_\beta)}{area(H_\alpha)} \tag{7.1}$$

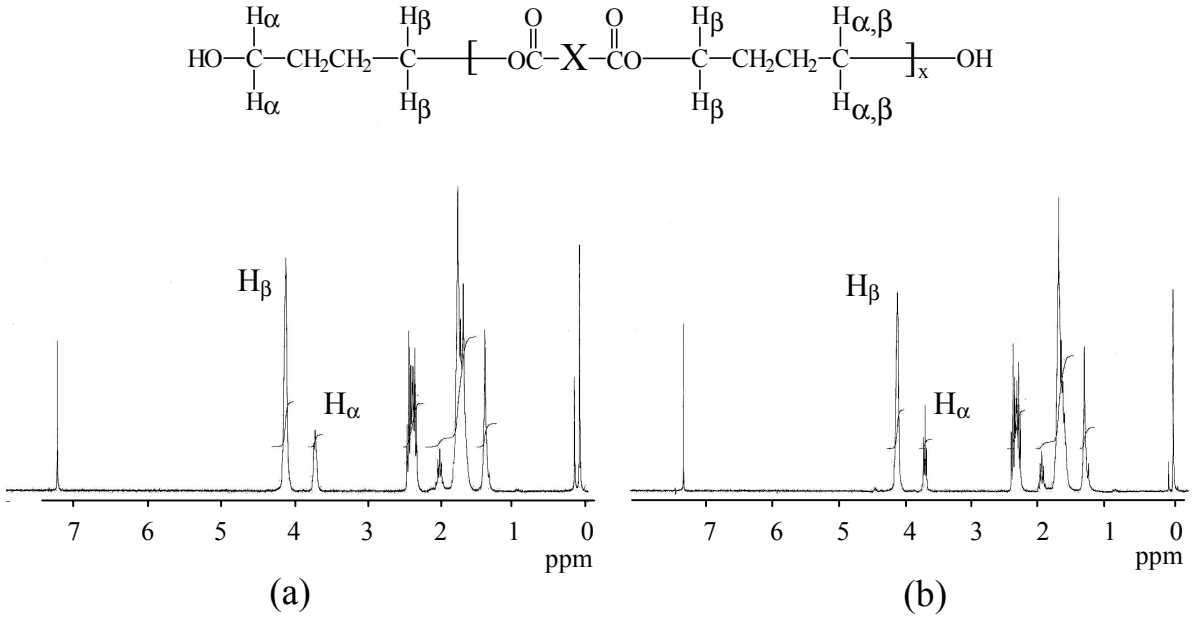


**Figure 7.2** Proton NMR spectra of the linear solventless liquid oligoesters before and after partial fluorination: (a) Oligo-II and (b) Oligo-II-F. Insert indicates position of α and β.

Thus, the average molecular weight ($M_n$) of the oligoester can be calculated by the following equation:

$$M_n = d_C[MW_{(\text{diacid})} + MW_{(\text{diol})} - 2MW_{(\text{water})}] + MW_{(\text{diol})} \tag{7.2}$$

where $MW_{(\text{diacid})}$, $MW_{(\text{diol})}$, and $MW_{(\text{water})}$ are the molecular weights of diacids, diol, and water, respectively. The molecular weight of three-armed oligoesters can be estimated similarly, but the $d_C$ would be half of the ratio of $area(H_\beta)/area(H_\alpha)$. In Table 7.1 the average molecular weights for various solventless liquid oligoesters are listed, ranging from 800 to 1000. The melting points of linear oligoesters are in the range of -5 to 0 °C (a single melting transition), as determined by differential scanning calorimetry (DSC) on a Perkin-Elmer 7 instrument, whereas a glass transition temperature was not observed. For the three-armed oligoester, on the other hand, only one glass transition temperature at –60 °C was detected. A low melting temperature or low $T_g$ is indicative of the liquid state of these oligoesters at ambient temperature.

**Table 7.1** Molecular weights of the solventless liquid oligoesters.

| Oligoester [a] | Area($H_\beta$, 4.1ppm) /Area($H_\alpha$, 3.7ppm) | MW by $^1$H-NMR | Hydroxyl number (mg KOH/g) | MW by titration |
|---|---|---|---|---|
| Oligo-II | 3.7 | 874 | 119 | 939 |
| Oligo-II-F | 4.3 | - | 110 | - |
| Oligo-III | 2.5[b)] | 914 | 184 | 915 |
| Oligo-III-F | 3.1[b)] | - | 137 | - |

[a] Oligo-II and -III represent the oligoesters from diol and triol, respectively; an "-F" means the partially fluorinated oligoester. Oligo-II-F is the product of Oligo-II and PFOA, while Oligo-III-F is the product of Oligo-III and PFOC.

[b] The peak area is the sum of a few split peaks around 4.1 and 3.7 ppm, respectively.

It can be also seen from Figure 7.2 and Table 7.1, that the peak area ratio of $H_\beta$ over $H_\alpha$ shows a small increase after partial fluorination, indicating a few hydroxyl groups have indeed been substituted by perfluoroalkyl carbonyl groups. The small peak at 4.4 ppm corresponds to the product $R_f$-CO-O-C$\underline{H}_2$-.

In order to stoichiometrically match the molar ratio between OH and NCO during curing reaction, the content of hydroxyl groups in the synthesized oligoesters must be known prior to the formulation of the coating films. The hydroxyl number can be readily determined by titration, as described in the Experimental Section. The hydroxyl numbers for several oligoesters before and after fluorination are given in Table 7.1. The molecular weight of oligoesters can also be deduced from the hydroxyl number, considering all chains ends are ended with hydroxyl groups. These MW values are also listed in Table 7.1, which are in good agreement with those determined by $^1$H-NMR.

### 7.3.2 Characterization of Fluorinated Oligoesters

To understand the partial fluorination in detail, a model oligoester (polybutylene adipate, PBA) was synthesized. One out of five hydroxyls was then replaced by a perfluoroalkyl group [$CF_3(CF_2)_6CO$]. Similar as described above, the molecular weight for PBA was determined from $^1$H-NMR and titration of the hydroxyl groups. Both methods yield a number-average molecular weight before partial fluorination equal to 914.

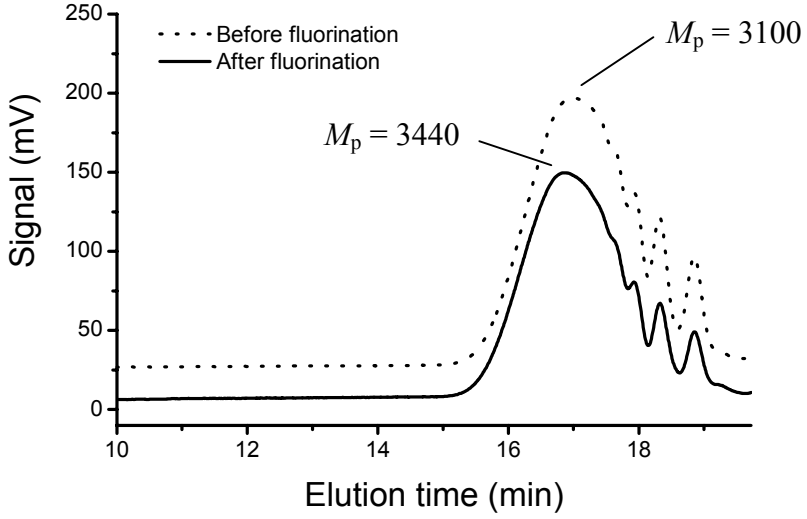


**Figure 7.3** Size exclusion chromatograms of PBA before and after partial fluorination.

The molecular weights determined by SEC are apparent values relative to a PS calibration curve. Because of the significant difference in polarity and likely difference in conformational characteristics and excluded volume effects between hydroxyl end-capped PBA and polystyrene standards, the molecular weights from SEC may deviate considerable from those determined by NMR and titration. Since SEC chromatograms (Figure 7.3) are multimodal, possibly due to individual oligomers, attention will be paid on the major peak value ($M_p$). As can be seen in Figure 7.3, $M_p$ slightly shifts from 3100 to 3440 after the partial fluorination. However, due to uncertainty in the molecular weight determination of the oligoester, it would be inappropriate to draw any firm conclusions from SEC.

Although some minor differences, both in SEC and NMR spectra, before and after partial fluorination are observed, almost no details about the molecular structure of the fluorinated oligomers have been revealed. To obtain the molecular information use was made of the MALDI-TOF MS technique. MALDI is a soft ionization process that allows desorption and ionization of polymers with molecular weight up to hundreds of kilodaltons with very little or no fragmentation.[24] A key advantage of MALDI MS is that the absolute molecular weight of individual polymer chains can be determined,[25] instead of obtaining relative average molecular weights by chromatographic techniques. Thus, details of molecular structure may be revealed by MALDI; for instance, the existence of perfluoroalkyl group in a partially fluorinated oligoester can be directly identified.

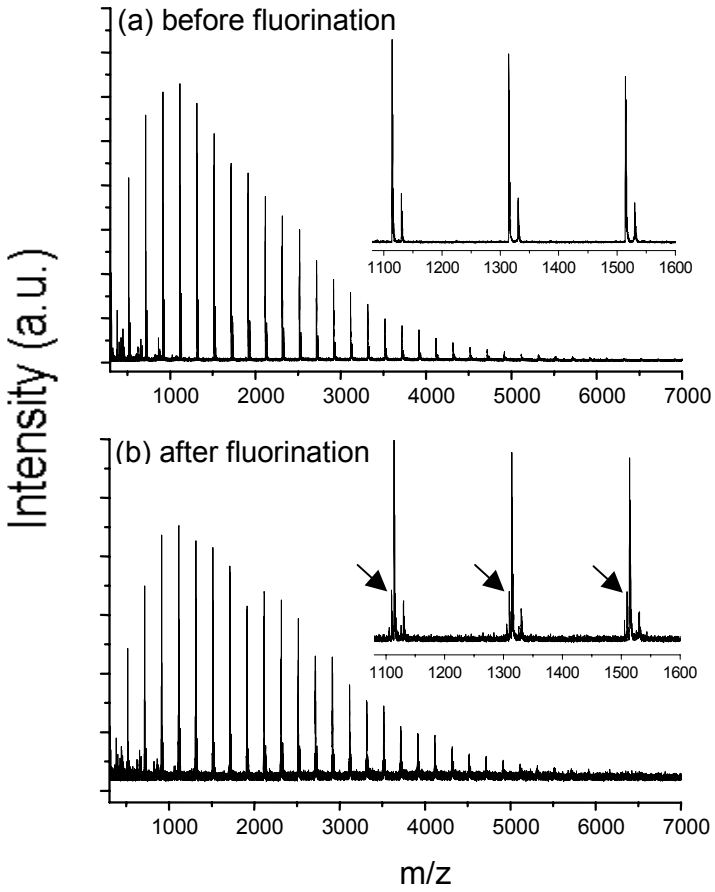


**Figure 7.4** Full MALDI mass spectra for PBA (a) before and (b) after partial fluorination. Peaks indicated by arrows are from mono-fluorinated PBA.

A typical full positive-ion MALDI mass spectrum for PBA before partial fluorination is shown in Figure 7.4a. The sets of signals are separated by 200 Da, characteristic of the butylenes adipate (BA) repeating unit. The molecular weight of the individual mean peaks correspond to the expected structure: $[HO\text{-}(CH_2)_4\text{-}O\text{-}(CO(CH_2)_4CO\text{-}O\text{-}(CH_2)_4\text{-}O)_n\text{-}H + Na]^+$. The molecular weight for PBA of different degrees of condensation ($n$) is $MW_{\text{BA-unit}} \times n + MW_{\text{diol}}$. For example, for $n = 5$ species, the molecular weight was determined to be 1091.21 Da (after subtracting 22.98 for sodium), almost the same as the theoretical value of 1090.29. For species with a degree of condensation greater than 5, Hercules *et al.*[26,27] reported the existence of cyclic oligoesters and monocarboxyl-terminated esters. These species were not found in our results. However, at lower molecular weight region, very small peaks at 423, 623, and 823 Da can be seen, corresponding to the cyclic oligoester with a degree of condensation of 2, 3, and 4, respectively. Although the cyclic structures may affect the molecular weight determination by titration, the effect would be very small since these peaks are about 2 orders of magnitude smaller than the major peaks.

The mass spectrum (Figure 7.4b) after partial fluorination looks quite similar to that of normal PBA (Figure 7.4a); major peaks are located at the exactly same positions. Only when carefully examined, a small but very important difference is noticeable: some small peaks neighboring major peaks appear, as pointed out by the arrows in the inset of Figure 7.4b. It is these small peaks that indicate the presence of the fluorinated species.

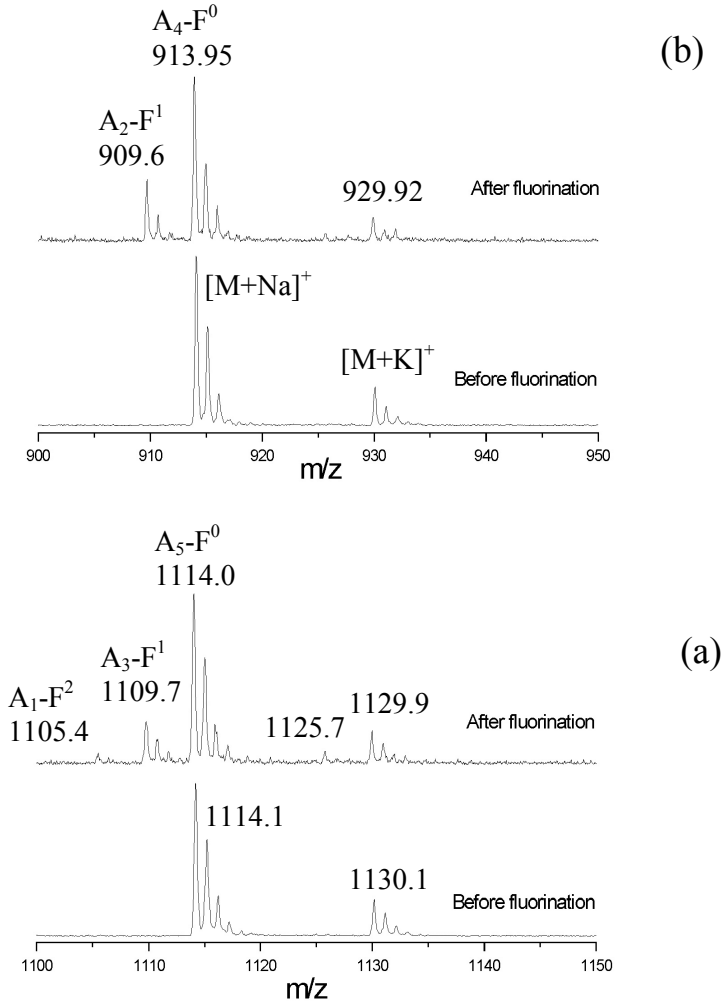


**Figure 7.5** MALDI mass spectra for PBA before and after partial fluorination: (a) degree of condensation, $n = 5$; (b) degree of condensation, $n = 4$.

Some details of the mass spectra are shown in Figure 7.5. Figure 7.5a gives the spectra of BPA before and after partial fluorination in the *m/z* region of 1100-1150. Before fluorination, two series of peaks at 1114.19 and 1130.16 Da with $n = 5$ are shown, corresponding to the sodium and potassium adducts, respectively. The observed isotope distribution (from C, H, and O) is in very good agreement with the simulated one as calculated by the instrument (Voyager–DE Pro) software. On the other hand, after partial fluorination the major peaks at 1114 ($A_5$-$F^0$, in Figure 7.5a) and 1130 Da remain the same,

indicating that a large amount of hydroxyl end-capped PBA remains unsubstituted. However, a few additional peaks due to fluorinated species show up. The peak at 1109.77 Da ($A_3$-$F^1$) results from the monosubstituted perfluoroalkyl oligoester of a lower degree of condensation ($n$ = 3) with the following structure: $[HO\text{-}(CH_2)_4\text{-}O\text{-}(CO(CH_2)_4CO\text{-}O\text{-}(CH_2)_4\text{-}O)_3\text{-}CO\text{-}C_7F_{15} + Na]^+$. The theoretical molecular weight for this species is 1109.33 Da. A corresponding potassium adduct can also be found at 1125.77 Da. Even more interesting, an even smaller peak at 1105.46 Da ($A_1$-$F^2$) is also visible, which comes from a di-substituted perfluoroalkyl oligoester with $n$ = 1 as follows: $[C_7F_{15}\text{-}CO\text{-}O\text{-}(CH_2)_4\text{-}O\text{-}(CO(CH_2)_4CO\text{-}O\text{-}(CH_2)_4\text{-}O)_1\text{-}CO\text{-}C_7F_{15} + Na]^+$. This unambiguously shows that a small amount of di-substituted species will be obtained even when a reaction is carried out at an acid chloride/hydroxyl ratio of 1/5, in accordance with statistical considerations.

In general, both mono- and di-substituted perfluoroalkyl oligoesters can be seen for the oligomer fraction with $n$ = 1-10, while only monosubstituted perfluoroalkyl oligoester can be found when $n$ = 11-14. When $n$ is greater than 14, no substituted species are visible presumably because of the small amount of high molecular weight species. For instance, in the *m/z* region between 900 and 950 (Figure 7.5b) a peak at 909.68 Da is due to a monosubstituted PBA with an $n$ = 2. Furthermore, in the low molecular weight region, no peaks were found at either 509 Da for $[HO(CH_2)_4O\text{-}CO\text{-}C_7F_{15} + Na]^+$ or 437 Da for $[C_7F_{15}COOH + Na]^+$. This suggests that no small fluorinated molecules are present after partial fluorination.

### 7.3.3 Wetting Characteristics from Contact Angles

The surface tension of a polymer can be evaluated by various methods. Among them the contact angle method gives the information for the top surface, such as wettability.[28] Here, we will employ the geometic mean method of Owens and Wendt[29] in combination with the Young's equation (see Chapter 2). Deionized water ($\gamma^d$ = 21.8 mN/m; $\gamma^p$ = 51.0 mN/m) and diiodomethane ($\gamma^d$ = 49.5 mN/m; $\gamma^p$ = 2.3 mN/m) were used as wetting liquids.[29]

In Table 7.2 the contact angle data are shown for the films based on mixtures of linear oligoesters (Oligo-II and Oligo-II-F) and polyisocyanate crosslinker. The films were cured at 80 °C for 30 minutes. When about 2.8 wt% of fluorine was introduced to the film, both advancing and receding angles exhibited a considerable increase for both wetting liquids, compared to the film without fluorine. The contact angle measurement was repeated either a few weeks later or after the film was rinsed with acetone to verify whether the fluorinated

species were crosslinked into the coating matrix. The change of the contact angle was found within ± 2°, implying the film surface was stable, and the decrease of surface tension was not caused by the existence of small fluorine-containing molecules which otherwise would have been removed by acetone. The increase of contact angle by the addition of fluorinated species corresponds to the decrease of the surface tension of the film, *i.e.*, from 34 to 21 mN/m.

**Table 7.2** Contact angle data for films based on linear oligoesters and poly-isocyanate crosslinker cured at 80 °C.

| | Water contact angle (degree) | | $CH_2I_2$ contact angle (degree) | | Surface tension (mN/m) [b] | | |
|---|---|---|---|---|---|---|---|
| Film [a] | $\theta_{adv}$ | $\theta_{rec}$ | $\theta_{adv}$ | $\theta_{rec}$ | $\gamma_S^d$ | $\gamma_S^p$ | $\gamma_S$ |
| Without F | 78 | 66 | 56 | 46 | 25.7 | 8.1 | 33.8 |
| With F | 92 | 77 | 78 | 65 | 15.1 | 5.7 | 20.8 |

[a] Film without F was based on a stoichiometrical mixture of Oligo-II and Desmodur N3300, while for F-containing film, 4 wt% of F was incorporated into the Oligo-II-F (Fluorine content in the film is 2.83 wt% after the composition correction for the amount of polyisocyanate crosslinker added).

[b] Surface tension was calculated from advancing contact angles.

The surface tension was also estimated by the so-called group contribution theory for the linear oligoesters.[30] For Oligo-II, with x = 3, the calculated $\gamma$ is 42 ± 3 mN/m, while for Oligo-II-F, $\gamma$ is 28±3 mN/m. The large difference in surface tension between normal and fluorinated oligoesters is the driving force leading to the enrichment with F-containing species at the surface. This is also one of the most important strategies to prepare self-stratifying coatings.

The packing of perfluoroalkyl groups at the surface is far away from the close-packed structure. For self-assembled perfluoroalkyl acid monolayer (in the surface a close-packed array of $CF_3$ groups), the water advancing contact angle is 112-120°,[31] and even for polytetrafluoroethylene (PTFE) films (parallel chain packing), the angle is measured to be 109°.[32] The highest value in our experiments is about 98°. Therefore, based on the current contact angle data it is not possible to define any picture on polymer orientation and architecture at the polymer-air interface. The observed contact angle hysteresis, on the other hand, may imply that domains of hydrocarbon-rich species (with higher surface tension) are

also present at the surface. The film surface roughness in 10 μm × 10 μm range is within 5 nm (measured by AFM) and seems therefore not to be the source for contact angle hysteresis. One other possible cause for the hysteresis is the surface rearrangement upon the exposure to the testing liquids, or so-called "kinetic hysteresis".[28,33]

**Table 7.3** Contact angle data for films based on three-armed oligoesters and poly-isocyanate crosslinker cured at 80 °C.

| Film[a] | Wt% of added F | Water contact angle (degree) | | $CH_2I_2$ contact angle (degree) | | Surface tension (mN/m) [b] | | |
|---|---|---|---|---|---|---|---|---|
| | | $\theta_{adv}$ | $\theta_{rec}$ | $\theta_{adv}$ | $\theta_{rec}$ | $\gamma_S^d$ | $\gamma_S^p$ | $\gamma_S$ |
| F-0 | 0 | 63 | 54 | 38 | 29 | 32.7 | 13.5 | 46.2 |
| F-1 | 0.18 | 86 | 63 | 51 | 35 | 30.7 | 3.3 | 34.0 |
| F-2 | 0.36 | 91 | 69 | 59 | 41 | 26.7 | 2.6 | 29.3 |
| F-3 | 0.72 | 93 | 70 | 60 | 40 | 26.5 | 2.1 | 28.6 |
| F-4 | 1.43 | 96 | 72 | 64 | 41 | 24.6 | 1.7 | 26.3 |

[a] Films were based on a mixture of Oligo-III and Oligo-III-F, and the stoichiometric amount of Desmodur N3300. Fluorine content in the film was calculated from the recipe for oligoester synthesis and the amount of polyisocyanate crosslinker added.

[b] Surface tension was calculated from advancing contact angles.

In Table 7.3 and Figure 7.6, contact angle data are shown for films based on three-armed oligoesters and polyisocyanate crosslinker cured at 80 °C for 30 minutes. As the content of fluorine in the film increases from 0 to 1.43 wt%, the advancing contact angle of water increases by more than 30°, while that of diiodomethane increases by about 25°. From Figure 7.6 it can be seen that the contact angles level off at a fluorine content of about 0.5 wt%. The decrease of the surface tension of the films demonstrates a similar trend, as listed in Table 7.3. From these data it can be observed that surfaces of the films become saturated by fluorine at a bulk fluorine content of 0.5 wt%. At a fluorine content of 1.43 wt%, the surface tension of the film is 26.3 mN/m, much lower than that of a film without fluorine (46.2 mN/m). This, once again, clearly shows a segregation of fluorine-containing species towards the surface.

The effect of curing temperature on film surface properties was also investigated. Contact angles on films that were cured for 30 min at 120 °C or at 80 °C showed an increase

with increasing fluorine content. However, the increase was less pronounced for curing at 120 °C. This may be due to the faster reaction rate at 120 °C between the hydroxyl groups of the oligoester and the isocyanate group of Desmodur N3300, which leads to a faster formation of the crosslinked network. As a direct consequence, the viscosity of the system becomes high enough in a short period (compared to the case where a curing temperature of 80 °C was used) to effectively reduce the extent of migration of fluorine-containing species.

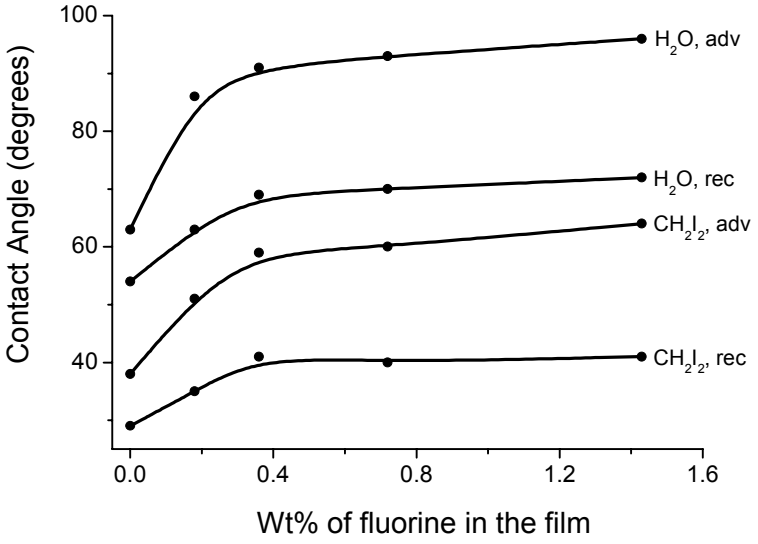


**Figure 7.6** Contact angle change as a function of fluorine content in films cured at 80 °C and based on three-armed oligoesters and polyisocyanate crosslinker.

### 7.3.4 Chemical Composition of Fluorinated Oligoester Films

As described above, introduction of fluorocarbons as end-groups can dramatically alter the surface properties due to the segregation of fluorinated species to the coating-air interface. To obtain chemical information at the surface XPS measurements were performed with 60° with respect to the surface normal.

The $C_{1s}$ and $F_{1s}$ regions of the XPS spectra for films with different fluorine concentrations are shown in Figure 7.7 (for codes of the films see Table 7.3). These films, cured at 80 °C, were based on mixtures of Oligo-III- and Oligo-III-F, with a stoichiometric amount of Desmodur N3300. Films from the linear oligoesters gave similar XPS spectra. In the $C_{1s}$ region of the XPS spectra, discrete peaks can be assigned to different functional groups. The peak assignments are (in eV, after charge correction): C-H, 284.6; C-O/C-N: 285.8; C=O, 288.8; $CF_2$, 291.5; and $CF_3$, 293.9. The intensities of the $–CF_2$- and the $–CF_3$ peaks (the fluorocarbons) relative to those of the aliphatic carbons, increase gradually with

increasing amount of fluorine in the coating formulation. A similar trend can be observed for the $F_{1s}$ spectra.

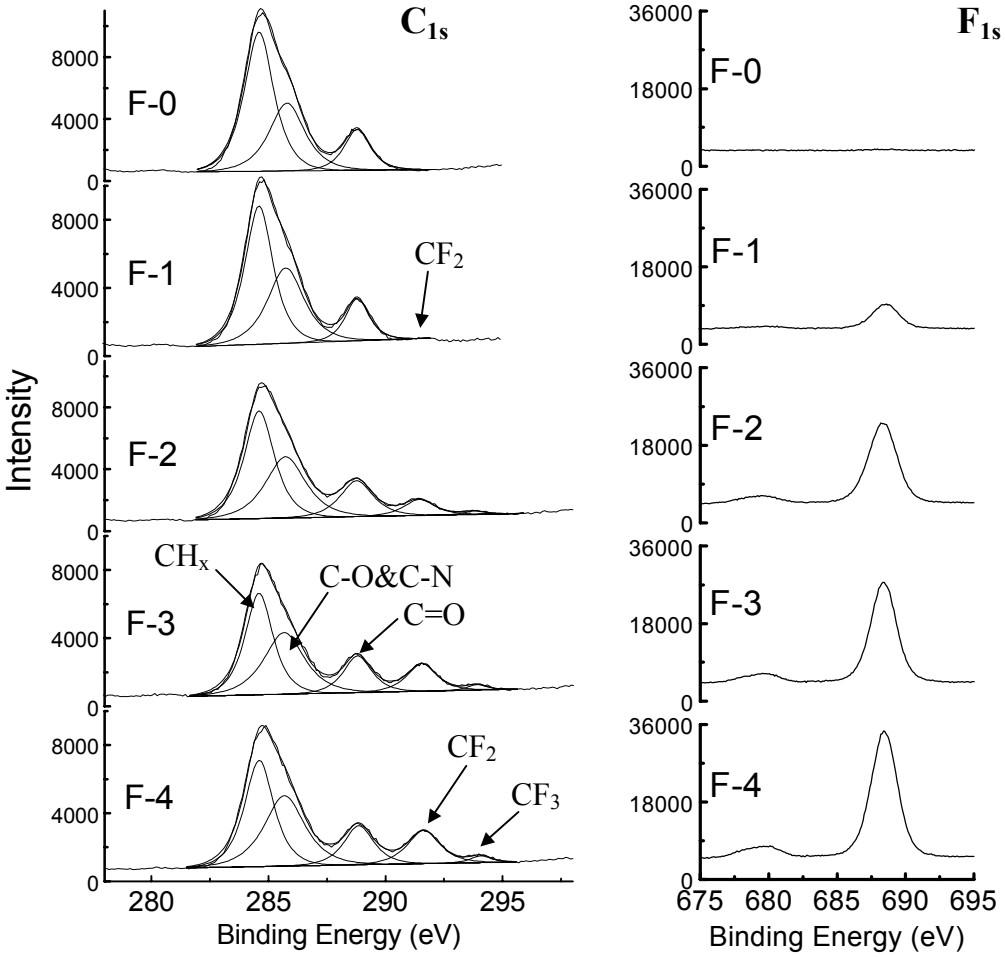


**Figure 7.7** High-resolution XPS spectra of the films from a mixture of Oligo-III and Oligo-III-F, and a stoichiometric amount of Desmodur N3300 after curing at 80 °C. The angle between the surface normal and the electron detector is 60°.

There are two ways to evaluate the surface composition from XPS data: elemental analysis and curve fitting (see Chapter 2). The XPS sampling depth depends on both the angle with respect to the surface normal and the kinetic energy of the emitted photoelectrons. At a particular angle, therefore, the signals from emitted photoelectrons reflect different sampling depths for each element. Because of the small amount of fluorocarbon in some of the $C_{1s}$ spectra, it is difficult to curve fit the region of the fluorocarbons. Therefore the approach of elemental analysis was chosen in such a case. Although this approach makes the quantitative analysis of the surface composition difficult due to the significant difference in sampling depths between fluorine and carbon, it will show the tendency of the surface segregation.

Note that the signal of the $C_{1s}$ will be relatively overestimated (deeper sampling depth), thereby resulting in lower apparent $F_{1s}/C_{1s}$ ratios.

**Table 7.4** XPS data for films based on oligoesters and polyisocyanate cross-linker.

| Sample | | $\left(F/C\right)^{XPS}_{peak\ area}$ | $\left(F/C\right)^{XPS}_{atomic}$ | $\left(F/C\right)^{mixing}_{atomic}$ | F surface enrichment factor[b] |
|---|---|---|---|---|---|
| Oligo-III | F-0 | 0.022[a] | 0.0044 | 0 | |
| | F-1 | 0.53 | 0.11 | 0.0021 | 52 |
| | F-2 | 1.77 | 0.36 | 0.0043 | 84 |
| | F-3 | 2.27 | 0.46 | 0.0085 | 54 |
| | F-4 | 2.52 | 0.51 | 0.017 | 30 |
| Oligo-II | Non-F | - | 0.028 | 0 | |
| | F-containing | 3.33 | 0.98 | 0.035 | 20 |

[a] Instrumental memory effect

[b] $\left(\left(F/C\right)^{XPS}_{atomic}\right)/\left(\left(F/C\right)^{mixing}_{atomic}\right)$

As listed in Table 7.4, the fluorine over carbon (F/C) intensity ratio increases upon increasing the fluorine content in the feed. Based on F/C intensity ratio, it was possible to estimate the F/C atomic ratio. In the analysis of XPS data, a uniform distribution of atoms is assumed and the elemental ratios are then determined by using XPS sensitivity factors (see Chapter 2). The relative sensitivity factors for the equipment used were determined using Teflon as a standard. The F/C atomic ratios for the systems involved, as obtained from XPS, are also given in Table 7.4 and plotted as a function of the theoretical fluorine content in the film (Figure 7.8). The nominal F/C atomic ratio is well below 0.02, but at the surface the fluorine segregation is substantial. For example, when the nominal atomic F/C ratio is only 0.0043, the surface F/C atomic ratio is 0.36, about 80-fold higher than the former. In this series of samples, the surface excess of fluorine (at a depth of about 4 nm) ranges from 30 – 80-fold above the corresponding bulk compositions. This surface enrichment is quite close to the results in the literature,[13] where the surface excess of fluorine was observed in the acrylic polymers containing about 1.5 wt% of (perfluoroalkyl)ethyl methacrylate. Also for the films based on linear oligoester, the surface enrichment of fluorine is unambiguous (see Table 7.5). Figure 7.8 also clearly indicates that the surface F/C ratio becomes almost unchanged at the fluorine content of about 1 wt%. This is in good agreement with the contact angle results as depicted in Figure 7.6. It can be concluded that with the addition of fluorinated species at a level of only 1 wt% of fluorine, it is possible to produce films with a fluorine-rich surface and

much lower surface energy. Such films have shown good repellency against water and common organic solvents.

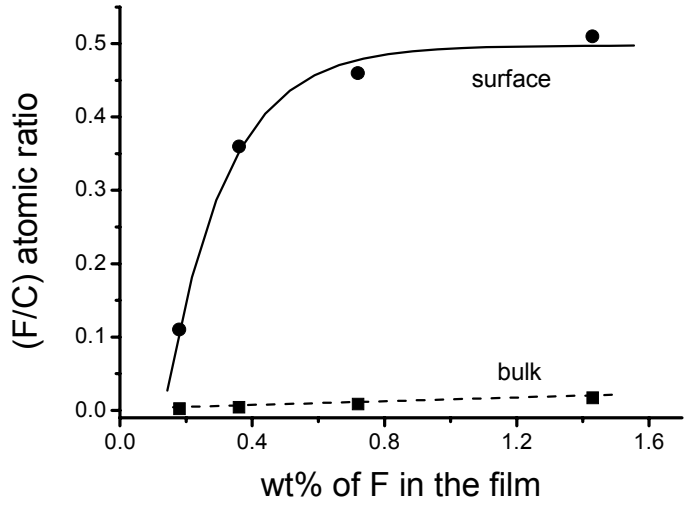


**Figure 7.8** F/C atomic ratio as a function of fluorine content in the films cured at 80 °C from a mixture of Oligo-III and Oligo-III-F, and a stoichiometric amount of Desmodur N3300.

Photocurable liquid oligoesters can be prepared by further substituting the remaining hydroxyl end groups in the 3-armed oligoester acrylic bonds. The obtained partially perfluoroalkyl end-capped, double-bond containing oligoester can be readily photo-cured under UV irradiation. Similar to thermally curable liquid oligoester described in this Chapter, the UV-cured coating showed an enrichment of fluorine at the surface.[34]

## 7.4 CONCLUSIONS

It has been demonstrated in this Chapter that surfaces with low energy can be produced by surface enrichment of fluorinated species in solventless liquid oligoester systems. In this way so-called "environmentally friendly" coating systems can be developed. Three-armed oligoesters are preferred over linear oligoesters to ensure chemical bonding between fluorinated tail and network. Contact angle and XPS studies showed that only 1.4 wt% of fluorine level is sufficient for producing a surface with a surface energy of about 26.3 mN/m. The fluorine level at the surface is many times higher than that in the bulk, caused by the migration of fluorine-containing species to the surface. Such a thin low surface energy layer may introduce many interesting properties to a coating, such as water/oil repellency, low coefficient of friction, and so on.

## 7.5 REFERENCES


[1] Wick, Jr., Z. W.; Jones, F. N.; Pappas, S. P. in *Organic Coatings; Science and Technology,* 2nd ed., Wiley-Interscience, New York, 1999.

[2] Schmidt, D. L.; Coburn, C. E.; DeKoven, B. M.; Potter, G. E.; Meyers, G. F.; Fisher, D. A. *Nature* **1994**, 368, 39.

[3] Anton, D. *Adv. Mater.* **1998**, *10*, 1197.

[4] Ciardelli, F.; Aglietto, M.; Dimirabello, L. M.; Passaglia, E.; Giancristoforo, S.; Castelvetro, V.; Ruggeri, G. *Prog. Org. Coat.* **1997**, *32*, 43.

[5] Höpken, J.; Moller, M. *Macromolecules* **1992**, *25*, 1461.

[6] Akiyama, S.; Kano, Y. in *Polymer Materials Encyclopedia,* Salamone, J. C. Ed., 1996.

[7] a) Yoon, S. C.; Ratner, B. D. *Macromolecules* **1986**, *19*, 1068 b) *ibid* **1988**, *21*, 2392, 2401.

[8] Yoon, S. C.; Ratner, B. D.; Ivan, B.; Kennedy, J. P. *Macromolecules* **1994**, *27*, 1548.

[9] Champan, T. M.; Marra, K. G. *Macromolecules* **1995**, *28*, 2081.

[10] Ho, T.; Malik, A. A.; Wynne, K. J.; McCarthy, T. J.; Zhuang, K. H. Z.; Baum, K.; Honeychuck, R. V. *ACS Symp. Ser.* **1996**, *624*, 362.

[13] Thomas, R. R.; Anton, D. R.; Graham, W. F.; Darmon, M. J.; Sauer, B. B.; Stika, K. M.; Swartzfager, D. G. *Macromolecules* **1997**, *30*, 2883.

[14] Thomas, R. R.; Anton, D. R.; Graham, W. F.; Darmon, M. J.; Stika, K. M. *Macromolecules* **1998**, *31*, 4595.

[15] Wang, J. G.; Mao, G. P.; Ober, C. K.; Kramer, E. J. *Macromolecules* **1997**, *30*, 1906.

[16] Hwang, S. S.; Ober, C. K.; Perutz, S.; Iyengar, D. R.; Schneggenburger, L. A.; Kramer, E. J. *Polymer* **1995**, *36*, 321.

[17] Kassis, C. M.; Steehler, J. K.; Betts, D. E.; Guan, Z. B.; Romack, T. J.; Desimone, J. M.; Linton, R. W. *Macromolecules* **1996**, *29*, 3247.

[18] Sun, F.; Castner, D. G.; Mao, G.; Wang, M.; McKeown, P.; Grainger, D. W. *J. Am. Chem. Soc.* **1996**, *118*, 1856.

[19] Affrossman, S.; Bertrand, P.; Hartshorne, M.; Kiff, T.; Leonard, D.; Pethrick, R. A.; Richards, R. W. *Macromolecules* **1996**, *29*, 5432.

[20] Iyengar, D. R.; Perutz, S. M.; Dai, C.; Ober, C. K.; Kramer, E. J. *Macromolecules* **1996**, *29*, 1229.

[21] Jones, F. N.; Fu, S.; Hua, J.; Yuan, X. *US Pat.* US 5587428.

[22] Kwok, R. W. M. http://www.chem.qmw.ac.uk/surfaces/#software

[23] Zisman, W. A. in *Contact Angle, Wettability and Adhesion*, F. W. Fowkes Ed., ACS Symp. Series, Vol. 43, Washington, DC, 1964.

[24] Wu, K. J.; Odom, R. W. *Anal. Chem*. **1998**, 70, 456A.

[25] Schriemer, D. C.; Li, L. *Anal. Chem*. **1996**, 68, 2721.

[26] Williams, J. B.; Gusev, A. I.; Hercules, D. M. *Macromolecules* **1997**, 30, 3781.

[27] Mehl, J. T.; Murgasova, R.; Dong, X.; Hercules, D. M. *Anal. Chem*. **2000**, 72, 2490.

[28] Johnson, R. E., Jr.; Dettre, R. H. in *Wettability*, Berg, J. C., Ed.; Marcel Dekker: New York, 1993; Chapter 1.

[29] Wu, S. *Polymer Interface and Adhesion*; Marcel Dekker: New York, 1982; Chapter 5.

[30] Van Krevelen, D. W. *Properties of Polymers: Their Estimation and Correlation with Chemical Structure*; Elsevier: Amsterdam, 1976; Chapter 8.

[31] Schönherr, H.; Ringsdorf, H. *Langmuir* **1996**, *12*, 3891.

[32] McLain, S. J.; Sauer, B. B.; Firment, L. E. *Macromolecules* **1996**, *29*, 8211.

[33] Chan, C-M. *Polymer Surface Modification and Characterization*; Hanser Publisher: Munich, 1994; Chapter 2.

[34] Ming, W.; van Ravenstein, L.; van de Grampel, R. D.; van Gennip, W.; Krupers, M; Niemantsverdriet, H; van der Linde, R. *Polym. Bull*. **2001**, 47, 321.

[35] This work has been published in: a) Ming, W.; Laven, J.; van der Linde, R. *Macromolecules*, **2000**, 33, 6886. b) Ming, W.; Lou, X.; van de Grampel, R. D.; van Dongen, J. L. J.; van der Linde, R. *Macromolecules*, **2001**, 34, 2389.

# Chapter 8

# Epilogue

## 8.1 GENERAL CONSIDERATIONS

The valuable technological properties of fluorinated polymer in films and coatings are associated both with perfluoroalkyl chain chemistry and chain orientation at the surface. For a detailed understanding of such systems it is therefore of paramount importance to elucidate the surface structure by adequate characterization methods to relate them to interfacial properties. The work described in this thesis is a contribution to this field where a correlation has been established between the surface tension and the surface constitution of partially fluorinated polymethacrylates. Contact angles, which are used to determine the surface tension, are highly sensitive to the composition and nature of surfaces. The combination of this information with the determination of the composition of exclusively the first atomic surface layer by LEIS enables a better understanding of the true origin of surface tension. Crucial in these investigations is the quantification of fluorine in fluorinated surfaces as described in Chapter 3. In these investigations, it has been clearly demonstrated that for partially fluorinated polymethacrylates the surface tension is linearly related to the fluorine concentration in the outermost layer of these polymers (Chapter 4).

Nevertheless, both the *composition* and the *orientation* in the interface have to be considered for the complete understanding of the molecular origin of the low surface tension of fluorinated surfaces. The combination of LEIS and a surface orientation-sensitive technique as near-edge X-ray absorption fine structure (NEXAFS) should in the future give access to both the chemical composition and structure of fluorinated surfaces in

unprecedented detail. This will result in the key elements for controlling the confined interfaces of 'self-assembled' partially fluorinated polymer films into specific morphologies and/or spatial orientations, *i.e.*, controlling *macroscopic* properties by manipulating *sub-nano* surface structures.

## 8.2 DOMAIN FORMATION IN THE SURFACE

The free surface of a copolymer melt is not necessary chemically homogeneous. When composition variations present themselves in the surface of a system, one may wonder whether this is an off-equilibrium effect, or a phenomenon that can be rationalized from equilibrium considerations. Unless there is a first-order lateral phase transition within the surface, where exactly at the coexistence condition two phases with equal surface pressure live side-by-side, the flat interface cannot tolerate lateral density gradients or surface composition variations that are larger than the equilibrium composition fluctuations. Typically, when the system is off-equilibrium there will be thermodynamical driving forces in the system that direct the system towards a stable equilibrium. In particular, density gradients in the lateral direction at the surface give rise to concomitant surface tension gradients. These surface tension gradients will push the system towards a laterally homogeneous surface.

The free surface, however, has a unique alternative to deal with lateral inhomogeneous compositions, and thus laterally inhomogeneous interfacial tensions. It is not necessary that the free surface remains flat. Such surface topologies may be studied by AFM analysis of polymer melts. Again, the question may arise whether these topologies are transient structures or represent a true equilibrium. More detailed questions may follow from this. For example, how can one envision that such interfaces can exist at a constant chemical potential for the polymer chains? Such questions can only be answered convincingly in a thermodynamically consistent analysis. The use of a mean-field description for inhomogeneous polymer systems as described in Chapter 5 starting from the Edwards diffusion equation could be used for this purpose. However, in order to study lateral inhomogeneous interfaces a two-dimensional gradient analysis has to be carried out instead of the one-dimensional approach described in Chapter 5.

## 8.3 SELF-STRATIFYING COATINGS

The technological value of placing low energy perfluoroalkyl groups at surfaces has been recognized since the pioneering studies of perfluorinated surfactants by Zisman and

coworkers.[1] In this respect it is generally accepted that fluorine is effective in lowering the surface tension, because fluorine has a small atomic radius and the highest electronegativity among atoms.

Fluorinated polymers are therefore a class of materials with exceptional properties, *i.e.* low surface energy, low electrostatic loading, low friction coefficient, hydrophobicity and lipophobicity. These properties render this class of polymers interesting materials for coating applications as described in Chapter 6 and 7. The fluorine-enriched surfaces described in this thesis are, however, rather thin which makes them unattractive in application such as anti-fouling. In that application a thicker layer of the low-surface tension polymer is necessary. Self-stratifying coatings, that are coatings capable of producing a multilayer structure in one operation, are better candidates for this application. The driving force leading to self-stratification may be the incompatibility between polymer components, including the surface tension difference, cross-linking effects, and so on. In particular the condition of spinodal decomposition in a two-component system seems interesting for creating macroscopically stratified layers.

This idea is similar to the principle of wetting-layer growth by Lipowsky and Huse[2] depicted in Figure 8.1. Near the surface a layer of material is depleted in the phase of low surface energy, which is in local equilibrium with the wetting layer. Diffusion of material from the bulk, driven by the concentration gradient, into the depletion region feeds the growth of the wetting layer. Both from a scientific and industrial point of view this will be a challenging task for the future. In this respect it would also be interesting to study stratification, induced in the presence of colloidal particles.[3,4]

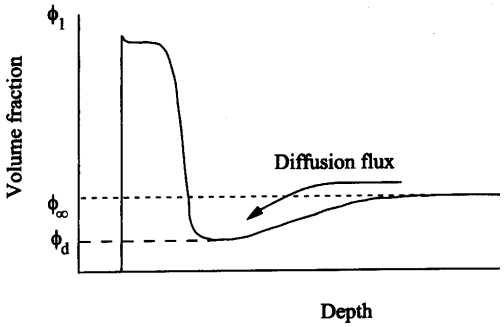


**Figure 8.1** A diffusion limited model for growth of a wetting layer. The wetting layer exists in local equilibrium with the depletion concentration $\phi_d$. Growth of the wetting layer is driven by diffusion of material from the bulk. Figure and legend are taken from reference 5.

## 8.4 WHICH SURFACE IS MORE HYDROPHOBIC ?

Another possible field, which has remained relatively unexplored in this thesis, involves topological and lateral distribution of the perfluorinated surface to affect performance. As described in Chapter 4 it is very likely that surface roughness on atomic scale (nano-scale topographies) plays a role in the wetting behavior of the partially fluorinated polymethacrylates. Films described in this thesis usually assume "the more, the better" principle for producing enriched perfluorinated surfaces to obtain the lowest surface tension of the polymer films. However, in nature, Lotus leaves exhibit extremely hydrophobic surfaces[6] without the use of perfluorinated surface chemistry. In recent work similar ultrahydrophobic behavior is achieved for non-fluorinated surfaces of fractal surface topology.[7,8] Additionally, lateral surface distributions of perfluorinated chemical domains with the order of size required to modulate properties, such as tribology, adhesion, and wetting, have not been explored. It is conceivable that total surface coverage with perfluorinated groups is not essential when lateral control of the density, orientation, topology and distribution of perfluorinated species are used in tandem in the film fabrication process. The control of these parameters will be essential for engineering of tailor-made surfaces.

## 8.5 REFERENCES


1 Zisman, W. A. in *Contact Angle, Wettability and Adhesion*, ed. F. W. Fowkes, ACS Symp. Series, Vol. 43, Washington, DC, 1964.

2 Lipowsky, R.; Huse, D. A, *Phys. Rev. Lett.* **1986**, 57, 353.

3 Pieranski, P.; Strzalecki, L.; Pansu, B. *Phys. Rev. Lett*. **1983**, 50, 900.

4 Thomas, R. R.; Lloyd, K. G.; Stika, K. M.; Stephans, L. E.; Magallanes, G. S.; Dimonie, V. L.; Sudol, E. D.; El-Aasser, M. S. *Macromolecules* **2000**, 33, 8828.

5 Jones, R. A. L.; Richards, R. W. *Polymers at Surfaces and Interfaces*, Cambridge University Press: Cambridge, 1999, Chapter 5.

6 Neinhuis, C.; Barthlott, W. *Annals of Botany* **1997**, 79, 667.

7 Onda, T.; Shibuichi, S.; Satoh, N.; Tsujii, K. *Langmuir* **1996**, 12, 2125.

8 Öner, D.; McCarthy, T. J. *Langmuir* **2000**, 16, 7777.

# Summary

Surfaces and interfaces play an important role in controlling the properties of a broad range of modern materials. Recent advances in the analytical techniques for surfaces have led to improved knowledge of material surfaces and interfaces. At the same time, synthetic and processing tools have been provided for a better control of surfaces and interfacial characteristics for specific applications. Within this framework, this thesis aimed at a better understanding of the correlation between the *physical chemical* surface properties and the *chemical* surface composition of perfluorinated surfaces.

It is generally accepted that the surface tension is primarily governed by interactions in the outermost surface layer. Thus consequently, the composition in the outermost atomic layer dictates the properties of the surface. It is therefore necessary to characterize in detail the composition of this outermost surface layer. Low-energy ion scattering (LEIS) measurements can give direct information of this composition. With the aid of reference samples even quantitative information on the surface composition can be extracted.

By this means, quantitative fluorine surface densities in the outermost atomic layer were determined by LEIS, using a freshly cleaved LiF (100) crystal as reference sample. The LEIS signal can then be translated into a fluorine surface concentration, expressed as the number of fluorine atoms per surface area. The validity of the quantification was proved by the determination of the fluorine concentration of self-assembled monolayers of perfluorinated thiols on gold. All concentrations are of the same order of magnitude ($10^{15}$ fluorine atoms/$cm^2$).

The synthesis and surface properties of a large variety of partially fluorinated polymethacrylates are described in Chapter 4. Incorporation of perfluoroalkyl moieties into a polymethacrylate reduces the surface tension of the polymer significantly, indicating a preferential orientation of the perfluorinated alkyl side chain towards the polymer-air interface (*intra*-molecular segregation). This preferential orientation was found by angle-dependent X-ray Photoelectron Spectroscopy (XPS). Considering the surface tension as a function of the fluorine concentration in the outermost surface as determined by LEIS one can discriminate three regimes. In an intermediate regime, exceeding a certain threshold concentration the surface tension shows a linear dependence on the fluorine concentration. Within the other two regions, the upper and the lower concentration regime, packing and ordering phenomena presumably disturb the linear dependence.

In the next step, compositional and thermodynamic properties of the partially fluorinated methacylate chains in the vicinity of the polymer-vapor interface were investigated within a theoretical model (Chapter 5). The analyses were carried out using a molecular-level self-consistent-field within the Scheutjens-Fleer theory. In these theoretical calculations also the influence of polymer architectures (random copolymers, end-capped polymers and block copolymers) on the surface tension were taken into account, providing essential knowledge for designing tailor-made surfaces.

Many specific applications of polymeric material require both favorable bulk properties and particular surface characteristics. Therefore, surface modification and interfacial engineering are essential in making sophisticated polymeric materials of outstanding bulk and surface properties. The combined knowledge from Chapter 4 and 5 was used to design novel low surface energy coatings systems *viz*. an epoxy-amine coating and an oligoester/isocyanate system.

Chapter 6 deals with the incorporation of perfluorinated epoxides into a thermally cured epoxy/amine coating system. XPS and contact angle measurements showed that the perfluorinated epoxides move to the air-coating interface via an *inter*-molecular segregation process before chemically incorporated in the epoxy matrix. Low surface energies could be obtained by the introduction of small quantities of perfluorinated organic moieties. The careful choice of the fluorinated components allows to control the surface tension of the final, cured films. By varying not only the kind of fluorinated species, but also their amounts, a large variety of low surface tension epoxy films can be obtained.

Chapter 7 provides another versatile method to modify the surface properties towards low surface tensions, keeping the bulk properties unchanged. In this Chapter an oligoester/isocyanate system is described, prepared from of a mixture of diacids of diols/triols. As found for the epoxide system (Chapter 6) only small amounts of the fluorinated species are sufficient to induce a large decrease of the surface tension. Fluorine levels as low as 1.5 wt% are sufficient to lower the surface tension of the films by 20 mN/m. The surface enrichment in fluorine-containing species is confirmed by X-ray Photoelectron Spectroscopy.

The practical examples given in Chapter 6 and 7 illustrate how refined knowledge on the self-organization of fluorinated polymer systems can advantageously be exploited to develop novel materials of added value.

# Samenvatting

Oppervlakken en grensvlakken spelen een belangrijke rol bij de sturing van de eigenschappen van een breed spectrum van materialen. Recente ontwikkelingen in de analysetechnieken van oppervlakken – een aantal worden besproken in Hoofdstuk 2 – hebben geleid tot een betere kennis van oppervlakken en oppervlakteverschijnselen. Ook is het mogelijk gebleken de aard en eigenschappen van oppervlakken beter te kunnen sturen. Het doel van het onderzoek zoals beschreven in dit proefschrift, is primair het begrijpen van de relatie tussen de oppervlaktesamenstelling en oppervlakte-eigenschappen zoals oppervlaktespanning. Als modelsysteem werd gekozen voor copolymeren opgebouwd uit gefluorideerde en niet-gefluorideerde monomeren.

Het is duidelijk dat de oppervlaktespanning vooral wordt bepaald door interacties in de allerbuitenste oppervlaktelaag (atoomlaag). Met andere woorden, de samenstelling in deze oppervlaktelaag bepaalt primair de eigenschappen van het oppervlak. Het is dus noodzakelijk de samenstelling van de buitenste laag in detail te kennen. Lage-energie-ionenverstrooiing (LEIS) metingen verschaffen informatie over deze samenstelling. Het is daarbij echter noodzakelijk de LEIS gegevens op een absolute concentratie schaal d.w.z. de gegevens dienen geijkt te worden. Dit gebeurt met behulp van metingen aan een referentiemateriaal.

Kwantitatieve bepaling van fluorconcentraties in de allerbuitenste oppervaktelaag kan worden uitgevoerd met behulp van een LiF (100) kristal, gesneden direct voorafgaand aan de meting. Op deze wijze kan het LEIS-signaal worden omgezet in een fluorconcentratie per eenheid van oppervlak. De geldigheid van deze methode werd bewezen door de bepaling van fluorconcentraties in de buitenste atoomlaag van zelfordenende monolagen van thiolen op goud. Deze concentraties waren alle in de orde van $10^{-15}$ fluoratomen per $cm^2$. Hoewel de

electronische structuur van het anorganische LiF-oppervlak sterk verschilt van dat van organische oppervlakken, bleken er geen matrixeffecten op te treden bij de metingen.

In Hoofdstuk 4 worden de synthese en de oppervlakte-eigenschappen van een groot aantal gedeeltelijk gefluorideerde polymethacrylaten beschreven. De inbouw van perfluoroalkyleenheden in het methacrylaatpolymeer laat een significante daling van de oppervlaktespanning zien. Dit wijst op een preferente aanwezigheid van de perfluoroalkyl-zijgroepen in het polymeer-lucht grensvlak. Deze preferentiële aanwezigheid kan ook worden aangetoond door middel van foto-electronspectroscopie (XPS) metingen.

In het gevonden verband tussen oppervlaktespanning en fluorconcentratie (bepaald door LEIS) in de buitenste atoomlaag konden drie gebieden onderscheiden worden: een gebied met een lineair verband met aan weerszijden ervan een gebied met een niet-lineair verband. In de beide niet-lineaire gebieden, met respectievelijk een lage en een hoge fluorconcentratie, wordt deze lineaire afhankelijkheid waarschijnlijk verstoord door pakkings-effecten.

Tevens werd het polymeer/dampgrensvlak van deze polymeren met een theoretisch model bestudeerd. De analyses werden uitgevoerd met een Self-Consistent-Fieldmethode, gebruik makend van de statistisch-thermodynamische theorie van Scheutjens en Fleer (Hoofdstuk 5). Bij deze theoretische benadering werd ook de invloed van de polymere ketenarchitectuur op de oppervlaktespanning bestudeerd.

In veel gevallen is het noodzakelijk dat een polymeermateriaal met gewenste bulk eigenschappen voorzien wordt van een oppervlak met specifieke eigenschappen. De kennis, vergaard in Hoofdstuk 4 en 5, werd toegepast bij het ontwerpen van nieuwe coatingsystemen met een lage oppervlaktespanning, te weten een epoxy/amine coating en een vloeibaar oligo-estersysteem.

Hoofdstuk 6 beschrijft de inbouw van gefluorideerde epoxides in een thermisch vernet epoxy/aminesysteem. De combinatie van XPS en contacthoekmetingen liet zien dat de gefluorideerde epoxides preferent naar het coating/luchtgrensvlak bewegen. Reeds bij geringe inbouw van het gefluorideerde epoxide kon een zeer lage oppervlaktespanning worden verkregen. Het bleek mogelijk dit op een beheerste wijze te laten verlopen, waarbij zowel de hoeveelheid als ook de ketenlengte van de gefluorideerde epoxides een belangrijke rol speelt.

Hoofdstuk 7 beschrijft een ander systeem, waarvan eveneens de oppervlakte-eigenschappen veranderd worden, terwijl de samenstelling van de bulk ongewijzigd blijft. Oligo-esters werden gesynthetiseerd door uit te gaan van mengsels van organische, di-

basische zuren en twee- of driewaardige alcoholen. Evenals bij de epoxysystemen, beschreven in Hoofdstuk 6, bleek ook hier dat kleine hoeveelheden van gefluorideerde reagentia voldoende waren voor een grote afname van de oppervlaktespanning. Een gewichtspercentage van 1,5% gefluorideerd materiaal veroorzaakte een daling van 20 mN/m in de oppervlaktespanning. Zelfs bij lage bulkconcentraties gefluorindeerd material bleek de opppervlakte concentratie aanzienlijk te zijn. Dit kon aangetoond worden met behulp van XPS metingen.

# Dankwoord

Bij de totstandkoming van dit proefschrift ben ik een groot aantal mensen dank verschuldigd die op directe of indirecte wijze hun bijdrage hebben geleverd aan dit werk.

Mijn promotor, Rob van der Linde, wil ik hartelijk bedanken voor de mogelijkheid die hij mij heeft geboden om in zijn groep te gaan promoveren. Bijzonder veel waardering heb ik voor de grote mate van vrijheid die mij gegeven werd. Bert de With wil ik bedanken voor de grote interesse die hij voor het onderzoek heeft getoond. Het was een plezier om met je samen te werken. Mijn copromotor en directe 'praatpaal' Jos Laven dank ik voor zijn theoretische inbreng in het geheel. Bovendien zal ik de vele 'Chinese bezorgmaaltijden' op de TUE niet snel vergeten.

De leden van de leescommissie prof. dr. Bert de With, prof. dr. Hidde Brongersma en prof. dr. Gerard Fleer, wil ik bedanken voor hun snelle en kritische beoordeling van dit proefschrift.

Met veel plezier denk ik terug aan de verschillende samenwerkingsprojecten die in de loop van het onderzoek zijn aangegaan. Prof dr. Hans Niemantsverdriet dank ik voor de waardevolle discussies op het gebied van XPS. Wouter van Gennip, dank voor het feit dat je altijd klaar stond voor het meten van de vele XPS samples.

Hidde Brongersma (de man van het biljart spelletje met ionen) bedank ik voor het grote enthousiasme waarmee we de fluor-oppervlakken hebben bestudeerd. Jos Maas en later Anja Gildenpfennig ben ik erkentelijk voor het uitvoeren van de talloze LEIS metingen binnen Calipso.

Aan de hand van Frans Leermakers ben ik het terrein van de SCF simulaties binnengewandeld. Termen als ana-files, goliath en dreuzel zijn nu geen onbekenden meer voor mij. Bedankt Frans voor de waardevolle bijdrage aan mijn proefschrift.

Maarten Krupers, jouw enthousiasme voor het onderzoek heeft mij door de moeilijke beginfase geholpen.

Dank aan de studenten, Jan van Geldrop voor de kinetisch bepalingen, Ben Wassing voor het pionierswerk aan de epoxy systemen, en Frans van der Velden en Tijn de Gouw die dit

pionierswerk succesvol hebben afgerond. Frans, jij in het bijzonder bedankt om in de allerlaatste fase van het proefschrift nog het een en ander door te meten!
Wieb Kingma wil ik bedanken voor de altijd zeer snelle GPC analyses. Dat het 'I love you' virus geen schade heeft aanbracht (ondanks dat ik het drie keer had aangeklikt) is te danken aan de goede computer ondersteuning van Alfons Franken. Michel Peper bedank ik voor mijn introductie in de wereld van de Raman spectroscopie. I like to thank Mingwen Tian for performing several AFM measurements. Emilio Jiménez Piqué (the man of adobe photoshop) mucho gracias for the time you spend in improving the resolution of the pictures in my thesis.
Het secretariaat, 'bevrouwd' door onze steunpilaren Helly van der Heijden en Caroline van Os, stond altijd voor mij klaar. Bijna niks was jullie te gek, ook al waren de verzoeken soms onmogelijk en moest altijd alles op het laatste momentje gebeuren!
Zonder mijn perfecte (nooit klagen over mijn gigantische puinzooi) kamergenoten, Marshall Ming en Chouiab Boukaftane, had ik nooit zoveel plezier op de TUE gehad. Thanks very much guys for this. One day we will celebrate my clean desk with some beers (Marshall) and some soft-drinks (Chouiab). Marshall, 非常感谢你阅读了本论文的初稿以及所提的宝贵意见，很荣幸能与你一起工作.
Verder wil ik natuurlijk iedereen van SPC, SVM, SVM-Coatings bedanken voor de gezellige werksfeer.
Martin Jung, ik stel je vriendschap zeer op prijs. Hopelijk hebben we weer snel bij HEMA in Helmond of HEMA in Mannheim een Italiaans etentje.
De emmer, oudhollands, en natuurlijk: 'wat vraag je' zijn begrippen die je alleen als echte DWS-2-er kent (Willy, Bas, Westers, Smeets, Aaltje, Cunni, Jan K., Jaap). Het was altijd een goede reden om richting één van jullie te rijden voor een biertje (vaak in Groningen).

Tenslotte wil ik mijn ouders bedanken, die altijd voor mij klaarstonden. Het is om deze reden dat ik dit proefschrift aan hen opdraag.

Last but not least, bedank ik Annemieke, ik heb je lief.

# Curriculum Vitae

Robert van de Grampel was born on the 1st of February, 1972 in Paterswolde. In 1990 he graduated from secondary school (Atheneum B, Sint Maartenscollege, Haren (Gr.) and started to study chemistry at the faculty of Mathematics and Natural Science at the University of Groningen. He specialized himself in Polymer Chemistry and did his major subject in the group of prof. dr. A.J. Pennings on synthesis and characterization of novel polycarbonates and polyesters for polymer optical fibres (POF's). He worked on a subsidiary subject on phosphazene-modified polysilanes in the group of Inorganic Ring Systems & Polymers at the same University. Polymeric phosphazene materials for membrane technology were studied at the University of Vermont, VT, USA, under the supervision of prof. dr. C.W. Allen. In June 1997 he joined the Polymer Chemistry & Coatings Technology Group as a PhD student under supervision of prof. dr. R. van der Linde, prof. dr. G de With, and dr. J. Laven at the Eindhoven University of Technology, The Netherlands.

In May 2002 he will join the GE Company, working at GE Plastics in Bergen op Zoom, The Netherlands.